

TWO-NUCLEON FORCES AND NUCLEAR MATTER

K. HOLINDE

Institut für Theoretische Kernphysik der Universität Bonn, Nußallee 14–16, D-5300 Bonn, W.-Germany



NORTH-HOLLAND PUBLISHING COMPANY - AMSTERDAM

TWO-NUCLEON FORCES AND NUCLEAR MATTER

K. HOLINDE

Institut für Theoretische Kernphysik der Universität Bonn, Nußallee 14–16, D-5300 Bonn, W.-Germany

Received July 1980

Contents

1. Introduction	123	6. Relativistic transition potentials	154
2. The tensor force in the two-nucleon interaction	126	6.1. Evaluation of iterative isobar diagrams	154
2.1. The one-pion-exchange potential (OPEP)	126	6.2. Results	158
2.2. ρ -exchange contribution to the NN-interaction	128	7. NN-scattering	162
2.3. The π NN form factor	130	7.1. Outline of the formalism	162
3. Transition from the two-body to the many-body problem	135	7.2. Results	163
3.1. Usual procedure	136	8. Nuclear matter	168
3.2. Brueckner theory including mesonic degrees of freedom	138	8.1. Outline of the formalism	168
3.3. Results for a one-boson-exchange model	139	8.2. Results	170
4. Explicit description of the intermediate-range attraction	143	9. Non-iterative diagrams	173
4.1. Role of the Δ -isobar	144	9.1. Non-iterative π -exchange diagrams involving two-nucleon intermediate states	173
4.2. Transition potentials	146	9.2. Non-iterative π -exchange diagrams involving $N\Delta$ intermediate states	176
4.3. Dispersion theory as a guide for explicit field-theoretic models	148	9.3. Effects in NN scattering	178
4.4. Role of ρ -exchange in the transition potentials	149	9.4. Effects in nuclear matter	182
5. Basic principles for a consistent treatment of the Δ -isobar in the two- and many-body system	150	9.5. Other non-iterative diagrams	182
5.1. Field-theoretic Hamiltonian	151	10. Summary and outlook	182
5.2. The two-nucleon problem	151	Appendix	183
5.3. Nuclear matter problem	153	References	187

Abstract:

Recent nuclear matter calculations have shown that (a) a precise knowledge of the tensor force in the nucleon–nucleon interaction, and (b) an explicit description of the intermediate-range attraction, are absolutely essential to obtain saturation at empirical density. This article describes the progress made recently with respect to these two topics.

Concerning the tensor force, we discuss the influence of π - and ρ -exchange and show the importance of a precise knowledge of the π NN-form factor. As to the second point, we demonstrate the outstanding role of the Δ -isobar. We emphasize the importance of a consistent treatment of the two-body and the many-body problem, starting from a field-theoretical Hamiltonian. We present an explicit boson-exchange model for the NN-interaction including the Δ , and show results for NN-scattering, the deuteron and nuclear matter.

Single orders for this issue

PHYSICS REPORTS (Review Section of Physics Letters) 68, No. 3 (1981) 121–188.

Copies of this issue may be obtained at the price given below. All orders should be sent directly to the Publisher. Orders must be accompanied by check.

Single issue price Dfl. 31.00, postage included.

1. Introduction

The nucleon–nucleon interaction is a fundamental problem in nuclear physics, since it is the starting point for any microscopic understanding of nuclear properties. A suitable procedure for a systematic application of a microscopic many-body theory to nuclear structure is assumed to consist of the following steps (advocated, for example, some years ago in the review article of Erkelenz [1]):

- (i) Determination of the free two-nucleon potential.
- (ii) Calculation of the binding energy and saturation density for the (hypothetical) system of infinite nuclear matter.
- (iii) Calculation of the binding energy, density distribution, and so forth, for real, finite nuclei.

In this scheme, the role of the nuclear matter system is the following: it is thought to be a suitable intermediate check for the reliability of a nucleon–nucleon potential before one starts doing extensive and complicated calculations in finite nuclei. (A numerical evaluation of nuclear matter properties is easier since the wave functions of this system are known to be plane waves, in contrast to finite nuclei, where the wave functions have to be determined selfconsistently.) The necessity for an intermediate check stems from the fact that the empirical two-body data (NN-scattering phase shifts and deuteron properties) do not sufficiently restrict the explicit form of the potential. Thus, a calculation of the properties of nuclear matter should rule out inadequate potential models, i.e. those which do not predict the correct saturation properties (since they are thought to necessarily fail in finite nuclei, too). The remaining (i.e. those giving correct nuclear matter results) are thought to predict adequate results in finite nuclei almost automatically.

Some years ago, the situation in nuclear matter was as follows: A first-order, standard Brueckner–Bethe calculation for different realistic potentials (i.e. those fitting the NN-data appropriately) predicted saturation points lying in a narrow band, the so-called Coester band, which does not meet the empirical value (see fig. 1). The discrepancies in the saturation points are remarkably independent of the specific structure and the type of derivation of the potential, but can be almost completely traced back to differences in the amount of tensor force; namely, the binding energy increases with decreasing tensor force. This is clear from the property of the tensor force being mainly a second-order contribution, which is suppressed in the medium. For example, as shown in fig. 1, the Reid soft core potential (RSC) [2], which has a D-state probability of $\approx 6.4\%$, binds at ~ 10 MeV, whereas one version of the Bonn potential (HM2 [4]), with a D-state probability of 4.3%, yields as much as 24 MeV binding. The crucial point is that, at present, the empirical information about the two-nucleon system is too crude to allow for a sufficiently reliable determination of the correct amount of tensor force: The empirical errors in the mixing parameter ϵ_1 and in the deuteron D-state probability p_D (which are quantities most sensitive to the tensor force) are so large that practically any tensor force (yielding values of p_D from 4 to 8%) is allowed by the two-body data. We should mention that the quadrupole moment of the deuteron is only of limited value for pinning down the correct amount of tensor force since meson-exchange-currents, which until now cannot be reliably calculated, are known to contribute.

Since, however, first estimates of higher-order contributions and many-body forces increased the saturation energy by about 5 MeV [8], more or less independently of the potential used, potential models like RSC appeared to be a realistic basis for microscopic calculations of finite nuclei. On the other hand, potential models with a low D-state probability (like HM2) were discarded. In the last few years, however, several new developments have changed the picture dramatically:

- (i) There are now ‘theoretical’ indications that the tensor force is in fact relatively weak, i.e. considerably smaller than that used in the RSC potential.

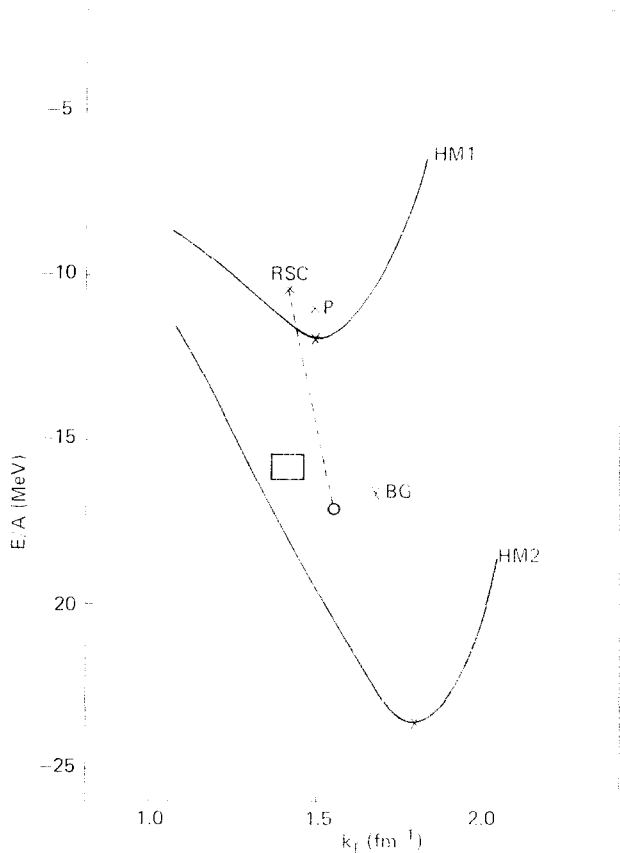


Fig. 1. Nuclear matter binding energy E/A as function of the Fermi momentum k_F . The lines show the results for two versions of the Bonn potential, HM1 [3] and HM2 [4], using first-order Brueckner theory. The crosses give the saturation points obtained by using the Reid soft-core potential [2] (RSC), the Paris potential [5] (P) and the OBE-potential of Bryan and Gersten [6] (BG), likewise in first-order Brueckner theory. The open circle (quoted from ref. [7]) denotes the saturation point of RSC, including higher-order Brueckner contributions. The box represents the empirical value.

(ii) New variational calculations of nuclear matter binding energy (in the Fermi-Hypernetted-Chain Approximation) led to a detailed reexamination of higher-order contributions in Brueckner theory. It now seems that even the RSC potential [2] tends to overbind nuclear matter, at too high a density, see fig. 1.

(iii) Already before these developments, the importance of meson and isobar degrees of freedom was realized. The consistent use of these degrees of freedom makes it possible to include many-body corrections in the NN-potential in a well-defined way, which result in a density-dependent suppression of the intermediate-range attraction and lead to considerably less nuclear matter binding.

Obviously, starting from the RSC potential, the inclusion of such degrees of freedom moves the saturation point away from the empirical one. Consequently, in the beginning (when the RSC potential was still thought to be realistic), those effects were not really taken seriously; they were often thought to be 'spurious' effects cancelled somehow by other many-body effects. Now, due to (i) and (ii), one believes more and more that a realistic description of nuclear matter cannot be achieved without the inclusion of such effects. This also means that any purely phenomenological potential will fail in dense matter, since the modifications due to the medium cannot be built in in a well-defined way. On the

other hand, such Pauli-blocking and dispersion effects arise naturally in a consistent many-body theory using a meson-theoretic framework. Thus, apart from a deeper understanding of the NN-interaction itself, a correct description of nuclear structure phenomena clearly makes it necessary to consider that the interaction between two nucleons is mediated by mesons.

Of course, the most appropriate approach for deriving a realistic two-nucleon force based on meson theory surely depends on what one wishes to do afterwards with this potential. In fact, if we would restrict our considerations to the two-nucleon problem, dispersion theory (as done e.g. in ref. [5]) is probably the best one can do since it provides strong constraints due to correlations with πN - and $\pi\pi$ -scattering data; the construction of explicit field-theoretical models would be a complete luxury. As another example, the final aim of the Nijmegen group [9] is to understand hyperon–nucleon scattering; they therefore rely on a pure OBE-model together with SU(3)-arguments to obtain the hyperon–nucleon interaction, which seems to be the best procedure in this case. However, if the final aim is to understand nuclear structure phenomena, we strongly believe that modifications of the NN-interaction due to the medium have to be taken into account. These can hardly be handled in a dispersion-theoretical treatment. Of course, the results of dispersion theory should be used as a constraint for explicit field-theoretical models in order to pin down ambiguities in propagators, form factors and so on.

Such an inclusion of mesonic and isobar degrees of freedom is an arduous task, and we are far from a complete treatment. In fact, due to its relatively large density, infinitely extended nuclear matter is physically a very complicated system and requires a much more extended picture than one realized before. Thus, also in view of the current difficulties concerning a reliable calculational procedure, it seems justified to raise doubts whether, at this point in time, nuclear matter can really play the role of a quick, intermediate check of an NN-interaction to be used in nuclear structure. In contrast, the three-body system and few-body reactions might be much more suitable candidates for such a first check, since the corrections due to the medium are obviously strongly density-dependent and should be small there, if not negligible. Such systems seem therefore appropriate to test the amount of tensor force, since the calculations are not spoiled by an incorrect calculational procedure (the Faddeev equations for the three-body system are well established and can be solved reliably for any kind of potential), or a possible mistreatment of many-body corrections, as in nuclear matter. Thus one could well advocate starting with the lightest nuclei and proceeding further to heavier nuclei extending the treatment with increasing density.

On the other hand, nuclear matter is certainly well suited to show up effects of modifications of the NN-interaction due to the medium, since these should be sizeable there precisely due to the large density. Thus, the role of the nuclear matter system might change: It may be no longer (at least in the moment) a candidate for a first check of a potential, but it is an appropriate system to study effects typical for dense matter in general.

It should be clear from the above that, in order to get a final understanding of nuclear structure, current research on the NN-interaction should concentrate on the following subjects:

- (a) to obtain precise and reliable information about the amount of tensor force present in the NN-system,
- (b) to obtain an explicit description of the intermediate-range attraction, which, in the two-body system, is consistent with what is known from dispersion theory.

Therefore, the purpose of this article is essentially twofold:

1. We want to describe what is known at present about the tensor force, especially, we will show the decisive role played by ρ -exchange and by the πNN -form factor.
2. We will show the point reached so far in building in mesonic and isobar degrees of freedom into the two-nucleon interaction and calculating their effects in the nuclear matter system.

2. The tensor force in the two-nucleon interaction

The tensor force is an essential quantity not only for the saturation properties of nuclear matter, but also for the binding energies of light nuclei: For example, two potential models, which differ by 1% in the deuteron D-state probability, predict saturation energies per particle, which differ by about 0.2 MeV in the case of the triton, by roughly 2 MeV for ^{16}O , and by as much as 10 MeV in nuclear matter. As expected, the effect depends strongly on the density of the system: For low density systems like the triton, the suppression of the tensor force due to the medium is small; it grows with increasing density.

Moreover, the amount of tensor force plays an important role in all sorts of few-body reactions like e.g. photodisintegration of the deuteron [10]. Thus it is of outstanding importance to know even the details of the tensor force in the NN-interaction as accurately as possible. Since, unfortunately, the empirical information in the moment is not sufficient to draw detailed conclusions, we are led to ask what the theory can tell us about this important quantity and whether, in the present stage, it is able to sufficiently pin down its behaviour.

According to meson field theory, the interaction between two nucleons is mediated by the exchange of various mesons. The nucleons and mesons are described by local and renormalizable field theories, in which the particles are considered as elementary and pointlike. On the other hand, people now believe in the quark model, where the nucleons consist of three quarks and the meson of a quark and an antiquark. The strong interaction between the quarks is due to the exchange of massless vector particles, called gluons. This whole system is described by a local renormalizable gauge field theory called quantum chromodynamics. Thus, in this scheme, the two-nucleon force is in fact a force between two three-body systems. To obtain from this picture an ‘effective’ nucleon–nucleon potential for application in nuclear structure is obviously very complicated and has not been done yet. (First calculations using the MIT bag model have been performed recently by DeTar [11].) In any case, in view of the composite structure of the hadrons predicted by the quark model, the concepts of field theory cannot be taken rigorously anymore. Of course, this does not mean that one should throw away all information about the NN-interaction obtained from usual meson theory. This picture had such an enormous success, correlating a great amount of data (from NN-, $\text{N}\pi$ - and $\pi\pi$ -scattering, electromagnetic form factor data) that it should be essentially right, at least for the outer- and intermediate-range part of the interaction. However, if one wants to have a detailed theoretical description of the very inner part of the interaction, it is plausible that the composite structure of the hadrons has to be taken into account in a realistic way, i.e. starting from the quark model. In fact, due to asymptotic freedom of the quarks, the description of the inner part in terms of quarks might be ultimately relatively simple since one can use perturbation theory. In the meantime, we might hope that, for low-energy NN-scattering and nuclear structure (which we are interested in here), the inner part of the NN-interaction need not be known in such detail and can be described by a global repulsion provided by ω -exchange.

2.1. The one-pion-exchange potential (OPEP)

The two simplest choices for the πNN -vertex are

$$\Gamma_{\pi,\text{ps}} = \sqrt{4\pi} g_{\text{NN}\pi} i\gamma^5 \tau \quad (2.1)$$

$$\Gamma_{\pi,pv} = \sqrt{4\pi} \frac{f_{NN\pi}}{m_\pi} i \gamma^\mu \gamma^5 k_\mu \tau \quad (2.2)$$

k_μ being the four-momentum of the π -meson. Both couplings are equivalent for on-mass-shell nucleons if we relate $g_{NN\pi}$ and $f_{NN\pi}$ by $g_{NN\pi} = (2m/m_\pi) f_{NN\pi}$, where m is the nucleon mass. However the off-shell contributions, i.e. those arising from antinucleons, are completely different: Unlike ps-coupling, pv-coupling strongly suppresses antiparticle contributions.

Historically, the ps-coupling was usually preferred over the pv-coupling since, in conventional field theory, the latter is not renormalizable. It is now understood that chiral invariance dictates addition of σ -degrees of freedom, which essentially converts ps-coupling into pv-coupling, at least for the description of low-energy phenomena [12].

$g_{NN\pi}$ (and $f_{NN\pi}$) are in fact not constants but, in general, $g_{NN\pi}$ is a function of the four-momenta involved at the πNN -vertex, i.e. $g_{NN\pi} = g_{NN\pi}(q^2, q'^2, k^2)$, see fig. 2. If we write

$$g_{NN\pi}(q^2, q'^2, k^2) = g_{NN\pi}(m^2, m^2, m_\pi^2) \cdot F_\pi(q^2, q'^2, k^2), \quad (2.3a)$$

the first term on the r.h.s. denotes the value of $g_{NN\pi}$ at the fully on-shell point and the second term, the so-called πNN form factor, describes the off-shell behaviour of $g_{NN\pi}$. From $\pi^\pm p$ dispersion relations [13] and analyses of $L \geq 4$ partial waves in NN scattering [14] one obtains for $g_{NN\pi}^2(m^2, m^2, m_\pi^2) \approx 14.5 \pm 0.5$. If we restrict our considerations to on-shell nucleons (which will be done in the following unless stated otherwise) we can write

$$g_{NN\pi}(k^2) = g_{NN\pi}(m^2, m^2, m_\pi^2) \cdot F_\pi(k^2) \quad (2.3b)$$

where $F_\pi(k^2)$ denotes the πNN form factor for on-shell nucleons.

The relativistic OPE-amplitude M_π contributing to NN-scattering is defined as

$$\langle f | M_\pi | i \rangle = \bar{u}(\mathbf{q}'_1, s'_1) \bar{u}(\mathbf{q}'_2, s'_2) \mathcal{M}_\pi u(\mathbf{q}_1, s_1) u(\mathbf{q}_2, s_2). \quad (2.4)$$

Here, $\mathbf{q}_i(\mathbf{q}'_i)$ are the incoming (outgoing) nucleon momenta and $s_i(s'_i)$ the corresponding spin components. The matrix \mathcal{M}_π acts in the two-particle Dirac spinor space and, for ps-coupling, is given according to the Feynman rules by

$$\mathcal{M}_\pi = \frac{\Gamma_{ps}^{(1)} \Gamma_{ps}^{(2)}}{k^2 - m_\pi^2}. \quad (2.5)$$

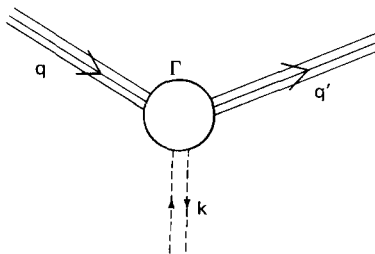


Fig. 2. Nucleon–nucleon–meson vertex.

Therefore

$$\langle \mathbf{f} | M_\pi | \mathbf{i} \rangle = 4\pi g_{NN\pi}^2 \frac{\bar{u}(\mathbf{q}'_2, s'_2) i\gamma^5 u(\mathbf{q}_2, s_2) \bar{u}(\mathbf{q}'_1, s'_1) i\gamma^5 u(\mathbf{q}_1, s_1)}{k^2 - m_\pi^2} \boldsymbol{\tau}_1 \cdot \boldsymbol{\tau}_2. \quad (2.6)$$

In the c.m. system and in the on-shell limit ($\sqrt{q'^2 + m^2} = \sqrt{q^2 + m^2}$) this becomes

$$\langle \mathbf{q}' s'_1 s'_2 | V_\pi | q s_1 s_2 \rangle = -4\pi \frac{g_{NN\pi}^2(k^2)}{4m^2} \frac{\boldsymbol{\sigma}_1 \cdot \mathbf{k} \boldsymbol{\sigma}_2 \cdot \mathbf{k}}{k^2 + m_\pi^2} \boldsymbol{\tau}_1 \cdot \boldsymbol{\tau}_2. \quad (2.7)$$

We should note that the on-shell limit is an excellent approximation over the whole energy range for nucleon–nucleon scattering ($0 < E_{\text{Lab}} \lesssim 350$ MeV), at least in the case of π -exchange [15]. Neglecting for the moment the k^2 -dependence of $g_{NN\pi}^2$, we obtain, after a Fourier-transformation, the well-known local expression in r -space (neglecting the δ -function piece)

$$V_\pi(r) = g_{NN\pi}^2 \frac{m_\pi^2}{4m^2} \frac{m_\pi}{3} \left[\boldsymbol{\sigma}_1 \cdot \boldsymbol{\sigma}_2 + S_{12} \left(1 + \frac{3}{m_\pi r} + \frac{3}{(m_\pi r)^2} \right) \right] \frac{\exp(-m_\pi r)}{m_\pi r} \boldsymbol{\tau}_1 \cdot \boldsymbol{\tau}_2 \quad (2.8)$$

with

$$S_{12} = 3 \frac{\boldsymbol{\sigma}_1 \cdot \mathbf{r} \boldsymbol{\sigma}_2 \cdot \mathbf{r}}{r^2} - \boldsymbol{\sigma}_1 \cdot \boldsymbol{\sigma}_2 \quad (2.9)$$

being the usual tensor operator; \mathbf{r} is the distance between the two interacting nucleons. Since the coupling constant is \mathbf{k}^2 -dependent, we must, in general, perform the Fourier-transformation numerically. Only for special, however, common choices for $F_\pi(k^2)$ the Fourier-transformation can still be done analytically.

Before discussing present information about $F_\pi(k^2)$, which, in fact, has considerable influence on all sorts of nuclear phenomena (e.g. three-body forces, pion–nucleus scattering, meson-exchange currents), we will turn in the next section to a brief description of what is known about the ρ NN-vertex, another important term for evaluating the tensor force.

2.2. ρ -exchange contribution to the NN-interaction

The ρ -meson (spin 1, negative parity, isospin 1) is a resonance at $m_\rho = 763$ MeV with a width of 146 MeV. The ρ NN-vertex is usually written as a sum of vector and tensor coupling

$$\Gamma_\rho = \sqrt{4\pi} \left[g_{NN\rho} \gamma^\mu + \frac{f_{NN\rho}}{2m} i\sigma^{\mu\nu} k_\nu \right] \boldsymbol{\tau}. \quad (2.10)$$

Here $g_{NN\rho}$ is the vector, $f_{NN\rho}$ the tensor coupling constant; $\sigma^{\mu\nu} = \frac{1}{2}i[\gamma^\mu, \gamma^\nu]$ and k_ν is the 4-momentum of the exchanged ρ -meson. The tensor coupling has to be taken into account in order to describe the anomalous magnetic moment of the nucleon. Note that for on-mass-shell nucleons, the vertex function (2.10) is equivalent to

$$\Gamma'_\rho = \sqrt{4\pi} \left[(g_{NN\rho} + f_{NN\rho}) \gamma^\mu - \frac{f_{NN\rho}}{2m} (q' + q)^\mu \right] \boldsymbol{\tau} \quad (2.11)$$

where q' , q are the four-momenta of the two nucleons at the vertex. The equivalence of eqs. (2.10) and (2.11) can be shown using the Gordon decomposition [16]. As noted already, these two vertex functions are only equivalent for on-mass-shell nucleons.

Analogous to eq. (2.4), the relativistic ρ -exchange amplitude M_ρ is defined as

$$\langle f | M_\rho | i \rangle = \bar{u}(\mathbf{q}'_1, s'_1) \bar{u}(\mathbf{q}'_2, s'_2) \mathcal{M}_\rho u(\mathbf{q}_1, s_1) u(\mathbf{q}_2, s_2) \quad (2.12)$$

where \mathcal{M}_ρ is given by

$$\mathcal{M}_\rho = \Gamma_\rho^{(1)} \frac{-g_{\mu\nu} + k_\mu k_\nu / m_\rho^2}{k^2 - m_\rho^2} \Gamma_\rho^{(2)}. \quad (2.13)$$

Let us first consider the second term $k_\mu k_\nu / m_\rho^2$ in the ρ -meson propagator. Due to the antisymmetry of $\sigma^{\mu\nu}$, this term does not contribute to the tensor part of the interaction. It does, however, contribute to the other parts unless nucleon 1 or 2 is on-mass-shell (and the mass of proton and neutron are assumed to be the same). In any case, this contribution turns out to be small [17].

Thus M_ρ can be written as (using the vertex function (2.10)):

$$\begin{aligned} \langle f | M_\rho | i \rangle = & -4\pi \boldsymbol{\tau}_1 \cdot \boldsymbol{\tau}_2 (k^2 - m_\rho^2)^{-1} \bar{u}(\mathbf{q}'_2, s'_2) \left[g_{NN\rho} \gamma^\mu + \frac{f_{NN\rho}}{2m} i\sigma^{\mu\nu} (q'_2 - q_2)_\nu \right] u(\mathbf{q}_2, s_2) \\ & \times \bar{u}(\mathbf{q}'_1, s'_1) \left[g_{NN\rho} \gamma_\mu + \frac{f_{NN\rho}}{2m} i\sigma_{\mu\alpha} (q'_1 - q_1)^\alpha \right] u(\mathbf{q}_1, s_1). \end{aligned} \quad (2.14)$$

In order to obtain a simple expression in r -space, which can be compared to $V_\pi(r)$, eq. (2.8), we first remove the γ^μ -term by means of the Gordon decomposition, neglect the convection-current-term $(q' + q)^\mu$, and obtain in the c.m. system and in the static limit

$$\langle q's'_1s'_2 | V_\rho | qs_1s_2 \rangle = 4\pi \boldsymbol{\tau}_1 \cdot \boldsymbol{\tau}_2 \frac{g_{NN\rho}^2}{4m^2} \left(1 + \frac{f_{NN\rho}}{g_{NN\rho}} \right)^2 (k^2 + m_\rho^2)^{-1} [-\mathbf{k}^2 \boldsymbol{\sigma}_1 \cdot \boldsymbol{\sigma}_2 + \boldsymbol{\sigma}_1 \cdot \mathbf{k} \boldsymbol{\sigma}_2 \cdot \mathbf{k}]. \quad (2.15)$$

Neglecting again the k^2 -dependence of the coupling constants, we obtain, after a Fourier transformation,

$$V_\rho(r) = g_{NN\rho}^2 \left(1 + \frac{f_{NN\rho}}{g_{NN\rho}} \right)^2 \frac{m_\rho^2}{4m^2} \frac{m_\rho}{3} \left[2\boldsymbol{\sigma}_1 \cdot \boldsymbol{\sigma}_2 - S_{12} \left(1 + \frac{3}{m_\rho r} + \frac{3}{(m_\rho r)^2} \right) \right] \cdot \frac{\exp(-m_\rho r)}{m_\rho r} \boldsymbol{\tau}_1 \cdot \boldsymbol{\tau}_2. \quad (2.16)$$

Comparing with $V_\pi(r)$ of eq. (2.8) we notice that the ρ -exchange tensor force has the opposite sign compared to OPEP, whereas the spin–spin term goes into the same direction. Using πN -scattering data, Höhler and Pietarinen [18] predicted for the coupling constants $g_{NN\rho}^2 (k^2 = m_\rho^2) \approx 0.55$ and for the ratio $f_{NN\rho}/g_{NN\rho} \approx 6.6$. Concerning electromagnetic nucleon form factors, such a large value for $f_{NN\rho}/g_{NN\rho}$ implies a bump-dip structure [19] in the imaginary part of $F_{2\nu}$ in order to account for the observed values of the anomalous magnetic moments of proton and neutron. In fact, according to ref. [19], the data require an additional pole contribution ρ' (with the same quantum numbers as ρ) at 1250 MeV, which suppresses the ρ -contribution at momentum transfer $t = 0$.

In principle, if one uses the above values for the NN-coupling constants in a nucleon–nucleon potential (eq. (2.16)), then, for consistency, one should also include the ρ' -contribution predicted in ref.

[19]. At first glance one might think that this contribution would also damp the effect of ρ -exchange, as it does in the form factor problem. We have checked however that, in low-energy nucleon–nucleon scattering, this contribution has a negligible effect only. It is much too short-ranged and is thus completely masked by the ω -repulsion. Furthermore, since there are two ρ NN-vertices involved in NN-scattering, this contribution goes in fact in the same direction as ρ -exchange.

We should note that this large value of $f_{NN\rho}/g_{NN\rho}$ has been recently confirmed by Grein [20], who gets $f_{NN\rho}/g_{NN\rho} = 6.0$ using NN forward dispersion relations.

This shows that the ρ -exchange potential is rather strong and consequently cuts down the OPE-tensor force in the inner region. Therefore, the deuteron D-state probability is reduced considerably. For example, in our potential version HM2 [4], the small D-state probability (4.3%) is to a large extent due to a strong ρ -coupling used there ($f_{NN\rho}/g_{NN\rho} = 6.2$). In fact, as pointed out by Lomon [21], a bulk of few-body reactions (like e.g. photodisintegration of the deuteron) now clearly favour low D-state probabilities.

2.3. The π NN form factor

For on-shell nucleons, the π NN form factor $F_\pi(k^2)$ is usually parametrized as

$$F_\pi(k^2) = \frac{\Lambda_\pi^2 - m_\pi^2}{\Lambda_\pi^2 - k^2}. \quad (2.17)$$

Here, Λ_π is the so-called cutoff-mass. This parameter is tried to be fixed either by certain empirical information or by theoretical estimates, to be discussed below. Eq. (2.17) shows that F_π suppresses the bare vertex for high $|k^2|$, which implies that the resulting potential is damped in the inner region. Λ_π governs the range of this suppression: For small values of Λ_π , $F_\pi(k^2)$ will be considerably smaller than 1 already for relatively small values of $|k^2|$, whereas for very large values of Λ_π , there will be a considerable deviation from 1 only for very large $|k^2|$. For example, $\Lambda_\pi = 1$ GeV modifies the bare OPEP already at $r \sim 1.5$ fm [22], whereas a value of $\Lambda_\pi \sim 3$ GeV will hardly have any effect on the final results.

In order to show the outstanding importance of a precise determination of the π NN form factor, we first study its influence on NN scattering phase shifts and deuteron observables, i.e. the sensitivity of these data to variations of Λ_π . We start from a momentum-space one-boson-exchange potential (OBEP) (for details see ref. [1]), using meson–nucleon form factors $F_\alpha(k^2)$, which are parametrized analogously to eq. (2.17), namely

$$F_\alpha(k^2) = \left(\frac{\Lambda_\alpha^2 - m_\alpha^2}{\Lambda_\alpha^2 - k^2} \right)^n \quad (2.18)$$

with $n = 1$ for $\alpha = \pi, \eta, \sigma, \delta$ and $n = \frac{3}{2}$ for $\alpha = \rho, \omega, \phi$ (in order to have sufficient convergence in the potential). In contrast to refs. [3, 23] we now use a common value for Λ_α .

We insert this potential in a Lippmann–Schwinger-type equation (see ref. [1]) and solve for the NN scattering phase shifts ($0 \leq J \leq 6$). The good quality of the fit is shown by the value for $\chi^2/\text{data} = 2.87$ using the error matrix as in ref. [5] based on the Livermore analysis [14] for $E_{\text{lab}} = 25, 50, 95, 142, 210$ and 330 MeV. (Fitting directly to the phase shifts like in refs. [3, 23] we obtain a value of $\chi^2/\text{data} = 2.85$.)

Table 1

Meson parameters obtained by fitting the NN-phase shifts. The first set shows the values if $\Lambda_\alpha = 1530$ MeV is taken for all meson contributions. $g_{NN\alpha}^2(k^2 = m_\alpha^2)$ are the coupling constants, $g_{NN\alpha}^2(k^2 = 0)$ the corresponding strengths. The number in brackets gives the tensor to vector coupling ratio $f_{NN\alpha}/g_{NN\alpha}$. m_α are the masses of the mesons exchanged. The second (third) set shows the values obtained if Λ_π is chosen to be 1265 (1000) MeV with $\Lambda_{\alpha \neq \pi}$ and m_α the same as before. The numerical calculations were performed with the values of $g_{NN\alpha}^2(k^2 = m_\alpha^2)$

Λ_α	1530		1265		1000	
	$g_{NN\alpha}^2(k^2 = m_\alpha^2)$	$g_{NN\alpha}^2(k^2 = 0)$	m_α	$g_{NN\alpha}^2(k^2 = m_\alpha^2)$	$g_{NN\alpha}^2(k^2 = m_\alpha^2)$	
π	14.4	14.17	138	14.4	14.4	
η	6	4.56	548.5	6	6	
	0.77	0.37	712	0.77	0.77	
ρ	(6.6)	(6.6)		(6.6)	(6.6)	
ω	23	9.25	782.8	23	23	
ϕ	5	0.85	1020	5	5	
σ	8.2	6.22	550	8.67	9.202	
δ	4.99	1.83	960	2.88	0.704	

The resulting meson parameters are shown in table 1. In addition to the coupling constants, i.e. $g_{NN\alpha}^2(k^2 = m_\alpha^2)$, we also give the values of $g_{NN\alpha}^2(k^2 = 0)$, which are a suitable measure of the strength of the corresponding interaction in NN scattering. The resulting NN phase shifts predicted by the present OBE-model are similar to those given by earlier versions [3, 23]. However, the resulting value for Λ_α is now the same for all mesons and equals 1530 MeV. It is important to note that, if we would not restrict Λ_π to be the same as $\Lambda_{\alpha \neq \pi}$, the resulting best fit value for Λ_π would be practically the same; in other words, the description of the data is not improved by using a smaller value of Λ_π . For larger values of Λ_π , the data becomes rather insensitive to variations of Λ_π .

In order to show the sensitivity of the data to variations of Λ_π , i.e. to modifications of the inner part of the tensor force, we changed Λ_π to 1000 MeV and 1265 MeV, respectively (keeping $\Lambda_{\alpha \neq \pi}$ unchanged). We readjusted only the scalar coupling constants (g_σ^2, g_8^2), see table 1. This guarantees that no additional, probably compensating change in the tensor force is made.

Typical results for the NN scattering phase shifts are shown in figs. 3–6: As a general feature, the results become very sensitive to variations of Λ_π , if $\Lambda_\pi < 1200$ MeV. In the 3D_2 wave, a long-ranged OPE-cutoff ($\Lambda_\pi \leq 1$ GeV) is able to remove the long-standing discrepancy between most realistic theoretical models and experiment. However, this is not the only possible tool: As is shown later in this article (e.g. fig. 36) retardation effects in the potential and the inclusion of explicit isobar diagrams are also able to achieve such an improvement. Furthermore, such a small value for Λ_π would have disastrous effects in lower partial waves; we show the results for the mixing parameter ϵ_1 and 3P_1 state. Since these partial waves are mainly influenced by the inner part of the potential (in contrast to D-waves) it is fairly obvious that $\Lambda_\pi \leq 1$ GeV suppresses the inner part of OPEP too strongly. Note that, according to our calculations, the situation is not essentially improved by readjusting also vector meson coupling constants.

Let us now look at the corresponding results for the deuteron observables, shown in table 2. We first note that the meson parameters of table 1 are in each case adjusted to reproduce the empirical value for the deuteron binding energy. The results show a strong sensitivity to variations of Λ_π . Concerning the quadrupole moment Q , meson-exchange-current corrections are supposed to give an additional con-

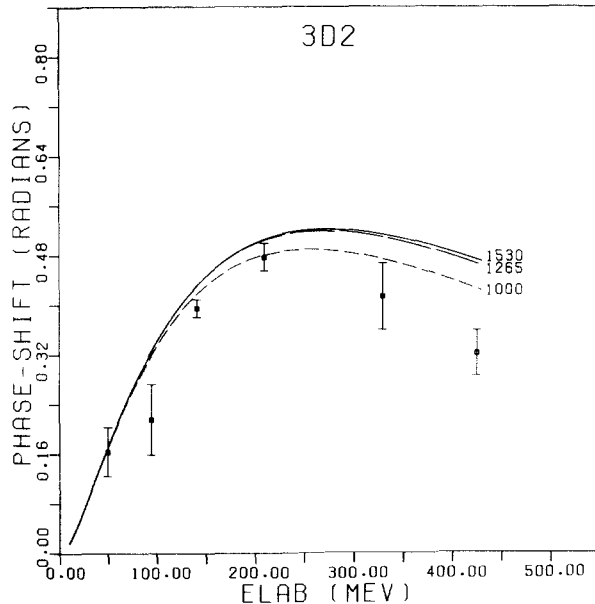


Fig. 3. 3D_2 -scattering phase shifts (in rad) predicted by an OBEP-version with $A_\alpha = 1530$ MeV for all mesons exchanged (solid line). The other lines are obtained if a fit with $A_\pi = 1265$ MeV (long-dashed) and $A_\pi = 1000$ MeV (short-dashed) is made. The error bars are taken from the energy-independent Livermore analysis [14].

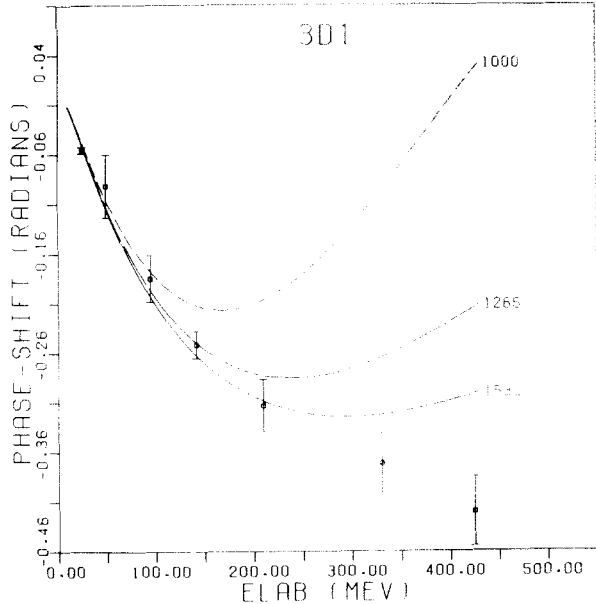


Fig. 4. As fig. 3, but for 3D_1 .

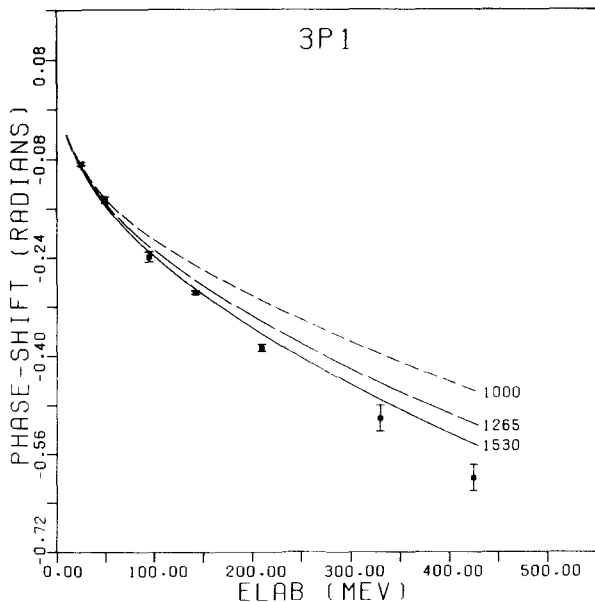


Fig. 5. As fig. 3, but for 3P_1 .

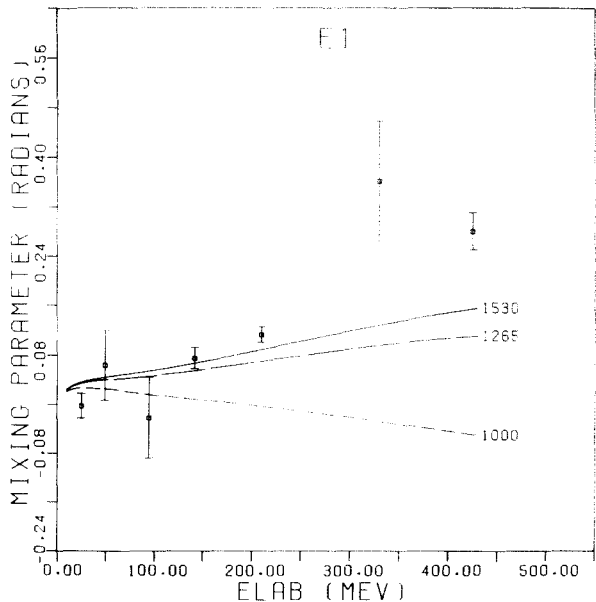


Fig. 6. As fig. 3, but for ϵ_1 .

Table 2
Deuteron data predicted by several OBEP-versions ($\Lambda_\pi = 1530, 1265$ and 1000 MeV) are compared with experiment

	exp	Λ_π		
		1530	1265	1000
E_b (MeV)	2.22462 ± 0.00006	2.225	2.223	2.223
Q (fm 2)	0.2860 ± 0.0015	0.281	0.277	0.263
P_D (%)	5 ± 2	5.18	4.70	3.63

tribution of ~ 0.01 fm 2 [24]. (According to ref. [25], the published values in ref. [24] are by a factor of 2 too large.) Thus the value for Q using $\Lambda_\pi = 1$ GeV seems to be ruled out, whereas $\Lambda_\pi \geq 1.2$ GeV is still acceptable. Since Q is mainly determined by the outer-range part of the deuteron D-wave (because of a factor r^2 in the integrand), this implies that the outer-range part of the tensor force can only be mildly suppressed if agreement with the empirical value for Q is to be maintained. Consequently, low partial waves in NN scattering together with the quadrupole moment of the deuteron seem to exclude a strong π NN form factor and to require $\Lambda_\pi \geq 1.2$ GeV throughout the whole range, at least in the OBE-framework.

Since the deuteron observables play an outstanding role in fixing properties of nuclei and nuclear matter, it is clear from the above that it is absolutely essential to know the π NN form factor as accurately as possible. In any case, it is highly unlikely that the deuteron D-state probability is larger than 6%. Even with a relatively short-ranged cutoff ($\Lambda_\pi = 1530$ MeV), p_D is only 5.2%. This is due to the relatively strong p-contribution favoured by the analyses of refs. [18, 20].

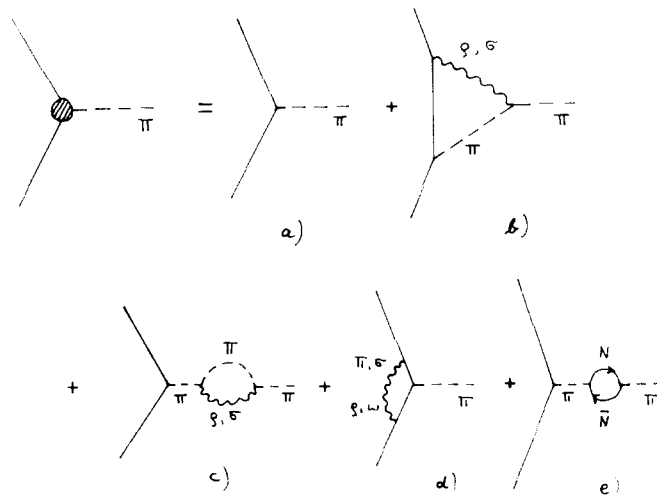
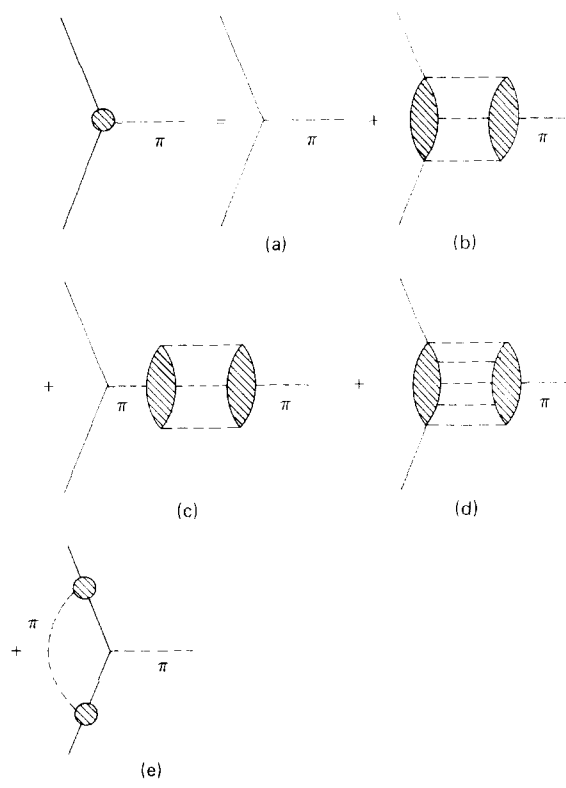
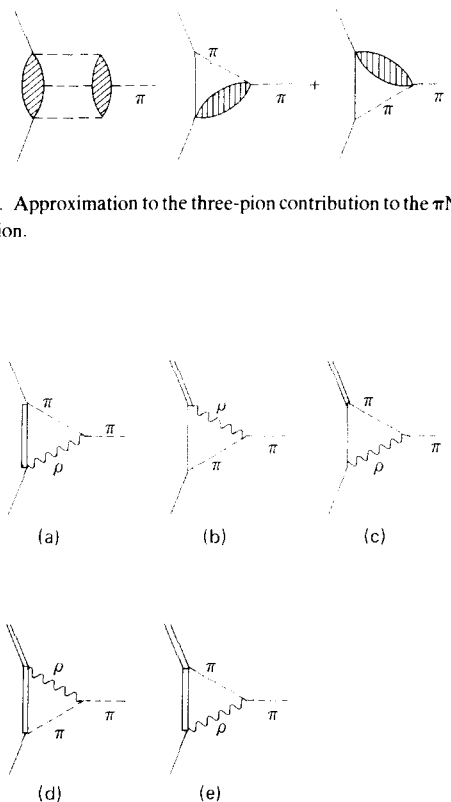
Recently, Brack, Riska and Weise [26] studied the process $\pi^+d \rightarrow pp$. Taking π - and p-meson rescattering into account they obtained cross sections in agreement with experiment provided they used a π NN form factor with $\Lambda_\pi > 1.2$ GeV. This is obviously consistent with the situation in NN scattering described before.

On the other hand, from an analysis of NN charge-exchange scattering data, Bongardt, Pilkuhn and Schlaile [27] deduced a rather low value, namely $\Lambda_\pi \approx 700$ MeV. Note however that their result was criticized recently by Dominguez and Verwest [28], who, with the same type of analysis, found $\Lambda_\pi = 900$ –1000 MeV.

The observed 6% discrepancy [29] in the Goldberger-Treiman relation [30] would lead to a value for Λ_π being as low as $4m_\pi$, if chiral symmetry were exact. Since it is not (the pion has a mass), the discrepancy can only be partly attributable to the π NN form factor, leading to a higher cutoff-mass.

A different approach pursued e.g. recently by Nutt and Loiseau [22] and Durso, Jackson and Verwest [31], is to construct a model for the π NN vertex function; either in field-theoretical language, where the π NN vertex is built up by the type of diagrams shown in fig. 7, or in a dispersion-theoretic approach, see fig. 8. In both figures, diagram (a) describes the bare vertex, whereas the other diagrams build up the π NN form factor. Processes (b) and (c) have low-mass cuts and should give the most significant contribution. A detailed analysis of these diagrams yields $\Lambda_\pi = 1$ –1.2 GeV, the result depending somewhat on off-shell ambiguities and the use of either ps- or pv-coupling. For details we refer to ref. [31].

Note that in the dispersion-theoretical calculation it is assumed that the 3π -intermediate state is dominated by two strongly interacting pions plus one free pion, see fig. 9. Furthermore, only the nearest s-channel singularity (the nucleon) is taken into account. Dillig and Brack [32] considered in addition

Fig. 7. Feynman diagrams contributing to the π NN-vertex function.Fig. 8. Dispersion-theoretic classification of the contributions to the π NN-vertex function.Fig. 9. Approximation to the three-pion contribution to the π NN-vertex function.Fig. 10. Diagrams contributing to the π NN-vertex function (a) and to the π N Δ -vertex function (b-e).

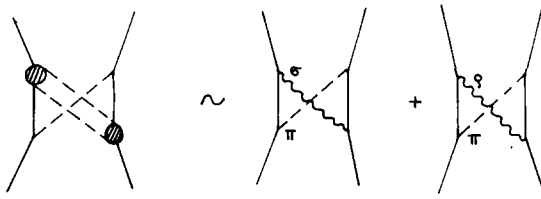


Fig. 11. Further contribution to the three-pion exchange.

the diagrams of fig. 10, which partly contribute also to the $\pi N\Delta$ vertex function. For the πNN vertex, they find a result comparable to that of ref. [31]. Moreover, the $\pi N\Delta$ vertex function should be similar to the πNN vertex function.

In summary, model calculations as well as direct empirical analyses seem to favour a value of $\Lambda_\pi \sim 1$ GeV, whereas more indirect studies, e.g. of low partial waves in NN scattering, seem to require $\Lambda_\pi > 1.2$ GeV, i.e. a softer form factor, especially for the inner-range part. Several reasons might be responsible for this discrepancy. First, low partial waves in NN scattering probe F_π at relatively large $|k^2|$, where diagrams like 7(d, e) should come into play, which, up to now, have been neglected. Second, additional contributions from 3π -exchange like those shown in fig. 11 might well reduce the strong damping effect of the πNN vertex function. (The need for such contributions was recently demonstrated [34].) In fact, in the framework of the Paris-potential, it is found [35] that the sum of πNN vertex corrections (fig. 8) and 3π -exchange contributions (fig. 11) is rather small and is significant only for internucleon distances $r \lesssim 0.8$ fm (whereas the vertex corrections alone influence the potential even at $r = 1.5$ fm). It thus appears that the value $\Lambda_\pi \sim 1.5$ GeV favoured in OBE-models is an effective quantity, which somehow takes into account the combined (small) effect of figs. 8 and 11.

Let us note finally that Bryan, Dominguez and Verwest [33] recently proposed a model for completely off-shell hadronic form factors $F(q^2, q'^2, k^2)$ based on the Veneziano formula.

3. Transition from the two-body to the many-body problem

We have seen in the last section that the inclusion of strong ρ -exchange (which is now to be preferred according to refs. [18, 20]) together with some structure at the πNN -vertex (whose precise shape is not known at present) cuts down the OPE-tensor force appreciably. This leads to a rather small value of the deuteron D-state probability, which seems to be required by a bulk of few-body reactions involving the deuteron [21]. This fact, together with new developments in the calculational procedure of the nuclear matter problem, implies that present realistic models of the NN-interaction overbind nuclear matter by several MeV, at a much too high density.

In this connection we would like to stress the following points:

(i) A search for potentials with still lower χ^2 for the fit to empirical two-body data will not help since, in the region of the χ^2 -values of present realistic potentials ($\chi^2/\text{datum} \lesssim 3$), the nuclear matter binding is rather insensitive to a variation of χ^2 (if the tensor force is kept unchanged). Conversely, potentials with the lowest χ^2 do not necessarily give the best results in nuclear structure. The decisive quantity is the amount of tensor force, which can be varied in a wide range without any appreciable change in the χ^2 -value.

(ii) Nuclear matter binding is rather insensitive to specific features of the NN-potential like e.g. non-localities or treatment of the intermediate-range attraction (dispersion-theoretic frame or narrow-

width σ), unless the amount of tensor force is affected. The reason is that such ingredients have roughly the same effect in two-body scattering and in nuclear matter and are thus ‘absorbed’ by fitting the empirical two-body data. In other words, apart from effects which modify the tensor force, nuclear matter binding does not probe specific details of the NN-interaction, provided a reasonable fit to the NN-scattering data is obtained.

3.1. Usual procedure

At first glance, a way out of this dilemma would be to construct potentials with an even larger amount of tensor force ($p_D \sim 8\%$ or more) compared to the Reid potential [2]. But this is in contradiction to all what we know at present about the tensor force (see section 2). Moreover, the Reid potential seems to underbind light nuclei, e.g. the triton and ^{16}O [36]. Thus, there appears to be an inconsistency, which obviously cannot be removed by modifying the tensor force; namely, the usual treatment of the many-body problem predicts relatively less binding for light nuclei than for dense systems like infinitely extended nuclear matter.

In our opinion, this problem has a rather deep origin: one does not take the fact rigorously into account that the NN-interaction is mediated by meson exchange. Let us describe in more detail what we mean by this statement, because it is an essential point.

In the two-body problem formulated in the framework of meson field theory, one usually starts from the relativistic, covariant Bethe–Salpeter equation [37]

$$M = K + KGM, \quad (3.1)$$

where M is the relativistic two-nucleon scattering amplitude, G is the relativistic free two-nucleon propagator and K is the (infinite) sum of all irreducible diagrams. Since this equation involves a four-dimensional integration over the intermediate nucleon four-momenta, it is difficult to solve, see ref. [38]. (In any case, the kernel K is usually truncated by considering one-particle-exchange mechanisms only.) Thus, one reformulates the problem by introducing a ‘simpler’ propagator g :

$$M = W + WgM \quad (3.2a)$$

$$W = K + K(G - g)W. \quad (3.2b)$$

Note that eqs. (3.2) are completely equivalent to eq. (3.1). g is chosen such that the scattering equation (3.2a) involves only a 3-dimensional integration; i.e. g contains a δ -function in the fourth component of the intermediate 4-momentum. This condition does not fix g uniquely; g has to be chosen in such a way that the ‘quasipotential’-equation (3.2b) can be replaced to a good approximation by

$$W = K + K(G - g)K \quad (3.3)$$

i.e. $(G - g)$ must be ‘small’. In spite of the fact that eq. (3.3) still involves a 4-dimensional integration due to the presence of G , it is much simpler to solve since it is not an integral equation (for given K) anymore.

It can be shown that, for reasonable choices of g , the approximation (3.3) is justified. However, one usually simplifies matters even more, taking $W = K$. In general, this is not such a good approximation

anymore, in the sense that now the final result for M depends on the specific choice of g . Using this prescription, eq. (3.2a) becomes

$$M = K + KgM. \quad (3.4)$$

Such an equation can easily be solved in momentum space. However, in order to obtain a potential which can be used in nuclear structure, one brings this equation into the form of the (non-relativistic) Lippmann–Schwinger equation:

$$T(z) = V + V \frac{1}{z - h_0} T(z) \quad (3.5)$$

where z is the starting energy for free two-body scattering and h_0 is the free Hamiltonian. The relations between M , K and T , V depend on the specific choice of g . For example, for the Blanckenbecler–Sugar choice of g [39], the corresponding relations are:

$$\begin{aligned} T(\mathbf{q}', \mathbf{q}) &= \sqrt{\frac{m}{E_{\mathbf{q}'}}} M(\mathbf{q}', \mathbf{q}) \sqrt{\frac{m}{E_{\mathbf{q}}}} \\ V(\mathbf{q}', \mathbf{q}) &= \sqrt{\frac{m}{E_{\mathbf{q}'}}} K(\mathbf{q}', \mathbf{q}) \sqrt{\frac{m}{E_{\mathbf{q}}}}. \end{aligned} \quad (3.6)$$

V is now regarded as a suitable potential to be used in the many-body problem. Thus V is used as input for the Bethe–Goldstone equation, which is the many-body analogue to the two-body Lippmann–Schwinger equation, and which determines the nuclear matter G -matrix $G(\tilde{z})$; (we refer to ref. [7] for more details):

$$G(\tilde{z}) = V + V \frac{Q}{\tilde{z} - h_0} G(\tilde{z}) \quad (3.7)$$

(setting the single-particle potential equal to zero above the Fermi sea). The Pauli-projector Q takes into account the presence of other nucleons in the medium. \tilde{z} is the starting energy for the scattering of two bound nucleons, which differs from the free starting energy z . In lowest order (two-hole-line approximation) the binding energy E of nuclear matter is obtained by

$$E = \sum_m \langle m | h_0 | m \rangle + \frac{1}{2} \sum_{m,n} \langle mn | G(\tilde{z}) | mn - nm \rangle. \quad (3.8)$$

Obviously, this is only an ad hoc procedure. After the definition of V by means of (3.5), one completely forgets about the origin and nature of V . Relativistic effects are in some way incorporated into the potential by the definition of V ; they are, however, to a large extent ‘absorbed’ by fitting the empirical NN-data.

Thus, even if one starts with a full-fledged meson theory in the two-body problem (either by using Lagrangian field theory or relying on dispersion-theoretical techniques), the fact that the NN-interaction is mediated by meson-exchange is suppressed (or forgotten) almost completely in the many-body

problem. In other words, meson theory is only used to define a convenient parametrization of the NN-interaction, the parameters being essentially the coupling constants and masses of the exchanged mesons. (There are strong constraints on these parameters by information from other sources, like e.g. πN - and $\pi\pi$ -interaction.)

However, if one goes to many-body systems, the usual treatment completely neglects from now on the dynamical presence of mesons in V . This implies that a purely phenomenological potential and a potential derived from meson theory give more or less identical results for the nuclear matter binding, provided the amount of tensor force is the same in both models and both describe the two-body data with the same quality. This is the reason why the phenomenological Reid potential [2] ($p_D = 6.47\%$) and the ‘dispersion-theoretic’ Paris-potential [5] ($p_D = 6.75\%$) give roughly the same result for the binding energy in nuclear matter. Thus nuclear matter seems not to care so much whether the potential is purely phenomenological or derived from a meson theory, at least in the frame described above. (Of course, meson theory is needed to fix the right amount of tensor force. We should note in this context that the currently favoured strong ρ -contribution (see refs. [18, 20]) has been included recently in the Paris potential [40].)

3.2. Brueckner theory including mesonic degrees of freedom

Obviously, the procedure described in the last subsection is unpleasant, at least from an aesthetic point of view. What one should do in principle is to start from a relativistic, covariant many-body equation, analogous to the Bethe-Salpeter equation (3.1) for the two-body case, and then do the corresponding reductions leading to (3.4). However, we prefer to follow an idea of Schütte [41]. He starts from a field-theoretic Hamiltonian H , leaving out antinucleons from the beginning, and treats H in three-dimensional perturbation theory [42]. The reason is the following: First, three-dimensional perturbation theory corresponds to standard non-relativistic many-body theory and will therefore allow a direct comparison with the usual procedure. Second, chiral invariance dictates that the nucleon–antinucleon (NN)-vertex is considerably suppressed compared to the NN-vertex.

For convenience, we give here the basic principles of this procedure, since it is the starting point for all calculations described in the next sections. For details of the formalism, we refer to ref. [41].

The starting point is the field-theoretic Hamiltonian

$$H = h_0 + t + W \quad (3.9)$$

with

$$h_0 = \sum_{\alpha} E_{\alpha} a_{\alpha}^+ a_{\alpha}, \quad t = \sum_k \omega_k b_k^+ b_k,$$

$$W = \sum_{\alpha\alpha'k} W_{\alpha'\alpha k} a_{\alpha'}^+ a_{\alpha} b_k + \text{h.c.}$$

Here, a_{α}^+ and b_k^+ are the creation operators for nucleons and bosons, respectively. α, k denote all quantum numbers which specify the state completely. E_{α} and ω_k are the relativistic kinetic energies of the nucleons and mesons, respectively. Thus, h_0 describes the kinetic energy operator of the nucleons and t the corresponding operator for the mesons. W represents the interaction term; $W_{\alpha'\alpha k}$ describes the structure of the NN-meson vertices.

3.2.1. The two-nucleon problem

We first define a transition matrix T (restricted to the two-nucleon space) by relating it to the standard S -matrix:

$$\langle \alpha' \beta' | S | \alpha \beta \rangle = \langle \alpha' \beta' | \alpha \beta \rangle - 2\pi i \delta(E_{\alpha'} + E_{\beta'} - E_\alpha - E_\beta) \langle \alpha' \beta' | T | \alpha \beta \rangle. \quad (3.10)$$

Here, $|\alpha \beta\rangle = a_\alpha^+ a_\beta^+ |0\rangle$, where $|0\rangle$ is the vacuum state. Treating H in three-dimensional perturbation theory, $\langle \alpha' \beta' | T | \alpha \beta \rangle$ can be represented by a series expansion defined by all diagrams containing two ingoing (α, β) and two outgoing (α', β') nucleon lines. This series can be partially summed by solving an integral equation of the Lippmann–Schwinger-type

$$T(z) = V(z) + V(z) \frac{1}{z - h_0} T(z). \quad (3.11)$$

Analogously to the Bethe–Salpeter kernel K in eq. (3.1), the energy-dependent ‘quasipotential’ $V(z)$ contains the (infinite) sum of all non-iterative diagrams, i.e. those with at least one meson present in each intermediate state.

3.2.2. Nuclear matter

Here, we first introduce a model Hamiltonian

$$h = \sum_\alpha \epsilon_\alpha a_\alpha^+ a_\alpha \quad (3.12)$$

with unperturbed ground state ϕ ; $h\phi = E_0\phi$. With respect to ϕ we define occupied single-particle states (denoted by a, b, \dots) and unoccupied single-particle states (denoted by A, B, \dots). The symbols α, β are used for either kind of single-particle state. Thus $E_0 = \sum_a \epsilon_a$ and $\phi = \pi a^+ |0\rangle$. We now define H' by

$$H = h_0 + t + W = h + t + H' \quad (3.13)$$

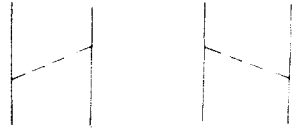
and treat H' within three-dimensional perturbation theory. The total energy E of the ground state of H can then be obtained from a series expansion quite analogous to standard many-body theory. In lowest order, E is again given by eq. (3.8); however, the Bethe–Goldstone equation (3.7) now becomes

$$G(\tilde{z}) = \tilde{V}(\tilde{z}) + \tilde{V}(\tilde{z}) \frac{Q}{\tilde{z} - h} G(\tilde{z}) \quad (3.14)$$

i.e. the ‘potential’ $\tilde{V}(\tilde{z})$ used in the Bethe–Goldstone equation now differs from the potential $V(z)$ used in the two-body scattering equation (3.11) in two respects: First, the starting energy \tilde{z} is different from the free starting energy z ; second, the propagator in \tilde{V} involves the model Hamiltonian h instead of h_0 . We will demonstrate this explicitly in the next section using an OBE-model as an example.

3.3. Results for a one-boson-exchange model

In this section we want to apply the principles outlined in the last section using a one-boson-exchange

Fig. 12. Diagrams contributing to $V(z)$ in the OBE-approximation.

model for the two-nucleon interaction. More details can be found in the papers of Kotthoff et al. [43, 44].

In the OBE-model, the quasipotential $V(z)$ is represented by the set of time-ordered diagrams given in fig. 12. The solid lines denote the nucleons, the dashed lines describe the mesons exchanged ($\pi, \eta, \sigma, \delta, \rho, \omega, \phi$). Algebraically, the matrix elements of $V(z)$ are represented as

$$\langle \alpha' \beta' | V(z) | \alpha \beta \rangle = \sum_{i=ps,s,v} \langle \alpha' \beta' | W^{(i)} \frac{1}{z - h_0 - t} W^{(i)} | \alpha \beta \rangle_{\text{linked}}. \quad (3.15)$$

where

$$W^{(i)} = \sum_{\alpha \alpha' k} W_{\alpha' \alpha k}^{(i)} a_{\alpha'}^+ a_{\alpha} b_k + \text{h.c.} \quad (3.16)$$

and

$$W_{\alpha' \alpha k}^{(ps)} = - \frac{\sqrt{4\pi} g_{ps}}{[2\omega_k^{(ps)}(2\pi)^3]^{1/2}} \delta(\mathbf{q}_{\alpha'} - \mathbf{q}_{\alpha} - \mathbf{k}) \bar{u}^{(r_{\alpha'})}(\mathbf{q}_{\alpha'}) i \gamma^5 u^{(r_{\alpha})}(\mathbf{q}_{\alpha}) \quad (3.17a)$$

$$W_{\alpha' \alpha k}^{(s)} = - \frac{\sqrt{4\pi} g_s}{[2\omega_k^{(s)}(2\pi)^3]^{1/2}} \delta(\mathbf{q}_{\alpha'} - \mathbf{q}_{\alpha} - \mathbf{k}) \bar{u}^{(r_{\alpha})}(\mathbf{q}_{\alpha'}) u^{(r_{\alpha})}(\mathbf{q}_{\alpha}) \quad (3.17b)$$

$$W_{\alpha' \alpha k}^{(v)} = - \frac{\sqrt{4\pi} \epsilon^{\mu}(\mathbf{k}, s)}{[2\omega_k^{(v)}(2\pi)^3]^{1/2}} \delta(\mathbf{q}_{\alpha'} - \mathbf{q}_{\alpha} - \mathbf{k}) \times \left[(g_v + f_v) \bar{u}^{(r_{\alpha'})}(\mathbf{q}_{\alpha'}) \gamma_{\mu} u^{(r_{\alpha})}(\mathbf{q}_{\alpha}) - \frac{f_v}{2m} \bar{u}^{(r_{\alpha'})}(\mathbf{q}_{\alpha'}) (q_{\alpha'} + q_{\alpha})_{\mu} u^{(r_{\alpha})}(\mathbf{q}_{\alpha}) \right] \quad (3.17c)$$

for pseudoscalar (π, η), scalar (σ, δ) and vector mesons (ρ, ω, ϕ), respectively. Contributions to $V(z)$ from the exchange of isospin 1 mesons have an additional factor $\tau_1 \cdot \tau_2$. The Dirac spinors $u^{(r)}(\mathbf{q})$ are normalized to $u^{(r)*} u^{(r)} = 1$. ϵ^{μ} is the polarization vector describing the vector mesons; $\omega_k^{(0)} = \sqrt{\mathbf{k}^2 + m^{(0)^2}}$.

For the π -exchange potential we obtain, omitting the δ -function which ensures 3-momentum conservation at the vertices,

$$\langle \mathbf{q}' s'_1 s'_2 | V_{\pi}(z) | \mathbf{q} s_1 s_2 \rangle = 2 \frac{4\pi}{(2\pi)^3} g_{NN\pi}^2 \tau_1 \cdot \tau_2 \frac{1}{2\omega_k^{\pi}} \frac{\bar{u}(\mathbf{q}'_2, s'_2) i \gamma^5 u(\mathbf{q}_2, s_2) \bar{u}(\mathbf{q}'_1, s'_1) i \gamma^5 u(\mathbf{q}_1, s_1)}{z - E_{q'} - E_q - \omega_k^{\pi}}. \quad (3.18)$$

Here $z = 2E_{q_0}$ is the starting energy. The factor $(2\pi)^{-3}$ is due to the specific ‘normalization’ used in the

scattering equation (3.11), the factor 2 arises because there are two diagrams (see fig. 12), which both give the same contribution. Note that the vertex structure (the numerator of eq. (3.18)) is the same as before (eq. (2.6)), whereas the denominator has changed. Neglecting however the recoil effects (i.e. putting $z = E_{q'} + E_q$), we obtain the usual OPE-propagator $k^2 + m_\pi^2$. If we iterate $V_\pi(z)$ by inserting it into eq. (3.11), the recoil effects tend to suppress the iterations of $V_\pi(z)$ since large intermediate momenta are involved. Consequently, these recoil effects reduce the OPE-tensor force (in addition to ρ -exchange and πNN -form factor). This has interesting consequences, see below.

Again, the meson parameters (coupling constants and masses) are determined by adjusting the resulting NN-partial wave phase shifts to the empirical phase shift analysis of ref. [14]. The resulting parameter values lie in the usual range, and the description of the NN-data is of the same quality as in other OBE-versions. One interesting point should be mentioned, however: In spite of the fact that this OBE-version has a relatively weak suppression of OPEP in the inner region ($\Lambda_\pi = 2.5$ GeV), the resulting deuteron D-state probability is only 4.4%, i.e. this potential has a rather weak tensor force. As described before, this feature can be traced back to the recoil effects in the potential propagator.

If we now do the analogous perturbation theory for the many-body system of nuclear matter, the resulting quasipotential, to be iterated in the Bethe–Goldstone equation, is not $V(z)$, but the propagator has to be modified in a well defined way; namely (for the example of π -exchange)

$$\langle q's'_1s'_2 | \tilde{V}_\pi(\tilde{z}) | qs_1s_2 \rangle \sim \frac{1}{\tilde{z} - \epsilon_{q'} - \epsilon_q - \omega_k^\pi} \quad (3.19)$$

i.e. the free starting energy z goes over into the starting energy \tilde{z} of two bound nucleons in the medium. Moreover, the free nucleon energies E_i go over into ϵ_i , the energies in the medium. For the ‘standard’ choice of single-particle energies above the Fermi sea ($\epsilon_i = E_i$), the iterative contributions of $\tilde{V}(\tilde{z})$ are suppressed compared to those of $V(z)$, since $\tilde{z} < z$. The change is appreciable for the π -exchange contribution, since, due to the small pion mass, the contribution is rather sensitive to changes in the recoil terms. Thus, the (attractive) contribution of the OPE-tensor force is further suppressed in the medium and gives comparatively less binding in nuclear matter. The situation is described graphically in fig. 13 showing one of the four twice-iterated π -exchange diagrams. In the usual treatment, the modifications due to the medium are taken into account only at the intermediate propagator 2 (see eq. (3.7)), whereas the propagators 1 and 3 (occurring in the potential) are taken over unmodified from free two-body scattering. In the extended treatment described above, also modifications at 1 and 3 are taken into account by changing $V(z)$ to $\tilde{V}(\tilde{z})$ in nuclear matter.

Of course, the additional modifications at 1 and 3 should be smaller than those at 2, especially for exchanges of mesons with large masses (like ω , ρ), since modifications in the recoil terms should play a minor role there. This might give some motivation for neglecting the modifications in the potential propagators, as is done in the usual treatment. It will turn out, however, that such effects cannot be neglected, at least in the case of π -exchange and with the standard choice of single-particle energies.

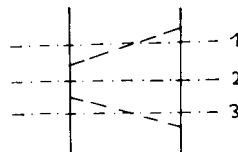


Fig. 13. Example of an iterative time-ordered diagram of fourth order in W .

Let us now come to the main results in nuclear matter (a more complete list can be found in ref. [44]). Using $\tilde{V}(\tilde{z})$ in eq. (3.14), and inserting the resulting G -matrix into eq. (3.8), we obtain (in lowest order) the binding energy per particle as function of the density, shown in fig. 14 (solid line). The influence of the modifications of V can be shown if eq. (3.14) is solved with $V(z)$, i.e. with the same quasipotential used in two-body scattering. (z is well defined in nuclear matter being just the sum of the relativistic kinetic energies of the two initial nucleons.) The result is given by the dashed line in fig. 14. Note that this saturation point corresponds well to the predictions of the usual treatment: For example, our OBE-version HM2 [4] with $p_D = 4.3\%$ (compared to 4.4% in the present case), treated in nuclear matter in the usual way, also predicts roughly 24 MeV binding at $k_F \sim 1.8 \text{ fm}^{-1}$. Fig. 14 shows that the use of $\tilde{V}(\tilde{z})$ (instead of $V(z)$) produces a sizeable discrepancy growing strongly with density, which can almost completely be traced back to the suppression of the OPE-tensor force in the ${}^3(\text{SD})_1$ -state. In view of the discussion in the introduction, this effect is welcome and goes qualitatively into the right direction: one obtains a repulsive many-body effect which reduces the overbinding produced by realistic potential models. Nevertheless, the density-dependence is not strong enough to come off the Coester line.

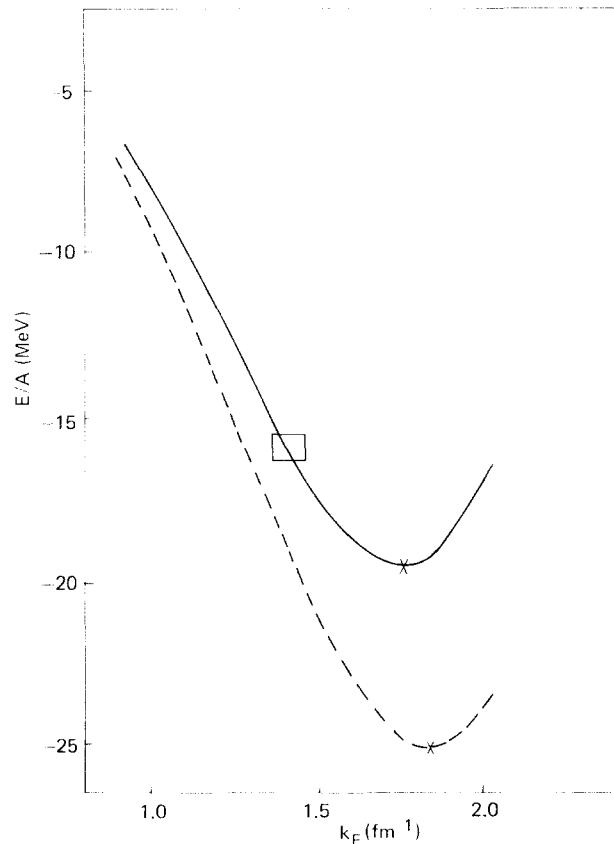


Fig. 14. Energy per particle in nuclear matter E/A (in MeV), as function of the Fermi momentum k_F (in fm^{-1}) (from ref. [44]). The solid (dashed) line is obtained using $\tilde{V}(\tilde{z})$ ($V(z)$) in eq. (3.14).

We should mention one important point concerning the wound integral κ . The value of κ belonging to $\tilde{V}(\tilde{z})$ (solid line) is in fact *lower* (by 10%) compared to the value belonging to $V(z)$ (dashed line). This is just opposite to the usual trend. The reason is quite obvious: In the usual treatment, decrease of nuclear matter binding is obtained by increasing the tensor to central force ratio, which increases the wound. Now, we obtain less binding by suppressing the (already weak) tensor force in the medium, which lowers the wound. A small wound is welcome because it should improve convergence properties of the hole-line expansion.

4. Explicit description of the intermediate-range attraction

We have seen in the last section that the consideration of mesonic degrees of freedom in the many-body problem resulted in less binding in nuclear matter compared to usual treatments, where these degrees of freedom are neglected. However, an even stronger suppression of binding is obtained by describing the intermediate-range attraction more explicitly than done in OBE- and dispersion-theoretic models.

In OBE-potentials, the intermediate-range attraction is described phenomenologically by a more or less fictitious scalar meson, the σ -meson. This particle effectively replaces the ($J^P = 0^+$, $I = 0$) part of the whole 2π -exchange contribution minus the twice iterated one-pion-exchange (which is already included in the scattering amplitude by iterating OPEP); see fig. 15.

Dispersion-theoretic methods (for an extensive description we refer to ref. [45]) obtain this contribution by using empirical πN - and $\pi\pi$ -data and performing an analytic continuation.

Explicitly, the 2π -exchange contribution can be split up into the type of diagrams shown in fig. 16. Here, N denotes an intermediate-nucleon state, whereas Δ represents an intermediate Δ -isobar ($m_\Delta = 1236$ MeV, spin 3/2, isospin 3/2). The last two terms in this figure show typical rescattering contributions.

If we want to describe only nucleon-nucleon scattering in free space, such an explicit dynamical model is a luxury since the dispersion-theoretic treatment automatically includes all such diagrams. (In this case, however, it might be worth-while to avoid the whole potential concept anyway.) However, if we wish to describe the nucleon-nucleon interaction in the presence of other nucleons, i.e. in a many-body system, an explicit dynamical model is necessary for the following reason: In an OBE- or dispersion-theoretic treatment, the 2π -exchange potential (fig. 15) is usually inserted unmodified, as part of V , into the Bethe-Goldstone equation (3.7). (The mesonic degrees of freedom discussed in the last section contribute negligibly to this part of the interaction.) However, as is seen from fig. 16, this contribution is in fact modified in the medium, since the internal nucleon and isobar interact with the other nucleons in the medium; for example, part of the intermediate-nucleon states are now forbidden

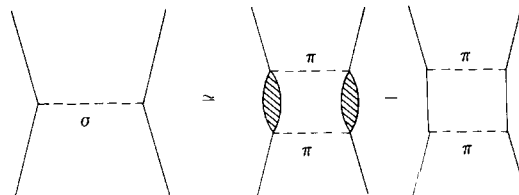
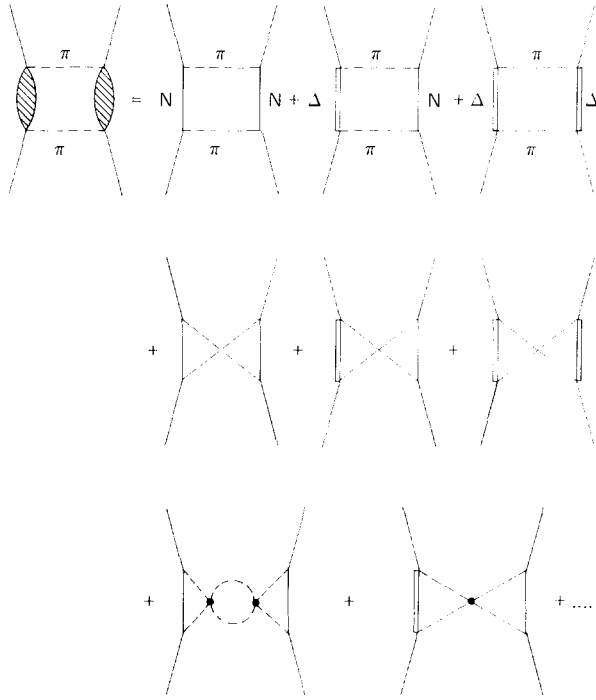
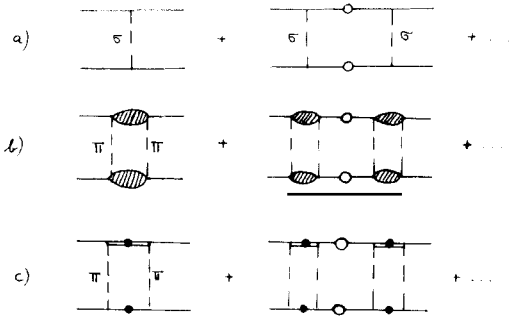


Fig. 15. Role of the σ -meson in OBEP.

Fig. 16. 2π -exchange diagrams.Fig. 17. 2π -exchange contribution: (a) OBE-model. (b) dispersion theory, (c) explicit model.

by the Pauli principle. Such effects can only be taken into account by using an explicit dynamical model for the intermediate-range attraction. In the usual dispersion-theoretic treatment (and, of course, also in an OBE-framework) such modifications cannot be handled in a well-defined way.

The essential difference is shown in fig. 17. At the open circles, many-body effects are included already in the usual treatment (e.g. due to the Pauli-projector Q in eq. (3.7)). In an explicit description, modifications of the NN-interaction can also be taken into account at the solid circles.

Thus, from a many-body view-point, a dispersion-theoretic treatment has no essential advantage compared to simple OBE-potentials. In a dispersion-theoretic potential, the blob of fig. 15 ultimately appears as if it arose from exchange of several scalar, isoscalar mesons with different masses (compared to a single resonance with definite mass in the OBE-framework). This ‘degree of freedom’, however, has negligible effects in the many-body system. Of course, dispersion theory has the essential advantage of predicting a more or less definite result for the 2π -exchange contribution in NN scattering (which is adjustable in OBE-models). Consequently, explicit field-theoretic models of the 2π -exchange can be tested by requiring them to be in an overall agreement with the dispersion-theoretic result in NN scattering, see section 4.3.

4.1. Role of the Δ -isobar

Of course, the explicit evaluation of all diagrams in fig. 16 would be an impossible task. One knows for example, that, apart from the Δ , higher resonances like $N_{11}(1470)$ give non-negligible contributions to the NN-forces [46]. Since such contributions are however shorter-ranged, many-body effects should

be relatively small there. (A short-ranged contribution is mainly built up by high-momentum components, which are less affected by Pauli blocking.) Consequently, an explicit treatment is not needed in a first step for those contributions, at least for not too high densities. We note in this context that, for the same reason, vertex functions are modified in the medium to a very small extent only, due to their relatively short range.

Thus it is reasonable to start with an explicit description of the long-ranged diagrams of fig. 16 and to describe the rest again by an effective scalar meson. How many of the diagrams have ultimately to be described explicitly depends on the density of the considered many-body system. This can be hardly decided ‘*a priori*’, but has to be settled by doing explicit calculations.

The first to study such many-body effects in nuclear matter were A. M. Green and coworkers (see e.g. ref. [25]). They used a different starting point, treating the Δ -isobar on the same footing as nucleons. Such a concept leads naturally to so-called transition potentials of the type shown in fig. 18 and to a coupled-channel problem. The authors of ref. [25] calculated the effect in the 1S_0 -partial wave, using transition potentials in the static limit together with a modified Reid potential (in order to reproduce the same empirical 1S_0 nucleon–nucleon phase shifts as before). Due to the above-mentioned many-body effects, the contribution arising from the transition potentials is quenched in nuclear matter, leading to a reduction of binding energy by about 5 MeV at nuclear matter density. Similar results were obtained by Day and Coester [47]. Such a coupled-channel treatment effectively includes some of the diagrams contributing to 2π -exchange. For example, if we iterate the first diagram of fig. 18 twice, we obtain the second diagram of fig. 16. However, the coupled-channel treatment includes many more diagrams, e.g. those involving the $\Delta\Delta$ -vertex. On the other hand, this framework is not able to handle crossed-box diagrams, which are known to be roughly as important as the uncrossed ones.

In this work, we prefer to follow the lines of fig. 16 and to avoid a complicated coupled-channel problem for the following reasons:

- (i) There are considerable uncertainties in the $\Delta\Delta$ -vertices (coupling constants etc.); they might in fact be negligible.
- (ii) A lot of contributions generated by the coupled-channel treatment are of higher order in the sense that they belong to $3, 4, \dots$ pion exchange contributing to the NN-interaction. Thus contributions of several-pion exchanges are mixed up, and it is hard to pin down model ambiguities by using dispersion-theoretic results of the 2π -exchange as a constraint.
- (iii) Crossed-box diagrams cannot be handled explicitly.

Thus, at the present stage, a fairly realistic model for the 2π -exchange is given by the contributions of fig. 19, where $\epsilon(J^P = 0^+, I = 0)$ and $\rho(J^P = 1^-, I = 1)$ now describe the part treated not explicitly, i.e. mainly the rescattering terms. A model for the total NN-interaction is then obtained by adding π -, η - and ω -exchange.

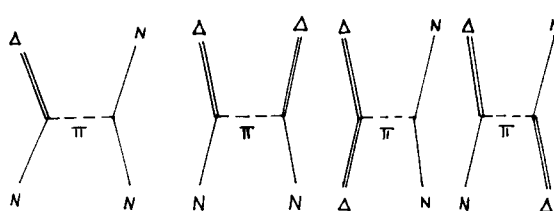
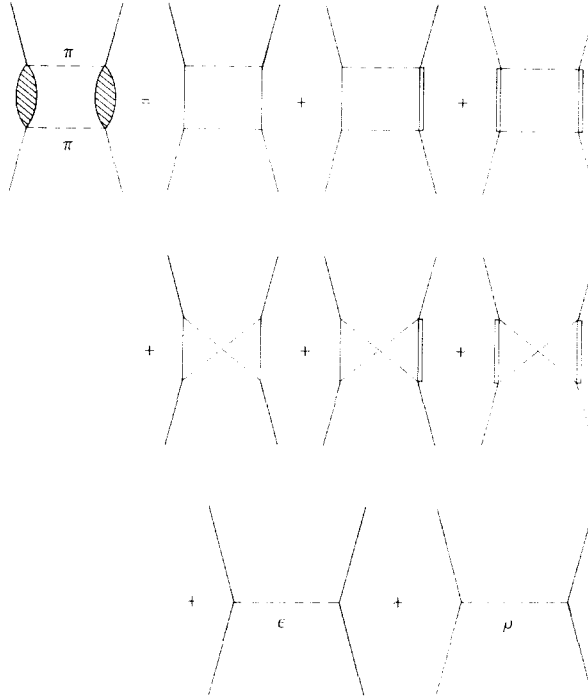


Fig. 18. Transition potentials.

Fig. 19. Model for the 2π -exchange contribution.

4.2. Transition potentials

As mentioned before, the first calculations with Δ -isobars were carried out using transition potentials in a coupled-channel framework. Such potentials were obtained by starting from a Lagrangian density coupling $N\Delta\pi$ given by

$$L_{N\Delta\pi} = \sqrt{4\pi} \frac{f_{N\Delta\pi}}{m_\pi} \bar{\psi} T \psi^\mu \partial_\mu \phi + \text{h.c.} \quad (4.1)$$

where $f_{N\Delta\pi}$ is the $N\Delta\pi$ coupling constant and T is the isospin transition operator. ψ denotes the nucleon field operator, ϕ the pion field and ψ^μ the field of the Δ -isobar. In the static limit, neglecting also the Δ -N mass difference, one then obtains for the transition potential $V_{N\Delta}^\pi$ describing the transition $NN \rightarrow N\Delta$

$$V_{N\Delta}^\pi(r) = f_{NN\pi} f_{N\Delta\pi} \frac{m_\pi}{3} \left[\boldsymbol{\sigma}_1 \cdot \boldsymbol{S}_2 + S_{12}^\Delta \left(1 + \frac{3}{m_\pi r} + \frac{3}{(m_\pi r)^2} \right) \right] \cdot \frac{\exp(-m_\pi r)}{m_\pi r} \boldsymbol{\tau}_1 \cdot \boldsymbol{T}_2 \quad (4.2)$$

where S_2 is a transition spin operator acting between a nucleon and a Δ -isobar (first introduced by Sugawara and von Hippel [48]), $f_{NN\pi} \equiv (m_\pi/2m)g_{NN\pi}$ and

$$S_{12}^\Delta = 3 \frac{\boldsymbol{\sigma}_1 \cdot \mathbf{r} \boldsymbol{S}_2 \cdot \mathbf{r}}{r^2} - \boldsymbol{\sigma}_1 \cdot \boldsymbol{S}_2. \quad (4.3)$$

Note that eq. (4.2) has the same structure as the OPEP (eq. (2.8)).

A similar expression is obtained for the transition potential $V_{\Delta\Delta}^\pi$ describing the transition $NN \rightarrow \Delta\Delta$

$$V_{\Delta\Delta}^\pi(r) = f_{N\Delta\pi}^2 \frac{m_\pi}{3} \left[\mathbf{S}_1 \cdot \mathbf{S}_2 + \mathbf{S}_{12}^{\Delta\Delta} \left(1 + \frac{3}{m_\pi r} + \frac{3}{(m_\pi r)^2} \right) \right] \frac{\exp(-m_\pi r)}{m_\pi r} \mathbf{T}_1 \cdot \mathbf{T}_2 \quad (4.4)$$

with

$$\mathbf{S}_{12}^{\Delta\Delta} = 3 \frac{\mathbf{S}_1 \cdot \mathbf{r} \mathbf{S}_2 \cdot \mathbf{r}}{r^2} - \mathbf{S}_1 \cdot \mathbf{S}_2. \quad (4.5)$$

The only new parameter is the coupling constant $f_{N\Delta\pi}$. There is some uncertainty about its value. From the width of the Δ ($\Gamma_\Delta = 120$ MeV) one obtains $f_{N\Delta\pi}^2 \approx 0.35$ (see ref. [48]). Chew-Low theory of pion-nucleon scattering predicts $f_{N\Delta\pi}^2 = 4f_{NN\pi}^2 \approx 0.32$ [49]. Höhler, Jacob and Strauss [50] point out that, instead of the rough estimate based on the width, a more elaborate treatment yields $f_{N\Delta\pi}^2 \approx 0.27$. Finally, the quark model predicts $f_{N\Delta\pi}^2 = \frac{72}{25} f_{NN\pi}^2 \approx 0.23$ (see ref. [25]).

However, it was shown recently by Durso et al. [51] that, in the derivation of suitable transition potentials, the Δ -N mass difference (≈ 300 MeV) cannot be neglected. This can be seen very simply by looking at the relativistic box diagram in fig. 19 involving a nucleon and a Δ -isobar in the intermediate state. This diagram is equivalent to a series of time-ordered diagrams shown in fig. 20, if we neglect antinucleon lines. Here only the first 4 (iterative) diagrams have a purely baryonic intermediate state and thus can be described by the iteration of a transition potential.

Treating all particles as scalars and keeping the initial nucleons at rest a suitable transition potential can be defined (neglecting recoil effects but keeping now the Δ -N mass difference),

$$V_{N\Delta}'(r) \sim \frac{1}{2} \left[\frac{\exp(-m_\pi r)}{r} + \frac{\exp(-\sqrt{(m_\Delta - m + m_\pi)m_\pi} r)}{r} \right]. \quad (4.6)$$

Compared to the former expression (4.2), half of the potential is now shorter-ranged due to the

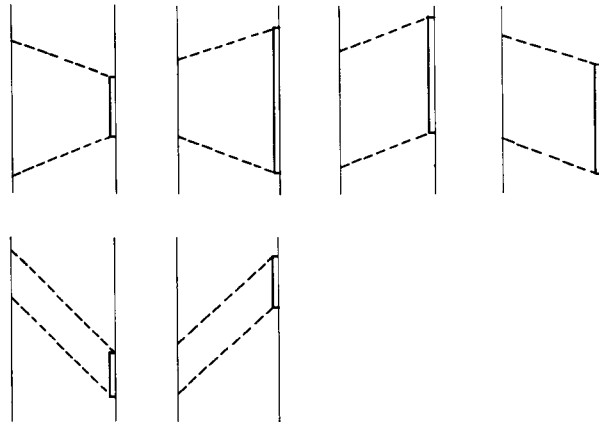


Fig. 20. Time-ordered diagrams involving the Δ -isobar.

inclusion of the Δ -N mass difference. Corresponding arguments yield for $V_{\Delta\Delta}^\pi$

$$V_{\Delta\Delta}'(r) \sim \frac{\exp(-\sqrt{(m_\Delta - m + m_\pi)m_\pi r})}{r} \quad (4.7)$$

These transition potentials are considerably smaller than the former expressions (4.2, 4.4). It will be shown later that the effect is even enhanced in a more exact treatment. Before, however, doing such extensive calculations we will sketch briefly in the next subsection how dispersion theory can be used as a guide for constructing relativistic dynamical models. We refer to ref. [51] for more details.

4.3. Dispersion theory as a guide for explicit field-theoretic models

In dispersion theory, the 2π -exchange potential can be schematically written as

$$V_{2\pi}(r) \sim \int_{4m_\pi^2}^{\infty} dt \rho(t) \frac{\exp(-\sqrt{tr})}{r} \quad (4.8)$$

This shows that $V_{2\pi}$ is built up by an ‘exchange’ of a particle with distributed mass \sqrt{t} weighted by the factor $\rho(t)$. Due to unitarity, $\rho(t)$ can be split up into possible on-shell intermediate states in terms of $f(t)$, the $N\bar{N} \rightarrow 2\pi$ amplitude, as shown in fig. 21.

The next step is the expansion of $f(t)$ into helicity amplitudes of definite angular momentum in the t ($N\bar{N} \rightarrow 2\pi$) channel. We will concentrate in the following on $f_+^{J=0}(t)$ (helicity non-flip) since, according to ref. [51], the Δ -isobar contributes mainly to this amplitude. Thus, the part of $V_{2\pi}(r)$ coming from distributed-mass scalar-isoscalar exchanges is given by

$$V_{2\pi}^{J=0}(r) \sim \int_{4m_\pi^2}^{\infty} \frac{\sqrt{\frac{1}{4}t - m_\pi^2} |f_+^{J=0}(t)|^2 \exp(-\sqrt{tr})/r}{-\sqrt{t} (m^2 - \frac{1}{4}t)^2} dt \quad (4.9)$$

(Note that the contribution from $J = 1$ -helicity amplitudes has the appearance of a potential from distributed-mass ρ -meson exchange.)

The crucial point is that $f_+^{J=0}(t)$ (also $f_-^{J=1}(t)$ etc.) can be determined from experiment. However, this cannot be done directly but requires an analytic continuation of experimental $\pi N \rightarrow \pi N$ scattering data to the pseudophysical $N\bar{N} \rightarrow 2\pi$ -amplitude needed in (4.9). If one assumes this analytic continuation to be accurate – an assumption not completely justified (as pointed out by G. E. Brown [12]) – one can view these analytically continued f 's to be empirical data and require that any dynamical model should at least roughly reproduce them.

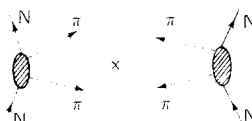


Fig. 21. Relation between $\rho(t)$ and the $N\bar{N} \rightarrow 2\pi$ amplitude $f(t)$.

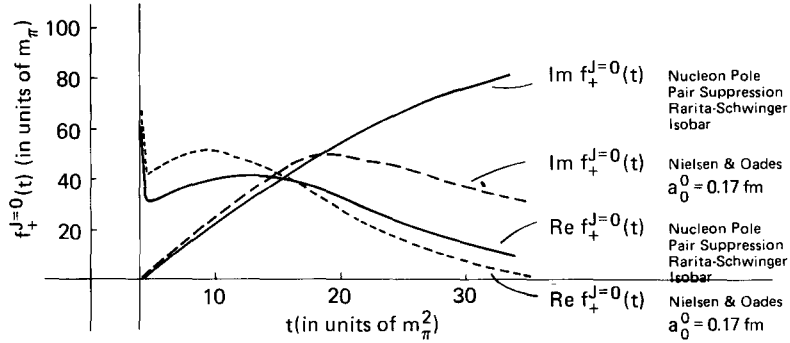


Fig. 22. Comparison of helicity amplitudes $\text{Re } f_+^{J=0}(t)$ and $\text{Im } f_+^{J=0}(t)$ calculated with the model of ref. [51], which includes the nucleon-pole term, calculated with pseudovector coupling, and the Rarita-Schwinger isobar. Real and imaginary parts are obtained by assuming the phase of the amplitude to be $\exp[i\delta_{\pi\pi}^{J=0}(t)]$, where the pion-pion phase shifts of Nielsen and Oades were used. For comparison the amplitudes of Nielsen and Oades, obtained by analytic continuations of the $\pi N \rightarrow \pi N$ amplitudes, are shown.

In ref. [51], a relativistic dynamical model for $f_+^{J=0}(t)$ was studied, including the nucleon (with pseudovector coupling) and the Δ -isobar (treated as a Rarita-Schwinger spinor). Pion rescattering effects were left out; thus the resulting $f_+^{J=0}(t)$ is completely real. Unitarity is enforced in an ad-hoc way by multiplying $f_+^{J=0}(t)$ by $\exp(i\delta_{\pi\pi}^0(t))$, where $\delta_{\pi\pi}^0(t)$ is the pion-pion S-wave phase shift. Such a phase factor does not affect $|f_+^{J=0}(t)|^2$, so the nucleon-nucleon interaction will remain unchanged. However, inclusion of this factor makes it possible to compare real and imaginary part of $f_+^{J=0}(t)$ obtained from the model directly with the empirical (analytically continued) ones.

Fig. 22 taken from ref. [51] shows the results. The solid lines represent the theoretical model calculation, the dashed lines are the empirical results of Nielsen and Oades [52]. We see that there is reasonable agreement. Furthermore, pion-rescattering effects are expected to remove the discrepancy for lower t , whereas the discrepancy at larger t is certainly suppressed by introduction of a pion form factor (which has not been included in the above model).

Thus, this relativistic dynamical model should be a reasonable starting point for an explicit description of the intermediate-range attraction. The usual non-relativistic transition potentials (4.2, 4.4) overestimate [51], however, the isobar-contribution of such a model by as much as a factor of 2 (see also the recent work of Saarela [53]). Therefore they are not able to describe the intermediate-range attraction in a realistic and adequate way. This shows that a careful, relativistic treatment of the diagrams in fig. 19 is needed. Especially nucleon- and isobar-recoil effects, which are also essential for a well-defined description of the many-body system (see section 3), should not be neglected.

4.4. Role of ρ -exchange in the transition potentials

Pion-exchange (see section 4.2) builds up only the long-range part of the transition potentials. It has been shown [54] that the inclusion of ρ -meson exchange drastically cuts down the inner part of eqs. (4.2, 4.4). (The exchange of isospin-zero mesons is forbidden because of isospin conservation since the Δ -isobar has isospin 3/2.)

Starting from the coupling

$$L_{N\Delta\rho} = \sqrt{4\pi} \frac{f_{N\Delta\rho}}{m_\rho} i\bar{\psi}\gamma^5\gamma^\mu T\psi (\partial_\mu\phi_\nu - \partial_\nu\phi_\mu), \quad (4.10)$$

where $f_{N\Delta\rho}$ is the $N\Delta\rho$ coupling constant, one obtains in the static limit (neglecting again the Δ -N mass difference) for the transition potentials involving ρ -exchange

$$V_{N\Delta}^{\rho}(r) = f'_{NN\rho} f_{N\Delta\rho} \frac{m_\rho}{3} \left[2\boldsymbol{\sigma}_1 \cdot \boldsymbol{S}_2 - \boldsymbol{S}_{12}^\Delta \left(1 + \frac{3}{m_\rho r} + \frac{3}{(m_\rho r)^2} \right) \right] \cdot \frac{\exp(-m_\rho r)}{m_\rho r} \boldsymbol{\tau}_1 \cdot \boldsymbol{T}_2 \quad (4.11)$$

with

$$f'_{NN\rho} = g_{NN\rho} \frac{m_\rho}{2m} \left(1 + \frac{f_{NN\rho}}{g_{NN\rho}} \right) \quad (4.12)$$

where $g_{NN\rho}$, $f_{NN\rho}$ are the usual vector and tensor ρ NN coupling constants defined in eq. (2.10). The analogous transition potential $V_{\Delta\Delta}^{\rho}(r)$ is found to be

$$V_{\Delta\Delta}^{\rho}(r) = f_{N\Delta\rho}^2 \frac{m_\rho}{3} \left[2\boldsymbol{S}_1 \cdot \boldsymbol{S}_2 - \boldsymbol{S}_{12}^{\Delta\Delta} \left(1 + \frac{3}{m_\rho r} + \frac{3}{(m_\rho r)^2} \right) \right] \cdot \frac{\exp(-m_\rho r)}{m_\rho r} \boldsymbol{T}_1 \cdot \boldsymbol{T}_2. \quad (4.13)$$

The value for $f_{N\Delta\rho}$ is usually obtained by using the quark model relation

$$f_{N\Delta\rho}^2 = \frac{f_{N\Delta\pi}^2}{f_{NN\pi}^2} f_{NN\rho}^{'2}. \quad (4.14)$$

A comparison with eqs. (4.2, 4.4) shows that ρ -exchange strongly suppresses the π -exchange tensor force (the spin–spin part is enhanced, however). Thus, the isobar–nucleon box diagram involving $\rho\pi$ -exchange should be repulsive since it cuts down the attractive contribution involving the exchange of 2 pions. The authors of ref. [51] claim that this $\rho\pi$ -exchange mechanism involving isobars can explain the long-standing discrepancy in $g_{NN\omega}^2(k^2=0)$ between the quark model value (~ 5) and effective values needed for description of NN-scattering (~ 10). Note however that the repulsion obtained by this $\rho\pi$ -exchange mechanism cannot be completely equivalent to pure ω -exchange. For example, the $\rho\pi$ -exchange mechanism is even attractive in the 3P_0 -channel since there the spin–spin part dominates the tensor part.

In fact, this strong state-dependence of the $\rho\pi$ -exchange mechanism helps to get a consistent description of the important 3P scattering phase shifts.

5. Basic principles for a consistent treatment of the Δ -isobar in the two- and many-body system

The discussion of the last section has shown that a careful relativistic treatment is needed in order to describe the isobar contributions in a realistic way. For example, static limits in the transition potentials (necessarily used by other groups working in r -space) cause serious errors and should be avoided. This suggests that one does the whole calculations in momentum space, which makes it possible to keep the full complexity of the $N\Delta$ -vertex. Furthermore, following the arguments of section 3, we again use a field-theoretic Hamiltonian together with three-dimensional perturbation theory in order to have a well-defined prescription for the transition from the two-body to the many-body system.

5.1. Field-theoretic Hamiltonian

In order to treat explicitly the contributions arising from the Δ -isobar, we now start from a Hamiltonian

$$H = h_0^{(N)} + h_0^{(\Delta)} + t + W^{(N)} + W^{(\Delta)} \quad (5.1)$$

where the quantities $h_0^{(N)}$, t , $W^{(N)}$ are defined in eq. (3.9) and

$$\begin{aligned} h_0^{(\Delta)} &= \sum_{\alpha} E_{\alpha}^{(\Delta)} c_{\alpha}^+ c_{\alpha} \\ W^{(\Delta)} &= \sum_{\alpha' \alpha k} W_{\alpha' \alpha k}^{(\Delta)} c_{\alpha'}^+ a_{\alpha} b_k + W_{\alpha' \alpha k}^{\prime (\Delta)} c_{\alpha'}^+ a_{\alpha} b_k^+ + \text{h.c.} \end{aligned} \quad (5.2)$$

Here, c_{α}^+ represents the creation operator for a Δ -isobar in the state α . It obeys commutation relations completely analogous to the nucleon case

$$\{c_{\alpha}, c_{\beta}^+\} = \delta_{\alpha\beta}, \quad \{c_{\alpha}, c_{\beta}\} = \{c_{\alpha}^+, c_{\beta}^+\} = 0. \quad (5.3)$$

Furthermore, the c 's commute with the a 's, i.e. the Δ -isobar is treated as a new particle, distinct from the nucleon. $E_{\alpha}^{(\Delta)}$ is the relativistic kinetic energy of the Δ ; thus, $h_0^{(\Delta)}$ is the corresponding kinetic energy operator. $W^{(\Delta)}$ describes the transition of a nucleon into a Δ (and vice versa). The Lagrangians (4.1, resp. 4.10) suggest the following form for the matrix elements $W_{\alpha' \alpha k}^{(\Delta)}$ (neglecting isospin)

$$W_{\alpha' \alpha k}^{(\Delta, \pi)} = -\sqrt{4\pi} \frac{f_{N\Delta\pi}}{m_{\pi}} \frac{1}{[2\omega_k^{(\pi)}(2\pi)^3]^{1/2}} \delta(\mathbf{q}_{\alpha'} - \mathbf{q}_{\alpha} - \mathbf{k}) i\Delta^{\mu} \bar{u}_{\mu}^{(r_{\pi})}(\mathbf{q}_{\alpha'}) u^{(r_{\pi})}(\mathbf{q}_{\alpha}) \quad (5.4)$$

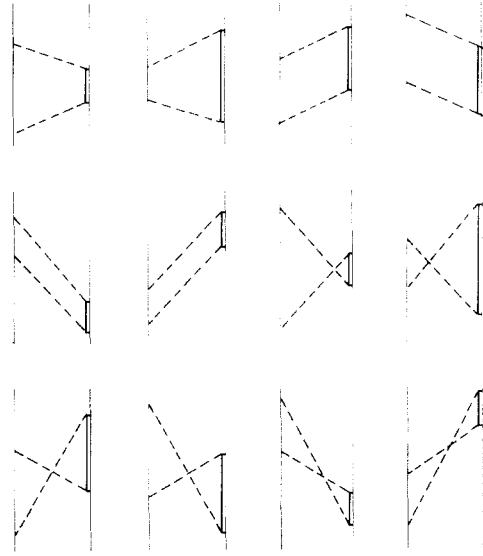
and

$$W_{\alpha' \alpha k}^{(\Delta, p)} = -\sqrt{4\pi} \frac{f_{N\Delta p}}{m_p} \frac{1}{[2\omega_k^{(p)}(2\pi)^3]^{1/2}} \delta(\mathbf{q}_{\alpha'} - \mathbf{q}_{\alpha} - \mathbf{k}) [\Delta_{\mu} \epsilon^{\nu}(\mathbf{k}, s) - \Delta^{\nu} \epsilon_{\mu}(\mathbf{k}, s)] \bar{u}_{\nu}^{(r_{\alpha})}(\mathbf{q}_{\alpha'}) \gamma^5 \gamma^{\mu} u^{(r_{\alpha})}(\mathbf{q}_{\alpha}) \quad (5.5)$$

where u^{μ} is the Rarita-Schwinger spinor describing the isobar. $W_{\alpha' \alpha k}^{\prime (\Delta)}$ is obtained from $W_{\alpha' \alpha k}^{(\Delta)}$ by taking the complex conjugate and changing \mathbf{k} to $-\mathbf{k}$ in the δ -function.

5.2. The two-nucleon problem

Treating $W = W^{(N)} + W^{(\Delta)}$ of H (eq. (5.1)) in three-dimensional perturbation theory, the transition matrix T defined in eq. (3.10) is again represented by a series expansion. However, in addition to the diagrams of section 3, the new series now contains diagrams involving intermediate Δ -isobars. For example, in lowest-possible order, the diagrams involving one Δ are those shown in fig. 23, i.e. those of fig. 20 plus the corresponding crossed-box diagrams. We call this sum $\bar{M}_{N\Delta}(z)$ (including those diagrams in which the Δ appears on the left hand side). A corresponding group of diagrams, $\bar{M}_{\Delta\Delta}(z)$, is obtained

Fig. 23. Time-ordered diagrams with positive-energy $N\Delta$ -intermediate states.

by replacing the intermediate nucleon in fig. 23 by a Δ -isobar, too. For completeness, we should then also consider the corresponding diagrams involving two intermediate nucleons, $\bar{M}_{NN}(z)$. (In section 3, only the first 4 were taken into account by iterating V_{OBE} .)

This suggests that we define an effective quasipotential (acting between two-nucleon states only)

$$V_{\text{eff}}(z) = V_{OBE}(z) + M'_{NN}(z) + \bar{M}_{N\Delta}(z) + \bar{M}_{\Delta\Delta}(z) \quad (5.6)$$

which generates the corresponding transition matrix $T(z)$ with the help of

$$T(z) = V_{\text{eff}}(z) + V_{\text{eff}}(z) \frac{1}{z - h_0^{(N)}} T(z). \quad (5.7)$$

Here, $V_{OBE}(z)$ is the quasipotential of OBE-type defined in section 3.3 (with modified parameters, of course, to be determined later by a fit to empirical NN-phase shifts). $M'_{NN}(z)$ is obtained from $\bar{M}_{NN}(z)$ by removing the iterative diagrams, since these are already included by iterating V_{OBE} in eq. (5.7).

More explicitly, the effective operator can be written as ($h_0 = h_0^{(N)} + h_0^{(\Delta)}$)

$$\begin{aligned} V_{\text{eff}}(z) = & W^{(N)} \frac{1}{z - h_0^{(N)} - t} W^{(N)} + W \frac{1}{z - h_0 - t} W \frac{1}{z - h_0 - t} W \frac{1}{z - h_0 - t} W \\ & - W^{(N)} \frac{1}{z - h_0^{(N)} - t} W^{(N)} \frac{1}{z - h_0^{(N)}} W^{(N)} \frac{1}{z - h_0^{(N)} - t} W^{(N)} \end{aligned} \quad (5.8)$$

where the first term is the OBE-part, the second term yields the sum of \bar{M}_{NN} , $\bar{M}_{N\Delta}$, $\bar{M}_{\Delta\Delta}$, and the third term is the iterative part of \bar{M}_{NN} to be subtracted.

5.3. Nuclear matter problem

We choose the same model Hamiltonian $h^{(N)}$ as in section 3 (eq. (3.12)) and the same unperturbed, pure nucleonic ground state ϕ . We now write H (eq. (5.1)) as

$$H = h^{(N)} + h_0^{(\Delta)} + t + H' \quad (5.9)$$

with

$$H' = W - (h^{(N)} - h_0^{(N)}) \quad (5.10)$$

and treat H' again in three-dimensional perturbation theory. The resulting diagrams can be partially summed by a Bethe–Goldstone-type equation

$$G(\tilde{z}) = \tilde{V}_{\text{eff}}(\tilde{z}) + \tilde{V}_{\text{eff}}(\tilde{z}) \frac{Q}{\tilde{z} - h^{(N)}} G(\tilde{z}) \quad (5.11)$$

with ($h = h^{(N)} + h_0^{(\Delta)}$)

$$\begin{aligned} \tilde{V}_{\text{eff}}(\tilde{z}) = & W^{(N)} \frac{Q}{\tilde{z} - h^{(N)} - t} W^{(N)} + W \frac{Q}{\tilde{z} - h - t} W \frac{Q}{\tilde{z} - h - t} W \frac{Q}{\tilde{z} - h - t} W \\ & - W^{(N)} \frac{Q}{\tilde{z} - h^{(N)} - t} W^{(N)} \frac{Q}{\tilde{z} - h^{(N)}} W^{(N)} \frac{Q}{\tilde{z} - h^{(N)} - t} W^{(N)} \end{aligned} \quad (5.12)$$

representing the analogous diagrams in the medium compared to $V_{\text{eff}}(z)$ of eq. (5.8) describing them in free two-body scattering. Note that, in the explicit evaluation of eq. (5.12), one has to take the Pauli principle into account, which forbids the intermediate nucleons to be in states occupied by the surrounding nucleons. To lowest order in G , the binding energy E of nuclear matter is obtained using eq. (3.8).

Finally, we have to give a recipe for the determination of the single-particle Hamiltonian $h^{(N)}$. In the following we shall use two choices:

(i) conventional choice

$$\begin{aligned} \epsilon_a &= E_a + \sum_b \langle ab | G(\epsilon_a + \epsilon_b) | ab \rangle \quad \text{for holes} \\ \epsilon_A &= E_A \quad \text{for particles} \end{aligned} \quad (5.13)$$

(ii) continuous choice

$$\begin{aligned} \epsilon_a &= E_a + \sum_b \langle ab | G(\epsilon_a + \epsilon_b) | ab \rangle \quad \text{for holes} \\ \epsilon_A &= E_A + \operatorname{Re} \sum_b \langle Ab | G(\epsilon_A + \epsilon_b) | Ab \rangle \quad \text{for particles.} \end{aligned} \quad (5.14)$$

This shows that the single-particle energies have to be determined self-consistently. Note also that, in this formalism, the quasipotential (5.12) depends on ϵ_a (through $h^{(N)}$) and thus has to be recalculated in every iteration step.

6. Relativistic transition potentials

The evaluation of $V_{\text{eff}}(\tilde{z})$ in eq. (5.8) is of course quite involved; we therefore will proceed in steps. This will also make our results more transparent and will facilitate a comparison with former work.

This section is devoted to a study of the iterative isobar box diagrams, i.e. the first four in fig. 23 together with those involving two Δ 's in the intermediate state. Of course, the others cannot a priori be neglected; however, this choice makes it possible to test the usual transition potential concept in a coupled-channel framework, since only the iterative diagrams (having no mesons in one intermediate state) should be described by iteration of a transition potential.

6.1. Evaluation of iterative isobar diagrams

In fig. 24, we redraw the first diagram of fig. 23, including kinematic notation. We first consider the case of π -exchange. According to standard rules (see refs. [41, 43]), using (3.17a) for the πNN -vertex and (5.4) for the $\pi N\Delta$ -vertex, we can write this diagram (denoted by $M_{N\Delta,1}^\pi$) as a second iteration of a transition potential $V_{N\Delta,1}^\pi$, in a helicity-state basis,

$$\langle \mathbf{q}' \Lambda'_1 \Lambda'_2 | M_{N\Delta,1}^\pi(z) | \mathbf{q} \Lambda_1 \Lambda_2 \rangle = \sum_{h_1, h_2^*} \int d^3 k \frac{\langle \mathbf{q}' \Lambda'_1 \Lambda'_2 | V_{N\Delta,1}^\pi(z) | \mathbf{k} h_1 h_2^* \rangle \langle \mathbf{k} h_1 h_2^* | V_{N\Delta,1}(z) | \mathbf{q} \Lambda_1 \Lambda_2 \rangle}{z - E_k^* - E_k} \quad (6.1)$$

with

$$\begin{aligned} \langle \mathbf{q}' \Lambda'_1 \Lambda'_2 | V_{N\Delta,1}^\pi(z) | \mathbf{q} \Lambda_1 \Lambda_2^* \rangle &= \frac{4\pi}{(2\pi)^3} \frac{g_{NN\pi} f_{N\Delta\pi}}{m_\pi} \frac{m}{E_{q'}} \left(\frac{mm_\Delta}{E_{q'} E_q^*} \right)^{1/2} \tau_1 \cdot T_2 \Delta_\mu F_\pi(\mathbf{q}', \mathbf{q}) \\ &\times \frac{\bar{u}_{\Lambda'_2}(-\mathbf{q}') u_{\Lambda'_2}^*(-\mathbf{q}) \bar{u}_{\Lambda_1}(\mathbf{q}') \gamma^5 u_{\Lambda_1}(\mathbf{q})}{2\omega_k^\pi (z - E_{q'} - E_q - \omega_k^\pi)} \end{aligned} \quad (6.2)$$

where $E_q = \sqrt{m^2 + \mathbf{q}^2}$, $E_q^* = \sqrt{m_\Delta^2 + \mathbf{q}^2}$, ($m = 938.9$ MeV, $m_\Delta = 1236$ MeV) and z is the starting energy;

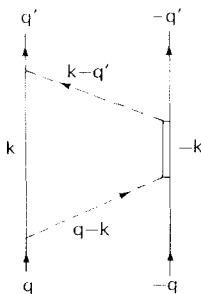


Fig. 24. Notation for the first diagram in fig. 23.

$\omega_k^\pi = \sqrt{(\mathbf{q}' - \mathbf{q})^2 + m_\pi^2}$, $\Delta^\mu = (0, \mathbf{q}' - \mathbf{q})$. Λ_1, Λ_2 resp. Λ'_1, Λ'_2 denote the helicities of the ingoing resp. outgoing nucleons. The summation goes over the helicities of the particles in the intermediate states, i.e. $h_1 = \pm\frac{1}{2}$, $h_2^* = \pm\frac{1}{2}, \pm\frac{3}{2}$, since the Δ -isobar has spin $\frac{3}{2}$. F_π is a phenomenological cutoff

$$F_\pi = \frac{\left(\frac{\Lambda_\pi^2 - m_\pi^2}{\Lambda_\pi^2 + (\mathbf{q}' - \mathbf{q})^2} \right)^2}{\dots} \quad (6.3)$$

with Λ_π a parameter, the so-called cutoff-mass.

The sum of the first four diagrams of fig. 23 plus those in which the Δ appears on the left hand side, can then be written as

$$\langle \mathbf{q}' \Lambda'_1 \Lambda'_2 | M_{N\Delta}^\pi(z) | \mathbf{q} \Lambda_1 \Lambda_2 \rangle = \sum_{h_1, h_2} \int d^3k \frac{\langle \mathbf{q}' \Lambda'_1 \Lambda'_2 | V_{N\Delta}^\pi(z) | k h_1 h_2^* \rangle \langle k h_1 h_2^* | V_{N\Delta}^\pi(z) | \mathbf{q} \Lambda_1 \Lambda_2 \rangle}{z - E_k^* - E_k} \quad (6.4)$$

with

$$V_{N\Delta}^\pi = (V_{N\Delta,1}^\pi + V_{N\Delta,2}^\pi) \sqrt{2}. \quad (6.5)$$

$V_{N\Delta,2}^\pi$ differs from eq. (6.2) only in the denominator where E_q has to be replaced by E_q^* .

Analogously, the sum of iterative diagrams involving $\Delta\Delta$ -intermediate states is given by

$$\langle \mathbf{q}' \Lambda'_1 \Lambda'_2 | M_{\Delta\Delta}^\pi(z) | \mathbf{q} \Lambda_1 \Lambda_2 \rangle = \sum_{h_1, h_2} \int d^3k \frac{\langle \mathbf{q}' \Lambda'_1 \Lambda'_2 | V_{\Delta\Delta}^\pi(z) | k h_1^* h_2^* \rangle \langle k h_1^* h_2^* | V_{\Delta\Delta}^\pi(z) | \mathbf{q} \Lambda_1 \Lambda_2 \rangle}{z - 2E_k^*} \quad (6.6)$$

with

$$V_{\Delta\Delta}^\pi = V_{\Delta\Delta,1}^\pi + V_{\Delta\Delta,2}^\pi \quad (6.7)$$

where

$$\begin{aligned} \langle \mathbf{q}' \Lambda'_1 \Lambda'_2 | V_{\Delta\Delta,1}^\pi(z) | \mathbf{q} \Lambda_1^* \Lambda_2^* \rangle &= \frac{4\pi}{(2\pi)^3} \frac{f_{N\Delta\pi}^2}{m_\pi^2} \frac{mm_\Delta}{E_q E_q^*} \mathbf{T}_1 \cdot \mathbf{T}_2 \Delta_\mu \Delta_\nu F_\pi(\mathbf{q}', \mathbf{q}) \\ &\times \frac{\bar{u}_{\Lambda'_2}(-\mathbf{q}') u_{\Lambda'_2}^*(-\mathbf{q}) \bar{u}_{\Lambda'_1}(\mathbf{q}') u_{\Lambda'_1}^*(\mathbf{q})}{2\omega_k^*(z - E_{q'} - E_q^* - \omega_k^*)} \end{aligned} \quad (6.8)$$

and $V_{\Delta\Delta,2}^\pi$ is the same as $V_{\Delta\Delta,1}^\pi$. Explicit expressions for the helicity-state matrix-elements can be found in the paper of Holinde and Machleidt [55]. Only the denominators have to be changed appropriately. (Note that also the denominators are the same if one neglects the recoil terms in eqs. (6.2, 6.8).)

Next we evaluate the contribution from ρ -exchange. Using (3.16a) for the ρ NN-vertex and (5.5) for the ρ N Δ -vertex, we obtain for the first 4 diagrams of fig. 23 (plus those where the Δ appears on the left hand side) with ρ -exchange

$$\sum_{h_1, h_2} \int d^3k \frac{\langle \mathbf{q}' \Lambda'_1 \Lambda'_2 | V_{N\Delta}^\rho(z) | k h_1 h_2^* \rangle \langle k h_1 h_2^* | V_{N\Delta}^\rho(z) | \mathbf{q} \Lambda_1 \Lambda_2 \rangle}{z - E_k^* - E_k} \quad (6.9)$$

with

$$V_{N\Delta}^p = (V_{N\Delta,1}^p + V_{N\Delta,2}^p)\sqrt{2} \quad (6.10)$$

where

$$\begin{aligned} \langle q' \Lambda'_1 \Lambda'_2 | V_{N\Delta,1}^p(z) | q \Lambda_1 \Lambda_2^* \rangle &= \frac{4\pi}{(2\pi)^3} \frac{f_{N\Delta p}}{m_p} \frac{m}{E_{q'}} \left(\frac{mm_\Delta}{E_q E_q^*} \right)^{1/2} \tau_1 \cdot T_2 F_p(q', q) \bar{u}_{\Lambda_2^*}(-q') \gamma^5 \gamma^\mu u_{\Lambda_1^*}(-q) \\ &\times \frac{-g_\nu^\beta \Delta_\mu + g_\mu^\beta \Delta_\nu}{2\omega_k^p(z - E_{q'} - E_q - \omega_k^p)} \bar{u}_{\Lambda_1^*}(q') \left[g_{NNp} \gamma_\beta + \frac{f_{NNp}}{2m} i\sigma_{\beta\alpha} \Delta^\alpha \right] u_{\Lambda_1}(q) \end{aligned} \quad (6.11)$$

and again, $V_{N\Delta,2}^p$ differs from $V_{N\Delta,1}^p$ only in the denominator, where E_q has to be replaced by E_q^* . Correspondingly,

$$\langle q' \Lambda'_1 \Lambda'_2 | M_{\Delta\Delta}^p(z) | q \Lambda_1 \Lambda_2 \rangle = \sum_{h_1 h_2} \int d^3 k \frac{\langle q' \Lambda'_1 \Lambda'_2 | V_{\Delta\Delta}^p(z) | kh_1^* h_2^* \rangle \langle kh_1^* h_2^* | V_{\Delta\Delta}^p(z) | q \Lambda_1 \Lambda_2 \rangle}{z - 2E_k^*} \quad (6.12)$$

with

$$V_{\Delta\Delta}^p = V_{\Delta\Delta,1}^p + V_{\Delta\Delta,2}^p \quad (6.13)$$

where

$$\begin{aligned} \langle q' \Lambda'_1 \Lambda'_2 | V_{\Delta\Delta,1}^p(z) | q \Lambda_1^* \Lambda_2^* \rangle &= \frac{4\pi}{(2\pi)^3} \frac{f_{N\Delta p}^2}{m_p^2} \frac{mm_\Delta}{E_q E_q^*} T_1 \cdot T_2 F_p(q', q) \\ &\times \bar{u}_{\Lambda_2^*}(-q') \gamma^5 \gamma^\mu u_{\Lambda_1^*}(-q) \bar{u}_{\Lambda_1^*}(q') \gamma^5 \gamma^\alpha u_{\Lambda_1^*}^\beta(q) \\ &\times \frac{\Delta_\mu \Delta_\alpha g_{\beta\nu} - \Delta_\mu \Delta_\beta g_{\nu\alpha} - \Delta_\nu \Delta_\alpha g_{\mu\beta} + \Delta_\nu \Delta_\beta g_{\alpha\mu}}{2\omega_k^p(z - E_{q'} - E_q^* - \omega_k^p)} \end{aligned} \quad (6.14)$$

and $V_{\Delta\Delta,2}^p$ is the same as $V_{\Delta\Delta,1}^p$. The form factor is chosen to be

$$F_p = \left(\frac{\Lambda_p^2 - m_p^2}{\Lambda_p^2 + (q' - q)^2} \right)^3 \quad (6.15)$$

with Λ_p being a cutoff-parameter. Explicit results for the specific matrix-elements of $V_{N\Delta}^p$ and $V_{\Delta\Delta}^p$ can be found in the paper of Holinde et al. [56]. The sum of all possible exchanges in the first four diagrams of fig. 23 (including those with mixed π, p -exchange) can then be written as

$$\begin{aligned} \langle q' \Lambda'_1 \Lambda'_2 | M_{N\Delta}(z) | q \Lambda_1 \Lambda_2 \rangle &= \sum_{h_1 h_2} \int \frac{d^3 k}{z - E_k^* - E_k} [\langle q' \Lambda'_1 \Lambda'_2 | V_{N\Delta}^p(z) | kh_1 h_2^* \rangle + \langle q' \Lambda'_1 \Lambda'_2 | V_{N\Delta}^p(z) | kh_1 h_2^* \rangle] \\ &\times [\langle kh_1 h_2^* | V_{N\Delta}^p(z) | q \Lambda_1 \Lambda_2 \rangle + \langle kh_1 h_2^* | V_{N\Delta}^p(z) | q \Lambda_1 \Lambda_2 \rangle] \end{aligned} \quad (6.16)$$

and for $\Delta\Delta$ -intermediate states

$$\begin{aligned} \langle q' \Lambda'_1 \Lambda'_2 | M_{\Delta\Delta}(z) | q \Lambda_1 \Lambda_2 \rangle &= \sum_{h_1^*, h_2^*} \int \frac{d^3 k}{z - 2E_k^*} [\langle q' \Lambda'_1 \Lambda'_2 | V_{\Delta\Delta}^\pi(z) | kh_1^* h_2^* \rangle + \langle q' \Lambda'_1 \Lambda'_2 | V_{\Delta\Delta}^o(z) | kh_1^* h_2^* \rangle] \\ &\quad \times [\langle kh_1^* h_2^* | V_{\Delta\Delta}^\pi(z) | q \Lambda_1 \Lambda_2 \rangle + \langle kh_1^* h_2^* | V_{\Delta\Delta}^o(z) | q \Lambda_1 \Lambda_2 \rangle]. \end{aligned} \quad (6.17)$$

We would like to make one final remark here: Of course, these iterative diagrams could have been obtained without introducing the concept of transition potentials. Specifically, the sum over intermediate helicities can be replaced by suitable projection operators (which is the adequate procedure for an evaluation of the non-iterative diagrams, see section 9).

However, transition potentials are explicitly needed in order to calculate isobar components of wave functions [57], which are of considerable importance in nuclear physics. We refer to a paper by Anastasio et al. [58], in which isobar configurations in light nuclei have been calculated with the transition potentials described in this section.

Before doing actual calculations, we have to expand the helicity state matrix-elements (eqs. (6.16, 6.17)) into angular momentum states $|J\Lambda_1 \Lambda_2\rangle$. If we choose the incident direction along the z -axis and the outgoing momentum to be in the xz -plane, the expansion, for a general matrix-element denoted by V , can be written as

$$\langle q' \Lambda'_1 \Lambda'_2 | V | q \Lambda_1 \Lambda_2 \rangle = \frac{1}{4\pi} \sum_J (2J+1) d_{\Lambda\Lambda}^J(\vartheta) \langle \Lambda'_1 \Lambda'_2 | V^J(q', q) | \Lambda_1 \Lambda_2 \rangle \quad (6.18)$$

where ϑ is the scattering angle between q and q' and $\Lambda = \Lambda_1 - \Lambda_2$, $\Lambda' = \Lambda'_1 - \Lambda'_2$. $d_{\Lambda\Lambda}^J(\vartheta)$ are the well-known reduced rotation matrices. Using this expansion, eq. (6.16) becomes

$$\begin{aligned} \langle \Lambda'_1 \Lambda'_2 | M_{N\Delta}^J(q', q|z) | \Lambda_1 \Lambda_2 \rangle &= \sum_{h_1^*, h_2^*} \int_0^\infty \frac{dk k^2}{z - E_k^* - E_k} [\langle \Lambda'_1 \Lambda'_2 | V_{N\Delta}^{\pi J}(q', k|z) | h_1^* h_2^* \rangle \\ &\quad + \langle \Lambda'_1 \Lambda'_2 | V_{N\Delta}^{o J}(q', k|z) | h_1^* h_2^* \rangle] [\langle h_1^* h_2^* | V_{N\Delta}^{\pi J}(k, q|z) | \Lambda_1 \Lambda_2 \rangle \\ &\quad + \langle h_1^* h_2^* | V_{N\Delta}^{o J}(k, q|z) | \Lambda_1 \Lambda_2 \rangle] \end{aligned} \quad (6.19)$$

and, correspondingly for eq. (6.17),

$$\begin{aligned} \langle \Lambda'_1 \Lambda'_2 | M_{\Delta\Delta}^J(q', q|z) | \Lambda_1 \Lambda_2 \rangle &= \sum_{h_1^*, h_2^*} \int_0^\infty \frac{dk k^2}{z - 2E_k^*} [\langle \Lambda'_1 \Lambda'_2 | V_{\Delta\Delta}^{\pi J}(q', k|z) | h_1^* h_2^* \rangle \\ &\quad + \langle \Lambda'_1 \Lambda'_2 | V_{\Delta\Delta}^{o J}(q', k|z) | h_1^* h_2^* \rangle] [\langle h_1^* h_2^* | V_{\Delta\Delta}^{\pi J}(k, q|z) | \Lambda_1 \Lambda_2 \rangle \\ &\quad + \langle h_1^* h_2^* | V_{\Delta\Delta}^{o J}(k, q|z) | \Lambda_1 \Lambda_2 \rangle]. \end{aligned} \quad (6.20)$$

The partial wave amplitudes of V can be obtained by inverting eq. (6.18)

$$\langle \Lambda'_1 \Lambda'_2 | V^J(q', q) | \Lambda_1 \Lambda_2 \rangle = 2\pi \int_{-1}^{+1} d \cos \vartheta d_{\Lambda\Lambda}^J(\vartheta) \langle q' \Lambda'_1 \Lambda'_2 | V | q \Lambda_1 \Lambda_2 \rangle. \quad (6.21)$$

In actual calculations they are evaluated numerically. Further details of the formalism can be found in ref. [55].

6.2. Results

The parameters in the transition potentials, used in the following calculations, are given in table 3. $f_{N\Delta\pi}^2$ is obtained from ref. [50] and $f_{N\Delta\rho}^2$ from eq. (4.14), with $g_\pi^2 = 14.4$, $g_\rho^2 = 0.55$ and $f_\rho/g_\rho = 6.6$.

In fig. 25 (solid line) we show the contribution of the first four diagrams of fig. 23 (plus those in which the Δ appears on the left hand side) involving only π -exchange, i.e. the contribution of eq. (6.4), in the 1S_0 -partial wave, for $q' = q_0 = 250$ MeV ($z = 2\sqrt{q_0^2 + m^2}$). The dashed line is obtained by replacing the time-ordered propagators in both $V_{N\Delta,1}^\pi$ and $V_{N\Delta,2}^\pi$ by simple pion-range propagators, i.e. by $(\mathbf{q}' - \mathbf{q})^2 + m_\pi^2$; in other words, retardation effects are neglected. It is seen that these retardation effects suppress the contribution by a factor of 3. Using the modification of the pion-range propagator proposed in ref. [51] (see eq. (4.6)), we see that the result (dash-dot line) goes in the right direction, however the effect is only 20% of the total retardation effect. That this modification underestimates the effect can be traced back to severe approximations used to derive it (initial nucleons at rest and neglect of nucleon recoil effects), as was already recognized in ref. [51].

Table 3
Parameters for the transition
potentials. (Here A_π and A_ρ are
given in MeV)

$f_{N\Delta\pi}^2$	$f_{N\Delta\rho}^2$	A_π	A_ρ
0.27	15.41	1200	1200

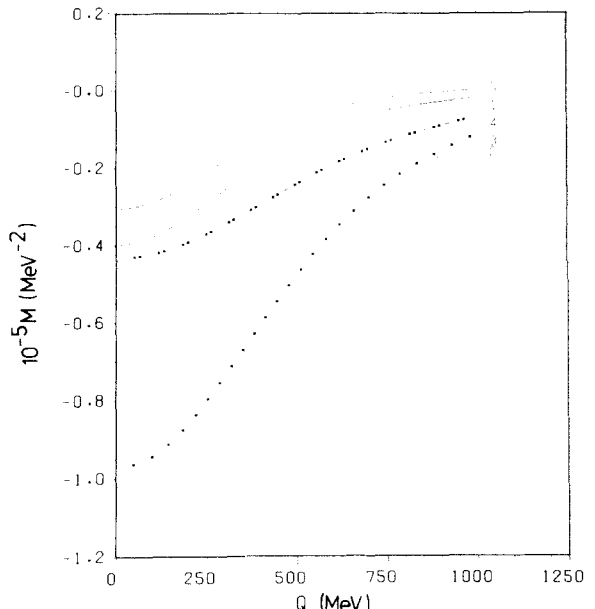


Fig. 25. The $N\Delta$ -contribution with only π -exchange, i.e. the contribution of $\langle \mathbf{q}' | M_{N\Delta}(z) | \mathbf{q} \rangle$ in eq. (6.4), for the 1S_0 -partial wave with $q' = q_0 = 250$ MeV ($z = 2\sqrt{q_0^2 + m^2}$) as a function of q is denoted by the solid lines. Curve 1 shows the full relativistic results while curve 5 shows the results when the static limit is taken at the $N\Delta$ -vertices. The dashed curve (curve 2) is obtained by replacing the time-ordered propagators in the transition potentials, $V_{N\Delta,1}^\pi$ and $V_{N\Delta,2}^\pi$, by simple pion-range propagators. The dash-dot (curve 3) is obtained using the prescription of ref. [51], i.e. taking $V_{N\Delta,1}^\pi$ as in curve 2 but using a range of $\sqrt{3}m_\pi$ in $V_{N\Delta,2}^\pi$. In the dashed-double-dot curve (curve 4) the range in $V_{N\Delta,1}^\pi$ is taken as $2m_\pi$ while it is taken as $4m_\pi$ in $V_{N\Delta,2}^\pi$.

This shows that, in order to simulate the exact time-ordered propagator, the range has to be chosen much shorter. If we arbitrarily choose $2m_\pi$ for $V_{N\Delta,1}$ (i.e. $(q' - q)^2 + 4m_\pi^2$ for the propagator) and $4m_\pi$ for $V_{N\Delta,2}$, we obtain the dash-double-dot curve. It is seen that this (phenomenological) prescription roughly agrees with the correct result for low momenta q , but overestimates it for higher q . This suggests that a very sophisticated prescription is needed in order to replace time-ordered propagators by manageable r -space expressions, see also ref. [53]. In any case, such a replacement destroys the specific structure of the propagator necessary for a well-defined prescription in going from two-body scattering to nuclear structure, see section 3.

In addition, we show the results if we go to the static limit at the $N\Delta$ -vertices in eq. (6.4), keeping the propagators the same. It reduces the exact contribution by roughly 25%. Our calculations have shown that this is true for all propagators considered in this figure. Thus the combined use of (i) the static limit at the vertices and (ii) pion-range propagator (as is usually done in r -space calculations) overestimates the contribution of an exact calculation by roughly a factor of 2.

Fig. 26 shows the corresponding results for the contribution of the iterative diagrams involving $\Delta\Delta$ -intermediate states, i.e. the contribution of eq. (6.6). The modifications of the range are, however, consistently changed compared to the former case: for the dash-dot line, m_π is now replaced by $\sqrt{3}m_\pi$ in the propagators of both $V_{\Delta\Delta,1}^\pi$ and $V_{\Delta\Delta,2}^\pi$; for the dash-double-dot line, m_π is replaced by $4m_\pi$ both in $V_{\Delta\Delta,1}^\pi$ and $V_{\Delta\Delta,2}^\pi$. There are characteristic differences compared to fig. 25: First, the relative contribution of higher momenta is much larger now; this shows that the $\Delta\Delta$ -contribution is considerably shorter-ranged than the $N\Delta$ -contribution of fig. 25. Second, for low momenta, the $N\Delta$ - and $\Delta\Delta$ -contributions are roughly the same for the pion-range propagator, whereas the use of the exact time-ordered propagators

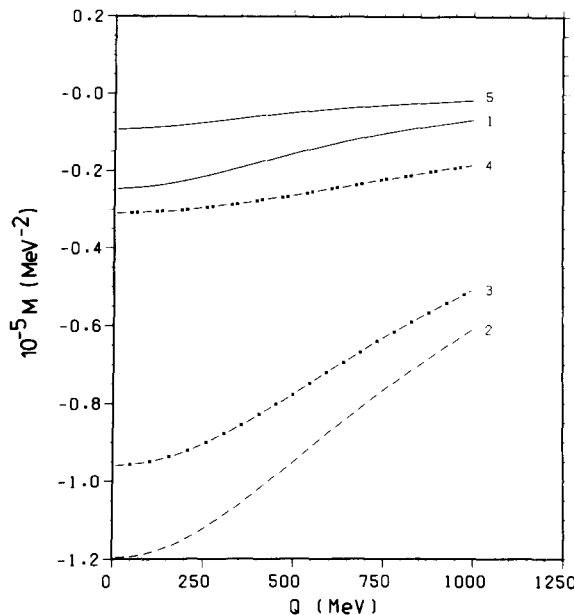


Fig. 26. The results for the $\Delta\Delta$ -contribution with only π -exchange, i.e. eq. (6.6), with the same notation as in fig. 25. For the Durso et al. [51] prescription (curve 3) both $V_{\Delta\Delta,1}^\pi$ and $V_{\Delta\Delta,2}^\pi$ have range $\sqrt{3}m_\pi$, while for curve 4 they both have range $4m_\pi$.

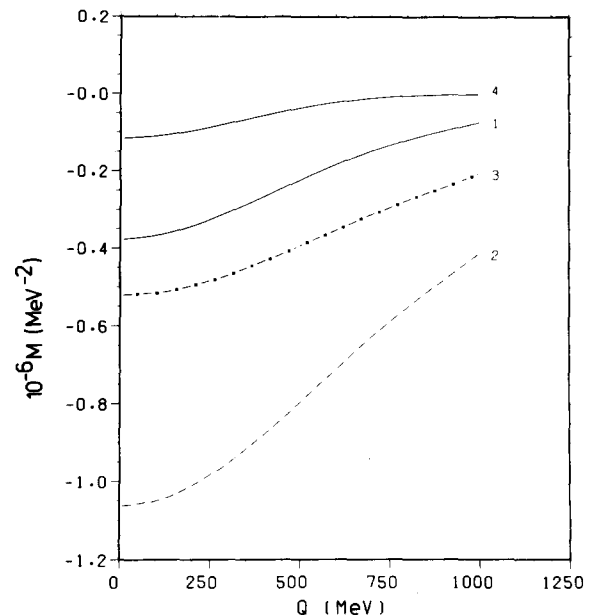


Fig. 27. The analogous $N\Delta$ -contribution to fig. 25 for only ρ -exchange. Again the solid curves denote the results for the full relativistic and static limit cases, curves 1 and 4 respectively. Curve 2 denotes the results with simple ρ -range propagators in $V_{N\Delta,1}^\rho$ and $V_{N\Delta,2}^\rho$ while for curve 3, when Durso et al. [51] prescription is used, m_ρ^2 is replaced by $m_\rho^2 + m_\rho(m_\Delta - m)$ in the propagator for $V_{N\Delta,2}^\rho$.

reduces the $\Delta\Delta$ -contribution relative to the $N\Delta$ -contribution. On the other hand, the effect of modifying the range is the same as in fig. 25. Also, the use of the static limit at the vertices together with the pion-range propagator overestimates the true contribution again by roughly a factor of 2.

A comparison with fig. 2 of ref. [55] shows that, for lower momenta, the sum of the $N\Delta$ - and $\Delta\Delta$ -contribution, i.e. the sum of eqs. (6.4) and (6.6), agrees roughly with the corresponding contribution using the pion-range propagator and $\Lambda_\pi \sim 850$ MeV (the different values for $f_{N\Delta\pi}^2$ used in this work and in ref. [55] have to be taken into account). In other words, the use of the exact time-ordered propagators allows the use of $\Lambda_\pi = 1200$ MeV instead of $\Lambda_\pi = 850$ MeV, which is in a much more reasonable range than before [55].

In figs. 27 and 28, we show the analogous contributions for ρ -exchange, i.e. eqs. (6.9) and (6.12). Again, the exact time-ordered propagators reduce the contribution obtained with the usual choice (i.e. $(q' - q)^2 + m_\rho^2$) by roughly a factor of 3 as in the case of pion exchange. This shows that the effect of time-ordered propagators cannot be neglected as suggested in ref. [53]. The dash-dot line again shows the result for a modification of the rho-range propagator according to ref. [51]: in fig. 27, m_ρ^2 is replaced by $m_\rho^{*2} = m_\rho^2 + m_\rho(m_\Delta - m)$ in the propagator of $V_{N\Delta,2}^\rho$ ($V_{N\Delta,1}^\rho$ is the same as for the dashed line); in fig. 28, m_ρ^2 is replaced by m_ρ^{*2} in the propagator of both $V_{N\Delta,1}^\rho$ and $V_{N\Delta,2}^\rho$. We see that the agreement with the exact result is much better than for the pion case. Again the combined use of the static limit at the vertices and simple ρ -range propagator overestimates the exact result by roughly a factor of 2.

The next two figures show the effect of combining the π - and ρ -exchange contributions. In fig. 29, the

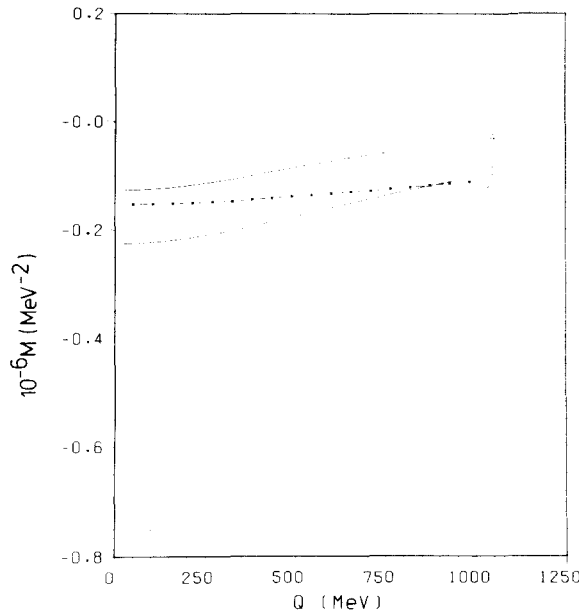


Fig. 28. The analogous $\Delta\Delta$ -contribution to fig. 26 for only ρ -exchange. The notation is the same as in fig. 27 except for curve 3 where m_ρ^2 is replaced by $m_\rho^2 + m_\rho(m_\Delta - m)$ in the propagators of both $V_{N\Delta,1}^\rho$ and $V_{N\Delta,2}^\rho$.

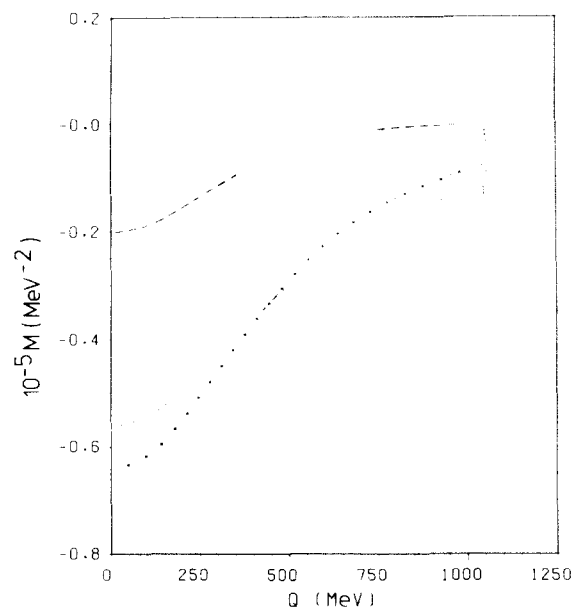


Fig. 29. Results from combining π - and ρ -exchange using time-ordered propagators. The solid curves denote the $N\Delta$ - and $\Delta\Delta$ -contributions with π - and ρ -exchange, i.e. $M_{N\Delta} + M_{\Delta\Delta}$. The dashed curves denote only the $N\Delta$ -contribution with π - and ρ -exchange, i.e. $M_{N\Delta}$. Both the full relativistic and static limit cases are shown, curves 1 and 3 and 2 and 4 respectively. The $N\Delta$ - and $\Delta\Delta$ -contribution with only π -exchange is also given by the dash-dot curve. As before, the results are shown for the 1S_0 -partial wave with $q' = q_0 = 250$ MeV.

two dashed lines show the $N\Delta$ -contribution, i.e. $M_{N\Delta}(z)$ of eq. (6.16), again in the 1S_0 -partial wave for $q' = q_0 = 250$ MeV. Curve 3 denotes the full (relativistic) result, whereas curve 4 shows the result if the static limit is taken at the $N\Delta$ -vertices. A comparison with fig. 25 shows that the inclusion of ρ -exchange suppresses the $N\Delta$ -contribution by a factor of 2 in this partial wave. The result for the static limit happens to be the same in spite of the fact that both π - and ρ -contributions are strongly modified separately. This feature, however, does not persist in higher partial waves.

The two solid curves (curves 1 and 2) denote the sum of $N\Delta$ - and $\Delta\Delta$ -contributions, for the relativistic case and the static limit respectively, i.e. the sum of eqs. (6.16) and (6.17). Thus the difference between curves 1 and 3 or between curves 2 and 4 gives the $\Delta\Delta$ -contribution. A comparison with fig. 26 shows that the $\Delta\Delta, \pi + \rho$ -contribution is in fact larger than the $\Delta\Delta, \pi$ -contribution, i.e. in this channel, the inclusion of ρ -exchange enhances the $\Delta\Delta$ -contribution. The strong reduction of the total contribution due to the static limit (nearly by a factor of 2) can be completely traced back to the reduction of the $\Delta\Delta$ -contribution. The dash-dot curve shows only the π -contribution ($N\Delta + \Delta\Delta$), which roughly agrees with the corresponding $(\pi + \rho)$ -contribution. Again, the strong reduction of the $N\Delta, \pi$ -contribution by adding ρ -exchange is partly cancelled by an increase of $\Delta\Delta, \pi$ due to the inclusion of ρ -exchange.

In fig. 30, the two solid lines (curves 1 and 2) again show the $(N\Delta + \Delta\Delta)$ -contribution arising from $(\pi + \rho)$ -exchange. The two dashed lines (curves 3 and 4) show the results when the time-ordered propagators in the transition potentials are replaced by usual pion-range and rho-range propagators (i.e. $(q' - q)^2 + m_\pi^2$, $(q' - q)^2 + m_\rho^2$). As before, curves 1 and 3 show the relativistic result and curves 2 and 4 the static limit at the $N\Delta$ -vertices respectively. Again we see that the use of the exact propagator reduces the contribution drastically. This figure also shows that the consistent use of the static limit in the whole expression (i.e. static limit at the vertices together with pion range) overestimates the exact contribution by a factor of 2.

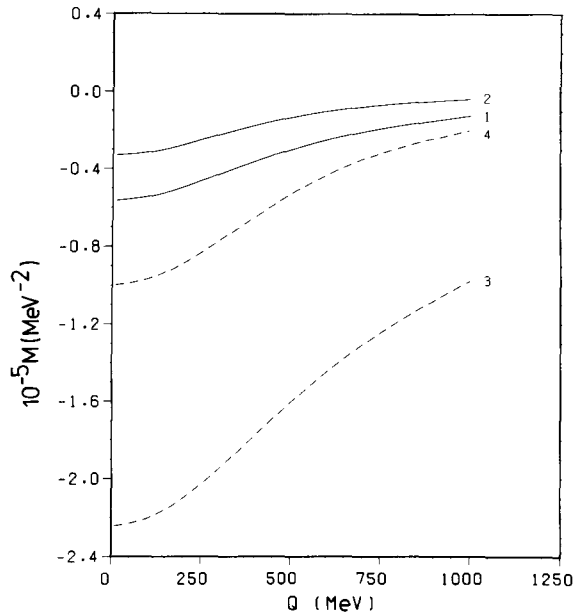


Fig. 30. Results from combining π - and ρ -exchange using simple π - and ρ -range propagators. The dashed curves denote the $N\Delta$ - and $\Delta\Delta$ -contribution with π - and ρ -exchange replacing the time-ordered propagators in the transition potentials by simple π - and ρ -range propagators. Both the full relativistic and static limit cases are shown, curves 1 and 3 and curves 2 and 4 respectively.

These results show that the possibility of using a reasonable value for the cutoff-mass in the $N\Delta$ -vertices is due to the combined use of time-ordered propagators and ρ -exchange. The effect of ρ -exchange is different in various partial waves (as will be seen below by looking at the effects on the NN-scattering phase shifts). This feature can be traced back to the fact that, in the static limit, ρ -exchange suppresses the tensor part, but enhances the spin-spin part, see section 4.4. It is just this property which helps in obtaining a consistent description of the data [59].

7. NN-scattering

A necessary (but of course not sufficient) condition for a realistic model of the nucleon–nucleon interaction to be applied in nuclear structure is a reasonable description of the empirical NN-data. Furthermore, these data are used to fix open parameters of the model.

7.1. Outline of the formalism

In order to calculate NN-scattering phase shifts, we start from the scattering equation (5.7) with an effective potential $V_{\text{eff}}(z)$ to be specified later. For practical calculations it is convenient to work with the R -matrix, which is related to the T -matrix by

$$T(z) = R(z) - i\pi R(z) \delta(z - h_0^{(N)}) T(z). \quad (7.1)$$

Thus, eq. (5.7) becomes in terms of $R(z)$

$$R(z) = V_{\text{eff}}(z) + V_{\text{eff}}(z) \frac{P}{z - h_0^{(N)}} R(z) \quad (7.2)$$

where P is the principal value, to be taken when carrying out the integration over the continuous spectrum of $h_0^{(N)}$. Thus we obtain for the helicity-state matrix elements of $R(z)$

$$\begin{aligned} \langle q' \Lambda'_1 \Lambda'_2 | R(z) | q \Lambda_1 \Lambda_2 \rangle &= \langle q' \Lambda'_1 \Lambda'_2 | V_{\text{eff}}(z) | q \Lambda_1 \Lambda_2 \rangle \\ &\quad + \sum_{h_1, h_2} P \int \frac{d^3 k}{z - 2E_k} \langle q' \Lambda'_1 \Lambda'_2 | V_{\text{eff}}(z) | kh_1 h_2 \rangle \langle kh_1 h_2 | R(z) | q \Lambda_1 \Lambda_2 \rangle \end{aligned} \quad (7.3)$$

and, after decomposition into angular momentum states (eq. (6.18)),

$$\begin{aligned} \langle \Lambda'_1 \Lambda'_2 | R^J(q', q|z) | \Lambda_1 \Lambda_2 \rangle &= \langle \Lambda'_1 \Lambda'_2 | V_{\text{eff}}^J(q', q|z) | \Lambda_1 \Lambda_2 \rangle + \sum_{h_1, h_2} P \int_0^\infty \frac{dk k^2}{z - 2E_k} \\ &\quad \times \langle \Lambda'_1 \Lambda'_2 | V_{\text{eff}}^J(q', k|z) | h_1 h_2 \rangle \langle h_1 h_2 | R^J(k, q|z) | \Lambda_1 \Lambda_2 \rangle. \end{aligned} \quad (7.4)$$

In fact, due to charge independence, there are two separate equations for isospin $I = 0$ and $I = 1$. Eq. (7.4) represents a coupled system of integral equations to be solved for R^J . This is done numerically in a

standard way. From the on-shell matrix-elements of R^J (putting $z = 2E_q$) one obtains the partial wave phase shifts. We refer to refs. [1, 43, 55] for further details.

7.2. Results

In this subsection we wish to present some typical results for NN-scattering phase shifts, using as effective potential

$$V_{\text{eff}}(z) = V_{\text{OBE}}(z) + M_{\text{NA}}(z) + M_{\Delta\Delta}(z). \quad (7.5)$$

Here, $V_{\text{OBE}}(z)$ is the one-boson-exchange potential of ref. [43] with suitably modified parameters. In contrast to ref. [43], we now make a more convenient choice for the form factors, i.e. in V_{OBE} we use

$$F_\alpha = \left(\frac{\Lambda_\alpha^2 - m_\alpha^2}{\Lambda_\alpha^2 - \Delta^2} \right)^n \quad (7.6)$$

at the vertices, with $n = 1$ for $\alpha = \pi, \eta, \sigma, \delta$ and $n = 3/2$ for $\alpha = \rho, \omega, \phi$; $\Delta^2 = (E_{q'} - E_q)^2 - (\mathbf{q}' - \mathbf{q})^2$. $M_{\text{NA}}(z)$ and $M_{\Delta\Delta}(z)$ are the iterative isobar box diagrams (eqs. (6.16, 6.17)) with parameters given in table 3. A reasonable description of all ($0 \leq J \leq 6$) partial wave phase shifts is obtained using for V_{OBE} the parameters shown in table 4.* There is an overall agreement of these couplings with what is known from other sources. (A survey of our present knowledge can be found in the recent work of Nagels et al. [60].) Figs. 31–36 show some of the resulting partial wave phase shifts as function of the nucleon lab energy. (A more complete list can be found in ref. [56].) The experimental error bars are taken from the energy-independent Livermore analysis [14]. The solid curves (curve 1) show the results if the full, unapproximated V_{eff} (eq. (7.5)) is taken. All other curves in figs. 31–36 are obtained by making certain approximations and by omitting specific contributions in V_{eff} , i.e. the parameters are kept unchanged. Curve 2 gives the result if the static limit is taken at all $N\Delta$ -vertices. The dashed curves (curves 3 and 4) show the results if $\Delta\Delta$ -contributions are omitted; in curve 3 the ρ -meson in the $\Delta\Delta$ -contribution is omitted, whereas for curve 4 the whole $\Delta\Delta$ -contribution is omitted. The dashed-dot curves (curves 5 and 6) show the analogous results for the $N\Delta$ -contributions when the whole $\Delta\Delta$ -contribution is omitted as well. The dashed-double-dot curve (curve 7) is obtained by omitting, in addition to the whole ($N\Delta + \Delta\Delta$)-contribution, also the σ -contribution, i.e. the total intermediate-range attraction is left out.

Table 4
Parameters for $V_{\text{OBE}}(z)$ defined in the text. (Here m_α and Λ_α are given in MeV. The number in brackets denotes the ratio of coupling constants f_ρ/g_ρ)

	π	η	σ	δ	ω	ρ	ϕ
$g_{N\text{Na}}^2(k^2 = m_\alpha^2)$	14.4		4.9978	12.795	0.373	30.012	0.4701 (6.61)
$g_{N\text{Na}}^2(k^2 = 0)$	14.263		4.274	7.928	0.077	13.965	0.253 (6.61)
m_α	138		548.5	599.7	960	782.8	712
Λ_α	2000		2000	1300	1300	1650	1020
							1650

* g_σ^2, g_δ^2 differ slightly from the values quoted in ref. [56] due to a former small inaccuracy in the computer code used in ref. [56]. The same is true for the values in table 5.

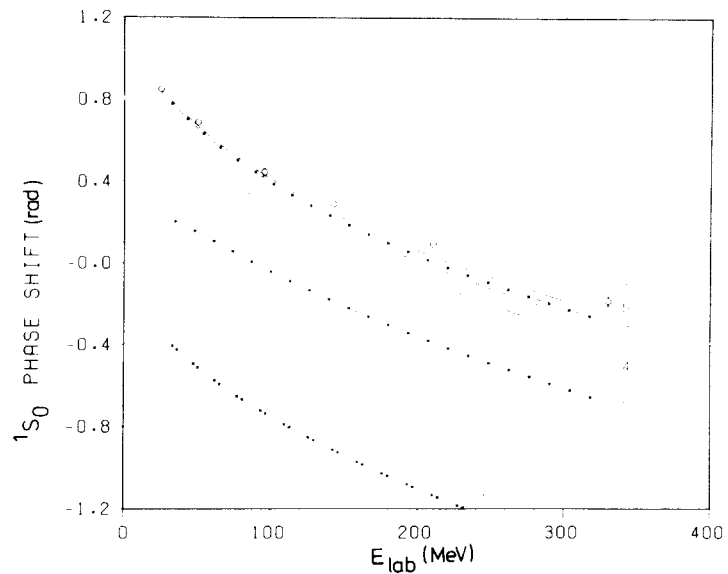


Fig. 31.

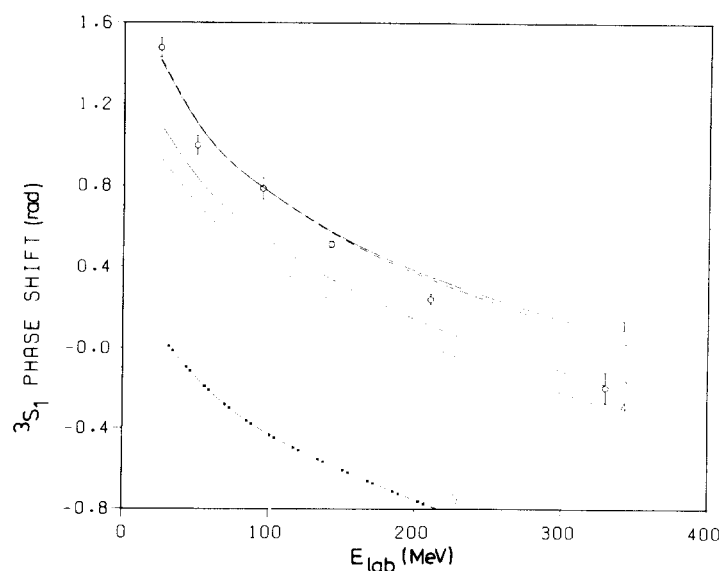


Fig. 32.

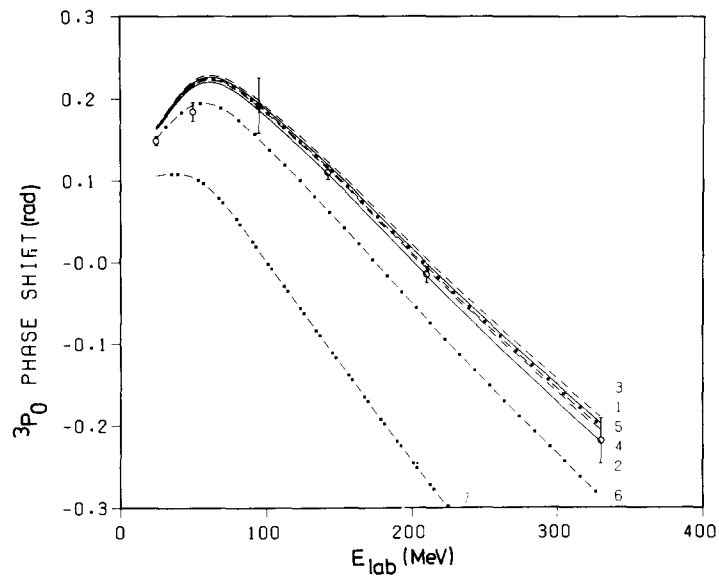


Fig. 33.

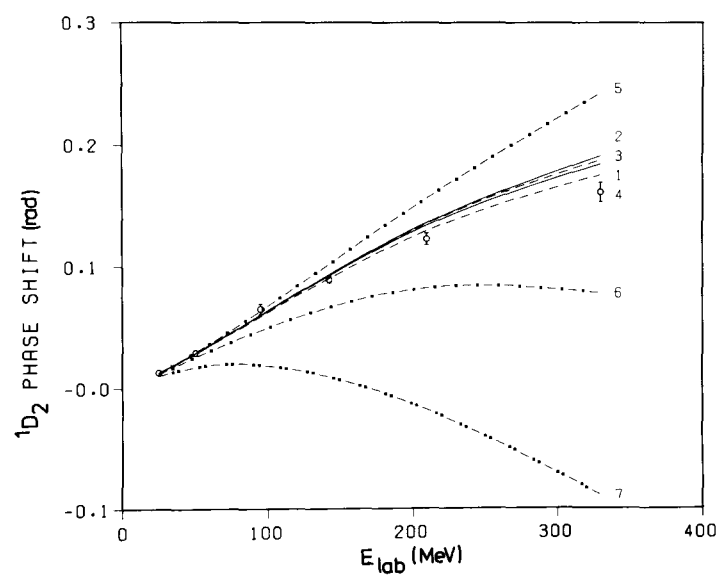


Fig. 34.

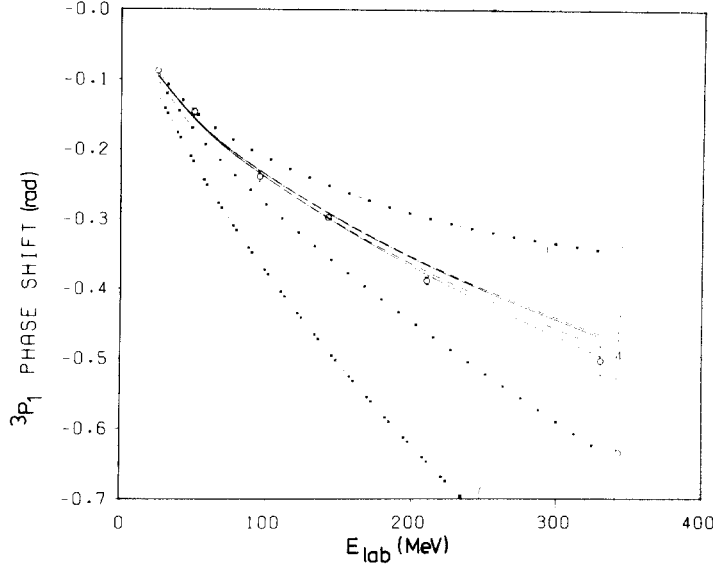


Fig. 35.

Figs. 31–35. Nucleon–nucleon nuclear bar phase shifts (in radians) as a function of the nucleon lab energy (in MeV). The error bars are taken from the energy-independent Livermore analysis [14]. Results for the full V_{eff} (eq. (7.5)) discussed in the text are denoted by the solid curves with the full relativistic and static limit cases taken at all the $N\Delta$ -vertices shown in curves 1 and 2 respectively. For the dashed curves $\Delta\Delta$ -contributions have been omitted from V_{eff} ; in curve 3 the $\Delta\Delta,\rho$ -contribution is omitted while in curve 4 the whole $\Delta\Delta$ -contribution is omitted. The dashed-dot curves denote the analogous results for the $N\Delta$ -contribution when the whole $\Delta\Delta$ -contribution is omitted as well. For curve 5 the $\Delta\Delta$ - and $N\Delta,\rho$ -contributions have been omitted from V_{eff} and for curve 6 both the whole $\Delta\Delta$ - and $N\Delta$ -contributions have been omitted. These two curves are not shown for $I = 0$ states since $N\Delta$ -states are forbidden there. The entire intermediate-range attraction is left out in curve 7, i.e. the $N\Delta$, the $\Delta\Delta$ - and the σ -contributions have been omitted from V_{eff} .

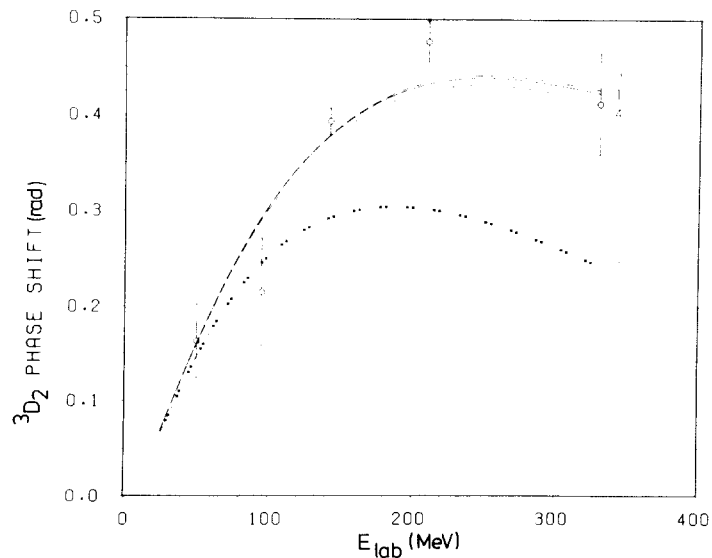


Fig. 36. The same notation as in figs. 31–35 is used except that curve 2 has been omitted since it cannot be distinguished from curve 1 in the figure.

There are, of course, no dashed-dot curves (curves 5 and 6) for isospin-zero states since $N\Delta$ -states are forbidden there.

The figures show that the use of the static limit at the $N\Delta$ -vertices in general reduces the isobar contribution (apart from 1D_2). The effect is large in S-waves: in 3S_1 , for example, where only $\Delta\Delta$ -states contribute, the isobar contribution is reduced to roughly one third of its original value. Fig. 29 shows that also in 1S_0 the main effect comes from the $\Delta\Delta$ -contribution, i.e. the $N\Delta$ -contribution does not change appreciably if the static limit is used. This is plausible, since, due to its shorter range, the $\Delta\Delta$ -contribution is more sensitive to the higher-momentum components, which, in turn, are more affected by the static limit. Thus, the effects of going to the static limit cannot be neglected anymore, in contrast to ref. [55], where the artificially strong cutoff ($\Lambda_\pi \sim 600$ MeV) suppressed strongly any effects in the high-momentum components. Furthermore, the relativistic $N\Delta$ -vertex can only partially be mocked up by increasing e.g. the σ -contribution, since the effect is different in different partial waves.

The effect of the $\Delta\Delta$ -contribution is comparable to the $N\Delta$ -contribution in the 1S_0 -partial wave, but is reduced in higher partial waves due to its comparatively shorter range, especially the $\Delta\Delta,\rho$ -contribution is strongly suppressed in waves ($L \geq 1$).

In general, ρ -exchange acts oppositely to π -exchange (see, however, 3P_0). The role of ρ -exchange is nicely demonstrated e.g. in the 3P_1 -partial wave. In fact, the different behaviour of ρ -exchange in different partial waves (e.g. 3P_0 , 3P_1) is helpful in obtaining a consistent description of the important 3P -states (see also ref. [59]). Note that our total Δ -contribution has roughly the same strength as the version in ref. [55] with $\Lambda_\pi \sim 700$ MeV (only π -exchange was considered there). With such a cutoff-mass, typical discrepancies showed up in ref. [55]; namely, 3P_1 - and 1D_2 phase shifts were too high, whereas 3P_0 -phase shifts were slightly too low. This, as seen from the present figures, is just cured by the inclusion of ρ -exchange.

In our opinion, this is the essential feature of the $N\Delta\rho$ -vertex. In fact, in this model, the repulsion in 1S_0 generated by the $N\Delta\rho$ -vertex is considerably smaller than suggested in ref. [51] ($\sim 15\%$ of the ω -contribution).^{*} This can also be seen from the resulting strength, $g_\omega^2(k=0)$ in table 4, which is in the same range as usual OBE-values.

Compared to the former procedure in ref. [55] (where the simple pion-range propagator was used) the total Δ -contribution is now suppressed much more in higher partial waves. This feature can be traced back to the much shorter range generated by the retardation effects of the time-ordered propagators.

In our model, the 3D_2 phase shift is considerably lowered compared to the results of other realistic models, see e.g. ref. [1], i.e. there is a strong improvement. The reason is the following: Part of the σ -exchange in OBE-models is now replaced by rather short-ranged diagrams involving $\Delta\Delta$ -intermediate states (the $N\Delta$ box diagrams do not contribute in isospin-zero states), which are strongly suppressed in D-waves, see fig. 36. The argument holds also if non-iterative diagrams are included, see section 9. Thus, referring to the discussion in section 2 about the πNN form factor, a strong (long-ranged) πNN form factor is not the only possible tool for removing the discrepancy in 3D_2 between theory and experiment.

Finally the low-energy scattering and deuteron data determined from the exact V_{eff} are given in table 5. Note the small value of the D-state probability in spite of the relatively weak πNN form factor used here. As in the pure OBE-model of ref. [43] (see section 3), this feature can be traced back to the retardation effects of the time-ordered propagators, which suppress higher-order contributions in V_{eff} ,

^{*} One could, however, argue that the relatively small value of $\Lambda_{N\Delta\rho}$ (= 1200 MeV) suppresses the $N\Delta\rho$ -vertex too strongly.

Table 5
Low-energy scattering and deuteron data

	Exp	eq. (7.5)	eq. (9.8)
E (MeV)	2.22462 ± 0.00006	2.2245	2.2238
Q (fm 2)	0.2860 ± 0.0015	0.280	0.2871
P_D (%)	5 ± 2	4.53	3.78
a_s (fm)	-23.715 ± 0.015	-23.70	-23.86
r_s (fm)	2.73 ± 0.03	2.72	2.68
a_t (fm)	5.423 ± 0.005	5.38	5.39
r_t (fm)	1.748 ± 0.014	1.69	1.74

i.e. contributions coming from the tensor force. Therefore it is possible to obtain a very low D-state probability (which nowadays seems to be favoured by certain few-body reactions, see ref. [21]) without using an unreasonably strong π NN form factor.

8. Nuclear matter

In this section, we want to apply our isobar model (eq. (7.5)) to nuclear matter.

8.1. Outline of the formalism

In first order of the Brueckner G -matrix, the (relativistic) energy E' of nuclear matter is obtained as

$$E' = \sum_a E_a + \frac{1}{2} \sum_{a,b} \langle ab | G(\epsilon_a + \epsilon_b) | ab - ba \rangle \quad (8.1)$$

where the sum goes over all occupied states. ϵ_a , ϵ_b are the relativistic single-particle energies (eqs. (5.13, 5.14)). Note that E_a (and thus E') contain the rest masses of the involved nucleons. The Bethe–Goldstone equation

$$G(\epsilon_a + \epsilon_b) = \tilde{V}_{\text{eff}}(\epsilon_a + \epsilon_b) + \tilde{V}_{\text{eff}}(\epsilon_a + \epsilon_b) \frac{Q}{\epsilon_a + \epsilon_b - h^{(N)}} G(\epsilon_a + \epsilon_b) \quad (8.2)$$

is written in terms of helicity-state matrix-elements as

$$\begin{aligned} \langle \mathbf{q}' \Lambda'_1 \Lambda'_2 | G(\epsilon_a + \epsilon_b) | \mathbf{q} \Lambda_1 \Lambda_2 \rangle &= \langle \mathbf{q}' \Lambda'_1 \Lambda'_2 | \tilde{V}_{\text{eff}}(\epsilon_a + \epsilon_b) | \mathbf{q} \Lambda_1 \Lambda_2 \rangle + \sum_{h_1, h_2} \int \frac{d^3 k \, Q(\mathbf{k}, \mathbf{P})}{\epsilon_a + \epsilon_b - E_{p+k} - E_{p-k}} \\ &\times \langle \mathbf{q}' \Lambda'_1 \Lambda'_2 | \tilde{V}_{\text{eff}}(\epsilon_a + \epsilon_b) | \mathbf{k} h_1 h_2 \rangle \langle \mathbf{k} h_1 h_2 | G(\epsilon_a + \epsilon_b) | \mathbf{q} \Lambda_1 \Lambda_2 \rangle \end{aligned} \quad (8.3)$$

where $\mathbf{P} = \frac{1}{2}(\mathbf{q}_a + \mathbf{q}_b)$ is the average momentum and \mathbf{q} , \mathbf{k} , \mathbf{q}' is the initial, intermediate and final relative momentum, respectively.

In principle, a \mathbf{P} -dependence arises not only in the propagator of eq. (8.3), but also in the numerator involving two-nucleon helicity states. Whereas, in free two-body scattering (section 7), a coordinate

system is (and can) always be chosen, in which $\mathbf{P} = 0$ (c.m. system), this cannot be done for the problem of two nucleons in the medium. Consequently, the matrix elements of \tilde{V}_{eff} in the medium contain a specific \mathbf{P} -dependence which can in principle be obtained from an evaluation of the potential matrix-elements for the general case $\mathbf{P} \neq 0$. This, however, would lead to enormous complications and require an effort which we feel is not justified at the present stage. It seems in fact that nature is so kind to keep the \mathbf{P} -dependence rather weak and unimportant:

(i) Due to γ^5 coupling, the πNN vertex depends to a good approximation (a numerical check for the OPEP was done in ref. [15]) only on the momentum transfer between ingoing and outgoing nucleons, which is independent of P .

(ii) Hajduk and Sauer [61] recently showed that the P -dependent terms in scalar and vector meson exchange contributions occurring in OBE-potentials are small and, moreover, cancel to a remarkable degree.

Therefore, throughout this article, we feel justified to neglect the P -dependence in all vertices building up \tilde{V}_{eff} .

Partial-wave decomposition of eq. (8.3) yields

$$\begin{aligned} \langle \Lambda'_1 \Lambda'_2 | G'(q', q) | \Lambda_1 \Lambda_2 \rangle &= \langle \Lambda'_1 \Lambda'_2 | \tilde{V}_{\text{eff}}^J(q', q) | \Lambda_1 \Lambda_2 \rangle + \sum_{h_1, h_2} \int_0^\infty \frac{dk \bar{Q}(k, P) k^2}{\epsilon_a + \epsilon_b - E_{P+k} - E_{P-k}} \\ &\quad \times \langle \Lambda'_1 \Lambda'_2 | \tilde{V}_{\text{eff}}^J(q', k) | h_1 h_2 \rangle \langle h_1 h_2 | G'(k, q) | \Lambda_1 \Lambda_2 \rangle \end{aligned} \quad (8.4)$$

where $\bar{Q}(k, P)$ represents the angle-averaged Pauli projector acting on the two-nucleon intermediate state.

For our specific model (involving only iterative isobar diagrams) the effective potential \tilde{V}_{eff} can be conveniently written in terms of transition potentials

$$\begin{aligned} \tilde{V}_{\text{eff}}(\epsilon_a + \epsilon_b) &= \tilde{V}_{\text{OBE}}(\epsilon_a + \epsilon_b) + \tilde{V}_{\text{N}\Delta}(\epsilon_a + \epsilon_b) \frac{Q_1}{\epsilon_a + \epsilon_b - h} \tilde{V}_{\text{N}\Delta}(\epsilon_a + \epsilon_b) \\ &\quad + \tilde{V}_{\Delta\Delta}(\epsilon_a + \epsilon_b) \frac{1}{\epsilon_a + \epsilon_b - h} \tilde{V}_{\Delta\Delta}(\epsilon_a + \epsilon_b). \end{aligned} \quad (8.5)$$

\tilde{V}_{OBE} , $\tilde{V}_{\text{N}\Delta}$ and $\tilde{V}_{\Delta\Delta}$ differ from V_{OBE} , $V_{\text{N}\Delta}$ and $V_{\Delta\Delta}$ (to be used in free NN-scattering) in that now the propagator contains the operator $h^{(N)}$ instead of $h_0^{(N)}$ (dispersion). Q_1 is the Pauli projector restricting the intermediate nucleon in the N Δ -state to be above the Fermi sea. Both modifications are seen to reduce the (attractive) isobar contribution and, therefore, lead to less binding in nuclear matter; an effect which is most welcome (see the discussion in the introduction).

In Brueckner theory, the single-particle energy ϵ is an auxiliary quantity introduced in order to improve the convergence of the hole-line expansion. In principle, the final result is independent of the specific choice. In practice, however, since one can calculate only three- (or at most four-) hole-line contributions, the result may depend on this quantity. If this is the case, it indicates that the result is not accurate, and one has to go to still higher orders. Thus a suitable single-particle potential should generate fast convergence and have a simple form, too.

Two alternative choices are currently used in the literature, namely eqs. (5.13) and (5.14). They are identical for holes according to the BBP-theorem [62], since this prescription cancels an important class

of higher-order diagrams. Unfortunately, there is no corresponding prescription for particle states. The conventional choice (eq. (5.13)) has a vanishing single-particle potential and, therefore, introduces a gap at the Fermi surface, whereas eq. (5.14), advocated for example by Mahaux et al. [63], is continuous there.

Using the conventional choice, the saturation points obtained with different NN-potentials differ widely (at least in lowest order). They lie on a narrow band, the so-called Coester band, which does not meet the empirical value. We believe that this deficiency is at least partly due to the neglect of higher-order contributions. As shown in ref. [7] for the RSC-potential, the three-hole-line contribution moves the lowest-order saturation point considerably off the Coester line, see fig. 1, and in the right direction regarding the empirical value.

It is interesting that, as shown in ref. [63] for the RSC-potential, the continuous choice (eq. (5.14)) moves the saturation point to higher energies (by roughly 4 MeV) compared to the conventional choice (comparing lowest-order results), but keeps the saturation density essentially the same. In fact, already in lowest order, the result for the continuous choice is very near to the saturation point obtained with the conventional choice after inclusion of the three-hole-line correction. In other words, a lowest-order calculation with the continuous choice in some way takes into account the three-body correlations obtained with the conventional choice (at least for the RSC-potential). Thus it seems that the problem of the Coester band is present only for lowest-order calculations based on the conventional spectrum.

8.2. Results

In this subsection we want to discuss some typical results. More details can be found in refs. [64, 65]. (The first reference contains also corresponding results for ^{16}O .)

Fig. 37 shows the binding energy per particle E/A ($E = E' - mA$, where E' is given by eq. (8.1)) as function of the Fermi momentum k_F , using eq. (8.5) as effective quasi-potential. The continuous choice gives roughly 3 MeV more binding. The fact that both prescriptions predict essentially the same saturation density, which was found already in ref. [63] for the phenomenological RSC-potential, obviously pertains for the extended and more realistic NN-interaction, eq. (8.5).

Note that the result for the standard choice, taken from ref. [65], is slightly more repulsive (about 1 MeV) compared to the result quoted in ref. [64]. The reason for this discrepancy is essentially the following: the former version [64], due to the mistake in the code (see footnote on p. 163), underestimated the isobar transition potentials and, consequently, the corresponding quenching of the NN-interaction in the medium by roughly 15% (see also the discussion below in connection with the wound integral).

In contrast to usual models, the choice of the single-particle energy in our case not only affects the propagator in the Bethe–Goldstone equation (8.4), but also all the propagators occurring in the quasi-potential $\tilde{V}_{\text{eff}}(\tilde{z})$ in eq. (8.5). Of course, the difference between the two (solid) curves in fig. 37 (“gap” and “cont”) is generated by the sum of both effects. Therefore, it is interesting to see how much of the total discrepancy is due to the change in $\tilde{V}_{\text{eff}}(\tilde{z})$. In order to answer this question, the following additional calculation has been done: we use the standard prescription (eq. (5.13)) in the propagator of eq. (8.4), but the continuous choice (eq. (5.14)) in $\tilde{V}_{\text{eff}}(\tilde{z})$, eq. (8.5), taking U_0 , M^* (which parametrize the single-particle energies) from the complete “gap”-calculation. The result is given by the dash-dot curve in fig. 37 and leads to the conclusion that the choice of the single-particle energy has little influence on $\tilde{V}_{\text{eff}}(\tilde{z})$: only 1/4 of the total difference is due to $\tilde{V}_{\text{eff}}(\tilde{z})$. At the first glance, this is surprising since the quasi-potential contains a lot of propagators (compared to one belonging to the equation).

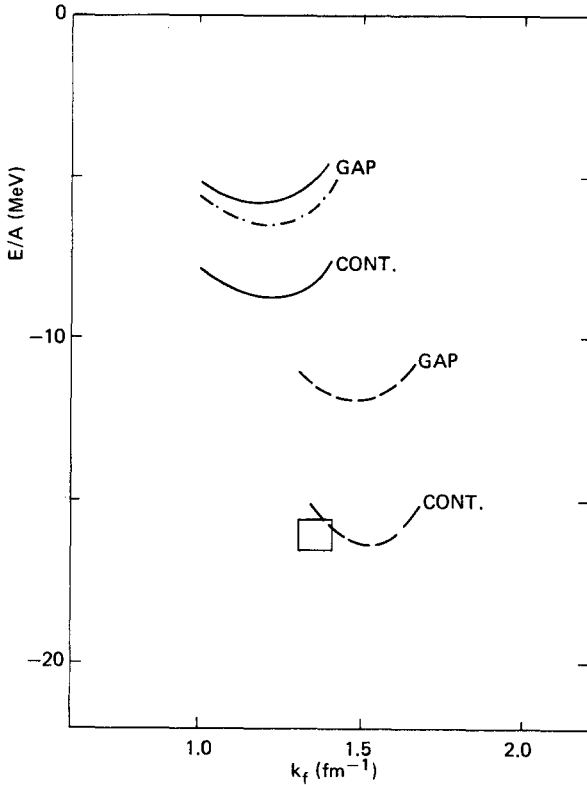


Fig. 37. Energy per particle E/A (in MeV) in nuclear matter as function of the Fermi momentum k_F (in fm^{-1}) using both the standard ("gap") and the continuous ("cont") choice. The solid lines are based on $V_{\text{eff}}(z)$ (eq. 7.5)), whereas the dashed lines are obtained using an OBE-potential [3]. The dash-dot curve is explained in the text. The box represents the empirical value.

However, these propagators contain additional terms from mesons and the Δ -N mass difference, which suppress the sensitivity to a change in $h^{(\text{N})}$.

In addition, fig. 37 shows the corresponding results (dashed lines) for a conventional OBE-potential [3] (HM1) which is not affected by a change in the single-particle energy. (Only the propagator in the Bethe–Goldstone equation is modified.) Nevertheless, the discrepancy is considerably larger there. The reason is that, in the scheme used in the present work, terms of higher order in the potential are very much suppressed due to energy-dependent recoil terms. This property also shows up in the small deuteron D-state probability of 4.53% (see table 5) and in the small value for the wound integral, see below. Therefore, inspite of additional terms depending on $h^{(\text{N})}$, the sensitivity to changes in $h^{(\text{N})}$ is comparatively small.

Table 6 presents the partial-wave contributions to the nuclear matter binding energy corresponding to the solid and dash-dot curves in fig. 37. As expected, the choice of the single-particle potential influences mainly the S-waves where higher-order contributions are most important. (Note that in the OBE-part of $\tilde{V}_{\text{eff}}(\tilde{z})$, the dependence on $h^{(\text{N})}$ drops out on-shell.)

Table 7 shows the results for specific contributions to the wound integral, κ_{NN} , $\kappa_{\text{N}\Delta}$, $\kappa_{\Delta\Delta}$ and their sum κ . These numbers were obtained according to the calculational method described in ref. [58] which deals with Δ -probabilities in ground states of nuclear systems in general. (Note that $\kappa_{\text{N}\Delta} = P_{\text{N}\Delta}$, but $\kappa_{\Delta\Delta} = \frac{1}{2}P_{\Delta\Delta}$.) Again there is a slight discrepancy between our values in table 7 for the standard choice

Table 6
Partial wave contribution (in MeV) to the binding energy of nuclear matter for $V_{\text{eff}}(z)$ at $k_F = 1.4 \text{ fm}^{-1}$

	gap	cont.	gap/cont.
1S_0	-13.32	-13.62	-13.52
3P_0	-3.64	-3.69	-3.65
1P_1	3.93	3.88	3.93
3P_1	12.99	12.47	12.83
3S_1	-18.76	-20.66	-18.99
3D_1	1.74	1.72	1.74
1D_2	-2.55	-2.58	-2.57
3D_2	-4.50	-4.56	-4.51
3P_2	-5.78	-6.01	-5.92
3F_2	-0.61	-0.61	-0.61
$J = 3$	3.24	3.19	3.23
$J = 4$	-1.77	-1.77	-1.77
$5 \leq J \leq 12$	0.51	0.53	0.52
potential energy	-28.50	-31.71	-29.29
kinetic energy	24.02	24.02	24.02
E	-4.48	-7.69	-5.27

Table 7
Contributions κ_{NN} , κ_{ND} , κ_{DD} to the wound integral and $\kappa = \kappa_{NN} + \kappa_{ND} + \kappa_{DD}$ (in %) at $k_F = 1.4 \text{ fm}^{-1}$ for the conventional ("gap") and continuous ("cont") choice

	κ_{NN}	κ_{ND}	κ_{DD}	κ
gap	6.4	2.9	4.2	13.5
cont.	10.3	3.2	4.2	17.7

and the corresponding values in ref. [58] because of the former incorrect numerical treatment mentioned before, which led to an underestimation of the isobar probabilities (which go like the square of the transition potentials) by roughly 30%.

As expected from the above discussion, the isobar contributions to the wound are rather insensitive to the choice of the single-particle potential. Only κ_{NN} changes appreciably, the value belonging to the standard choice being smaller simply because the gap suppresses higher-order contributions. According to our calculations, an explicit treatment of isobars increases the wound (through κ_{ND} , κ_{DD}) by roughly a factor of 2. Nevertheless, for our specific model, the total values are still reasonably small. In contrast, models which use the phenomenological RSC-potential with its unreasonably strong tensor force and static transition potentials overestimating grossly the isobar contribution, yield values for κ which are by a factor of 2–3 larger [66].

For the standard choice, neglecting the many-body corrections in $\tilde{V}_{\text{eff}}(\tilde{z})$, i.e. using $V_{\text{eff}}(z)$ also in the medium, eq. (8.2), we obtain a saturation energy of roughly -25 MeV, which agrees with the OBE-case, see fig. 14. This is not surprising, since both models have a similar amount of tensor force and are thus equivalent in nuclear matter. A consideration of many-body effects in the interaction, i.e. the use of $\tilde{V}_{\text{eff}}(\tilde{z})$ in eq. (8.2), leads however to a change of the saturation energy by as much as nearly 20 MeV. Only 1/3 of the effect arises from modifications of the OBE-potential, see fig. 14. The explicit description of part of the intermediate-range attraction by means of isobar diagrams therefore leads to a reduction of the binding energy by roughly 12 MeV.

In our case, the isobar box diagrams provide roughly 30% of the intermediate-range attraction in the NN-interaction. Without modifications, such contributions contribute 36 MeV to the binding energy of nuclear matter (which is reasonable since the total intermediate-range attraction of the nucleon–nucleon potential yields nearly 100 MeV binding). Consequently, Pauli- and dispersive effects reduce them by about 30%.

This strong quenching in the medium leads, in lowest-order Brueckner theory, to a saturation energy of -5.8 MeV at $k_F = 1.2 \text{ fm}^{-1}$, which is now far too low compared to the empirical value of $\approx -16 \text{ MeV}$, inspite of the small tensor force (deuteron D-state probability = 4.53%). As expected, the continuous choice for the single-particle energy yields a considerable improvement of the binding energy *and* the saturation density. Nevertheless, this result is still far away from the empirical value. Thus, if the situation would be the same as for the RSC potential (where, already in lowest order, the continuous choice seems to give a rather accurate result) the situation would be hopeless, especially if one realizes that a further reduction of the binding is expected if one takes also the modifications of the other diagrams of fig. 16 into account, see also the next section. Thus one might be tempted to conclude that such modifications are not really physical, but only spurious effects produced by some mathematical formalism.

There is, however, reason to believe that, for our model, the situation might be quite different because the field-theoretic Hamiltonian (containing as an interaction a vertex W instead of a potential V) generates a lot more diagrams in the perturbation expansion, see ref. [41]. Thus the contribution of all three-hole-line diagrams (including those coming conventionally from three-body forces) is perhaps considerably larger than suggested by the use of the continuous choice. A calculation of those diagrams is inevitably required before anything conclusive can be said.

In ref. [55] we found the density-dependence of such many-body corrections to go roughly like k_F^4 . In fact, the effect in ^{16}O is only 15% of the effect in nuclear matter; i.e. for the present model, the binding energy of ^{16}O is reduced only by $\approx 3 \text{ MeV}$, see ref. [64]. This is consistent with a density-dependence of k_F^4 since ^{16}O roughly corresponds to the nuclear matter system at $k_F \approx 1.1 \text{ fm}^{-1}$, see ref. [36]. Thus, many-body effects in ^{16}O are considerably reduced, but cannot be neglected. Furthermore, it seems that the inclusion of such effects improves the relation between the binding energy and the charge radius in ^{16}O , see ref. [64].

9. Non-iterative diagrams

Even after inclusion of higher-order contributions (e.g. three-hole-line contributions) in the many-body problem, it would be premature to expect detailed agreement since, up to now, our explicit description of the intermediate-range attraction is incomplete. So far our model contains only iterative isobar diagrams, which can be described in terms of transition potentials. In this section, we study some non-iterative diagrams, for example those of fig. 23 (apart from the first four).

The important role of non-iterative diagrams was first pointed out in ref. [51]. There it was shown that the inclusion of crossed isobar diagrams guarantees the whole Δ -contribution to be essentially isoscalar, a feature strongly suggested from dispersion-theoretic calculations.

On the other hand, Smith and Pandharipande [67] have shown that there are strong cancellations between the non-iterative diagrams involving NN-, $N\Delta$ - and $\Delta\Delta$ -intermediate states. However, their arguments critically depend on the detailed structure of the πNN - and $\pi N\Delta$ -vertices, which are not known to a sufficient accuracy. Nevertheless, it is clear from their calculations that not only the non-iterative isobar diagrams (involving $N\Delta$ - and $\Delta\Delta$ -intermediate states), but also the corresponding diagrams with two-nucleon intermediate states should be considered.

9.1. Non-iterative π -exchange diagrams involving two-nucleon intermediate states

We first consider the diagrams of fig. 38, i.e. the non-iterative diagrams involving two-nucleon

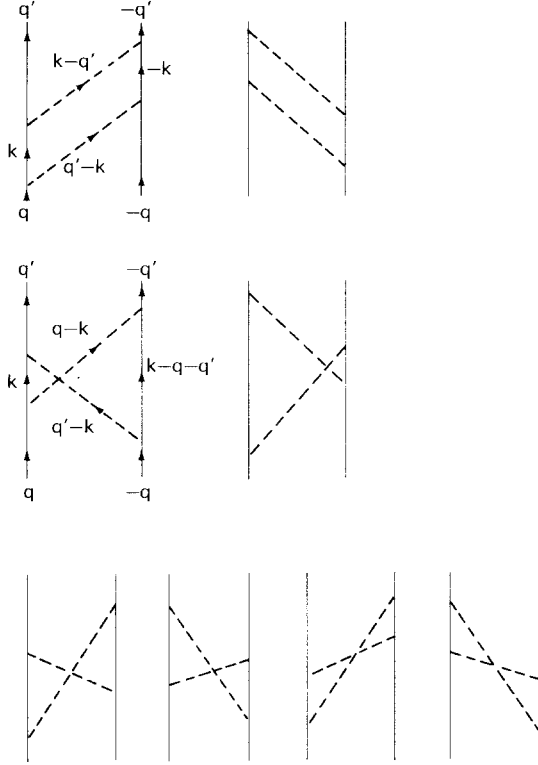


Fig. 38. Non-iterative diagrams involving two-nucleon intermediate states.

intermediate states, $M'_{NN}(z)$, together with 2π -exchange. As noted before, the iterative diagrams are included by iterating the one-pion-exchange potential.

The first diagram in fig. 38, i.e. one of the two non-iterative box diagrams, is written in a helicity-state basis, using pseudoscalar πNN -coupling,

$$\begin{aligned} \langle \mathbf{q}' \Lambda'_1 \Lambda'_2 | M'_{NN,1}(z) | \mathbf{q} \Lambda_1 \Lambda_2 \rangle &= \frac{(4\pi)^2}{(2\pi)^6} g_{NN\pi}^4 (3 - 2\boldsymbol{\tau}_1 \cdot \boldsymbol{\tau}_2) \sum_{h_1, h_2} \int \frac{d^3k F_\pi^2[(\mathbf{q}' - \mathbf{k})^2] F_\pi^2[(\mathbf{q} - \mathbf{k})^2]}{4\omega_{q-k}\omega_{q'-k}} \\ &\times \frac{\bar{u}_{\Lambda'_2}(-\mathbf{q}') i\gamma^5 u_{h_2}(-\mathbf{k}) i\gamma^5 u_{\Lambda'_1}(-\mathbf{q}) \bar{u}_{\Lambda'_1}(\mathbf{q}') i\gamma^5 u_{h_1}(\mathbf{k}) \bar{u}_{h_1}(\mathbf{k}) i\gamma^5 u_{\Lambda_1}(\mathbf{q})}{(z - E_{q'} - E_k - \omega_{q'-k})(z - E_{q'} - E_q - \omega_{q'-k} - \omega_{q-k})(z - E_q - E_k - \omega_{q-k})}. \end{aligned} \quad (9.1)$$

Here, $E_q = \sqrt{\mathbf{q}^2 + m^2}$, $\omega_q = \sqrt{\mathbf{q}^2 + m_\pi^2}$, and z is the starting energy. Furthermore, the form factor $F_\pi(\Delta^2)$ is parametrized as $F_\pi(\Delta^2) = (\Lambda_\pi^2 - m_\pi^2)/(\Lambda_\pi^2 + \Delta^2)$, Λ_π being the cutoff-mass and $\Delta^2 = (\mathbf{q}' - \mathbf{q})^2$. The spinors are normalized such that $u^\dagger u = 1$. The explicit evaluation of eq. (9.1) is described in detail in the appendix. The general structure of the result is as follows (c.p. eq. (A.11))

$$\begin{aligned} \langle \mathbf{q}' \Lambda'_1 \Lambda'_2 | M'_{NN,1}(z) | \mathbf{q} \Lambda_1 \Lambda_2 \rangle &= \frac{(4\pi)^2}{(2\pi)^6} g_{NN\pi}^4 (3 - 2\boldsymbol{\tau}_1 \cdot \boldsymbol{\tau}_2) \sum_{i=1}^4 A_i(\mathbf{q}' \Lambda'_1 \Lambda'_2; \mathbf{q} \Lambda_1 \Lambda_2) \\ &\times \int \frac{d^3k I_i^{(1)}(\mathbf{q}', \mathbf{q}, \mathbf{k}) F_\pi^2[(\mathbf{q}' - \mathbf{k})^2] F_\pi^2[(\mathbf{q} - \mathbf{k})^2]}{16E_k^2 \omega_{q-k} \omega_{q'-k} D_i^{(1)}(\mathbf{q}', \mathbf{q}, \mathbf{k})}. \end{aligned} \quad (9.2)$$

The second graph of fig. 38 gives exactly the same result, i.e. the contribution of the non-iterative box diagrams is twice the expression (9.2). The total sum of the crossed-box diagrams of fig. 38 is given by (see the appendix)

$$\begin{aligned} \langle \Lambda' \Lambda'_1 \Lambda'_2 | M'_{NN}^{(2)}(z) | \Lambda \Lambda_1 \Lambda_2 \rangle &= \frac{(4\pi)^2}{(2\pi)^6} g_{NN\pi}^4 (3 + 2\tau_1 \cdot \tau_2) \sum_{i=1}^4 A_i(\Lambda' \Lambda'_1 \Lambda'_2; \Lambda \Lambda_1 \Lambda_2) \\ &\times \int \frac{d^3 k I_i^{(2)}(\mathbf{q}', \mathbf{q}, \mathbf{k}) F_\pi^2[(\mathbf{q}' - \mathbf{k})^2] F_\pi^2[(\mathbf{q} - \mathbf{k})^2]}{16 E_k E_{k-q-q'} \omega_{q-k} \omega_{q'-k} D^{(2)}(\mathbf{q}', \mathbf{q}, \mathbf{k})}, \end{aligned} \quad (9.3)$$

where

$$\frac{1}{D^{(2)}} = \sum_{i=1}^6 \frac{1}{D_i^{(2)}}. \quad (9.4)$$

For the actual numerical calculations, we need the partial wave amplitudes. These can be obtained from eq. (6.21). The partial wave contribution of the iterative box diagrams can then be written as

$$\begin{aligned} \langle \Lambda' \Lambda'_2 | M'_{NN}^{(1)\mu}(q', q|z) | \Lambda \Lambda_2 \rangle &= 2\pi \cdot 2 \cdot \frac{(4\pi)^2}{(2\pi)^6} g_{NN\pi}^4 (3 - 2\tau_1 \cdot \tau_2) \\ &\times \sum_{i=1}^4 \int_{-1}^{+1} d \cos \theta d_{AA}^J(\theta) A_i(\Lambda' \Lambda'_1 \Lambda'_2; \Lambda \Lambda_1 \Lambda_2) \\ &\cdot \int \frac{d^3 k I_i^{(1)}(\mathbf{q}', \mathbf{q}, \mathbf{k}) F_\pi^2[(\mathbf{q}' - \mathbf{k})^2] F_\pi^2[(\mathbf{q} - \mathbf{k})^2]}{16 E_k^2 \omega_{q-k} \omega_{q'-k} D_i^{(1)}(\mathbf{q}', \mathbf{q}, \mathbf{k})}. \end{aligned} \quad (9.5)$$

Correspondingly, we obtain for the contribution of the crossed-box diagrams

$$\begin{aligned} \langle \Lambda' \Lambda'_2 | M'_{NN}^{(2)\mu}(q', q|z) | \Lambda \Lambda_2 \rangle &= 2\pi \frac{(4\pi)^2}{(2\pi)^6} g_{NN\pi}^4 (3 + 2\tau_1 \cdot \tau_2) \\ &\times \sum_{i=1}^4 \int_{-1}^{+1} d \cos \theta d_{AA}^J(\theta) A_i(\Lambda' \Lambda'_1 \Lambda'_2; \Lambda \Lambda_1 \Lambda_2) \\ &\cdot \int \frac{d^3 k I_i^{(2)}(\mathbf{q}', \mathbf{q}, \mathbf{k}) F_\pi^2[(\mathbf{q}' - \mathbf{k})^2] F_\pi^2[(\mathbf{q} - \mathbf{k})^2]}{16 E_k E_{k-q-q'} \omega_{q-k} \omega_{q'-k} D^{(2)}(\mathbf{q}', \mathbf{q}, \mathbf{k})}. \end{aligned} \quad (9.6)$$

The calculation of eqs. (9.3, 9.4) is straightforward and is based on the definitions given e.g. in ref. [1]. We evaluate the integrals numerically.

In fig. 39 (dot-dashed line) we show the contribution of the non-iterative box-diagrams, i.e. the first two in fig. 38, in the 1S_0 partial wave, for $q' = q_0 = 250$ MeV [$z = 2(q_0^2 + m^2)^{1/2}$], which is given by eq. (9.5). Here, we use $g_{NN\pi}^2 = 14.4$ and $\Lambda_\pi = 1.5$ GeV. The dashed line gives the corresponding con-

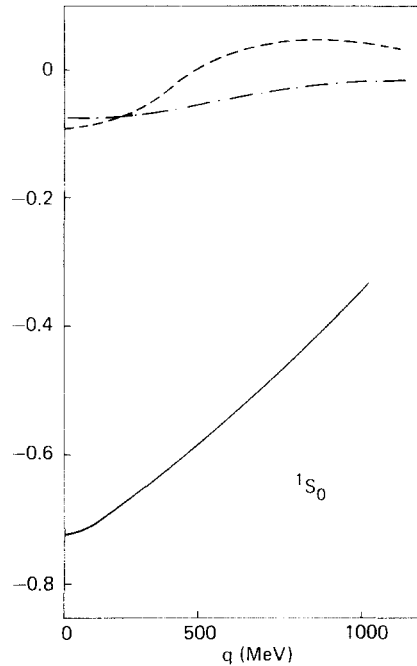


Fig. 39. Contribution of $M_{NN}^{\pi\pi}$ in the 1S_0 partial wave. The dot-dashed line displays the contribution of stretched-box diagrams (the first two of fig. 38) evaluated as given by eq. (9.5). The result for the crossed box diagrams (diagrams 3–8 of fig. 38, eq. (9.6)) does not contain the isospin factor and is given by the dashed line. The solid line shows the result for the corresponding iterative diagrams, which is the same as the first iteration of the one-pion-exchange potential. The results, plotted as a function of the relative momentum q are given in 10^{-8} MeV^{-2} . The values of q_0 , which defines the starting energy $z = 2(q_0^2 + m^2)^{1/2}$, and q' are 250 MeV. $g_{NN\pi}^2$ has been normalized to 1.

tribution of the crossed-box diagrams, i.e. diagrams 3–8 in fig. 38, given by eq. (9.6). For a better comparison of the relative sizes of these contributions we suppress the isospin factors (being one for box and 5 for crossed box in this partial wave). In addition, the solid line shows the contribution of the corresponding iterative diagrams, included already by the first iteration of the one-pion-exchange potential in the scattering equation.

It is seen that the non-iterative box diagrams give an attractive contribution which is, however, only $\approx 10\%$ of the dominant iterative diagrams in this partial wave. This can be traced back to the fact that in the case of the non-iterative box diagrams pions are involved in all intermediate states. This enlarges the energy denominators and thus suppresses the contribution compared to the iterative diagrams, in which one energy denominator involves two nucleons only. For the same reason, the contribution of the crossed-box diagrams is also relatively small. Note, however, that, owing to the isospin factor 5 suppressed in fig. 39, the crossed-box diagrams are of the same importance as the iterative box diagrams, at least in this partial wave.

The effect of these diagrams on NN-scattering data may be found in the paper by Holinde et al. [68], see also below.

9.2. Non-iterative π -exchange diagrams involving $N\Delta$ intermediate states

Here, we consider the analogous diagrams with $N\Delta$ intermediate states, i.e. the diagrams of fig. 38 with one intermediate nucleon replaced by the Δ -isobar. The explicit evaluation of such diagrams

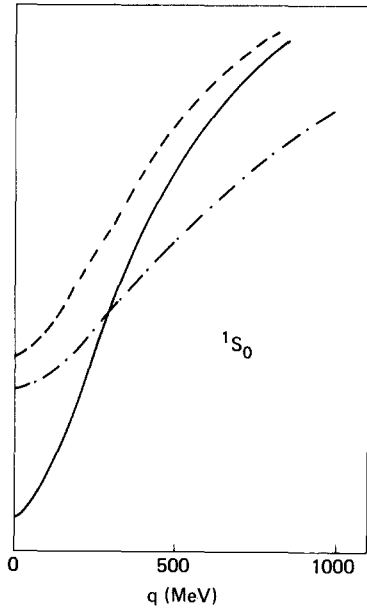


Fig. 40. The contribution of $M'_N\Delta^\pi$ in the 1S_0 partial wave is shown schematically as function of q for fixed q_0, q' , dropping the isospin factor. The dashed line displays the contributions of stretched-box diagrams multiplied by a factor 8/3. The dash-dot curve shows the contributions of crossed-box diagrams multiplied by a factor of 8/7. For comparison, the solid line gives the contribution of the corresponding iterative diagrams.

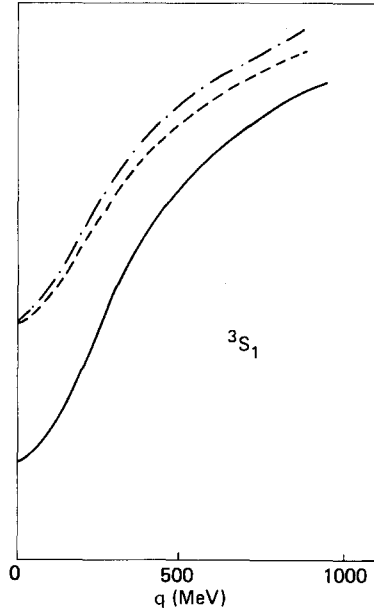


Fig. 41. The same for the (diagonal) 3S_1 partial wave.

proceeds in the same way as shown in the last section and in the appendix for the case of NN intermediate states, using now the well-known projection operator for the Δ -isobar (spin 3/2)

$$P^{\mu\nu}(\mathbf{k}) = \Lambda_+(\mathbf{k}) [-g^{\mu\nu} + \frac{1}{3}\gamma^\mu\gamma^\nu + \frac{2}{3}k^\mu k^\nu/m_\Delta^2 + \frac{1}{3}(\gamma^\mu k^\nu - \gamma^\nu k^\mu)/m_\Delta] \quad (9.7)$$

together with the isobar vertex-functions $W^{(\Delta,\pi)}$ (eq. (5.4)). Details may be found in ref. [69].

Neglecting isospin, it was pointed out in ref. [51] that, when all particles are at rest (i.e. energies are replaced by corresponding masses), the non-iterative box diagrams are 3/8 of the iterative ones and, moreover, the crossed-box diagrams give a contribution which is 7/8 of the iterative diagrams. Fig. 40 shows that this remains roughly to be true for our unapproximated model in the 1S_0 -channel; on the other hand, in the (diagonal) 3S_1 -channel shown in fig. 41, such an approximation grossly overestimates the contribution of the non-iterative diagrams (i.e. recoil effects suppress these contributions more strongly than the iterative ones).

Within this approximation (putting all particles at rest), the sum of all time orderings for crossed and uncrossed exchanges looks like the iteration of a Yukawa potential of pion range, usually used in the transition potential concept. Obviously, this statement is consistent with the result shown e.g. in ref. [56] that the use of pion range instead of exact time-ordered propagators enhances the contribution of the iterative isobar diagrams by a factor 2–3.

Consequently, a transition potential of pion range can approximate the exact result only in the 1S_0 -channel, it will considerably overestimate it in the 3S_1 -channel.

Including isospin, the above conclusions can be taken over for the isoscalar exchange piece of the sum of crossed and uncrossed diagrams, since there both terms have the same sign. Thus, a transition potential of pion range can describe this isoscalar piece roughly in the 1S_0 -channel, but overestimates it in the 3S_1 -channel. The isovector piece is relatively small since here crossed and uncrossed diagrams have opposite signs. Our explicit calculations have shown that the simple prescription of

- (i) taking a transition potential of pion range and
- (ii) dropping the isovector part is reasonable for 1S_0 , but overestimates the isobar contribution in the important 3S_1 -channel (only crossed diagrams occur there) by a factor of 2. (Of course, a transition potential with the complete isospin-dependence will yield no contribution at all in the 3S_1 -channel. Thus the true result lies between these two extremes.)

9.3. Effects in NN scattering

In order to show the effect of these non-iterative diagrams on nucleon–nucleon scattering phase shifts, we use as effective potential

$$V_{\text{eff}}(z) = V_{\text{OBE}}(z) + M_{N\Delta}(z) + M_{\Delta\Delta}(z) + M'_{NN}(z) + M'_{N\Delta}(z). \quad (9.8)$$

Here, V_{OBE} is the one-boson-exchange potential of ref. [43].* $M_{N\Delta}(M_{\Delta\Delta})$ denotes the sum of iterative diagrams with $N\Delta(\Delta\Delta)$ intermediate states including π - and ρ -exchange (eqs. (6.16, 6.17)). $M'_{NN}(M'_{N\Delta})$ denotes the sum of non-iterative diagrams with $NN(N\Delta)$ intermediate states including only π -exchange. The corresponding diagrams are shown in fig. 42. Using the formulas of section 7.1, the scattering phase shifts can be obtained from R^J in the usual way.

The meson parameters are shown in table 8. Concerning the $\pi N\Delta$ -coupling constant, we now take the value favoured by the quark model, i.e. we consider our Δ -isobar to be an explicit new particle (which is not necessarily identical with the empirical πN -resonance in the $(\frac{3}{2}\frac{3}{2})$ -channel). Otherwise, we would run into problems of double-counting, since e.g. we include also M'_{NN} . In the explicit higher-order diagrams, we use throughout $\Lambda_\pi = 1$ GeV, whereas the fit requires $\Lambda_\pi = 1.4$ GeV in V_{OBE} . We feel justified to use different values for Λ_π at the present stage. In our model, the form factors have still to be considered to be essentially phenomenological quantities, which effectively replace contributions still not included in the present model. For example, the inclusion of explicit 3π -exchange diagrams,

Table 8
Parameters for $V_{\text{eff}}(z)$ (eq. (9.8)). m_α and Λ_α are given in MeV. The number in brackets denotes the ratio of coupling constants f_ρ/g_ρ . Λ_α denotes the cutoff-mass in the OBE-vertices, whereas Λ'_α denotes the cutoff-mass at all other vertices

	π	η	σ	δ	ω	ρ
$g_{NN\alpha}^2(k^2 = m_\alpha^2)$	14.4	8.4	15.902	0.451	30	0.78 (4.85)
$g_{NN\alpha}^2(k^2 = 0)$	14.26	7.11	12.47	0.24	20.62	0.55 (4.85)
m_α	138	548.5	650	960	782.8	763
Λ_α	1400	1400	1400	1400	1400	1400
Λ'_α	1000				1500	
$f_{N\Delta\alpha}^2$	0.23				15.08	

* Now $F_\alpha \equiv (\Lambda_\alpha^2 - m_\alpha^2)/(\Lambda_\alpha^2 + (\mathbf{q}' - \mathbf{q})^2)$ at all vertices.

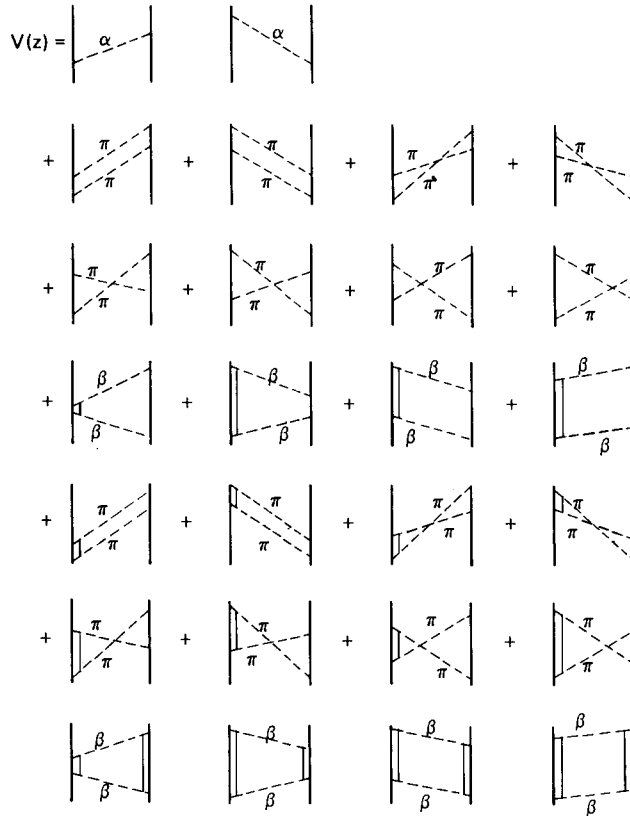


Fig. 42. Diagrams included in the model of eq. (9.8). The solid line denotes a nucleon, the double-solid line a Δ -isobar. $\alpha = \pi, \eta, \sigma, \delta, \rho, \omega$ and $\beta = \pi, \rho$. Corresponding diagrams where the Δ appears on the right-hand side are not shown but are included in the calculations.

which are expected to influence the inner part of the tensor force, might ultimately make it possible to use $\Lambda_\pi = 1$ GeV (which is suggested by model calculations [31]) throughout. Anyhow, due to their short range, a reliable description of form factors might require to take into account quark-theoretical view-points, which is only in its infancy nowadays. The parameters are partly adjusted in order to obtain a reasonable description of the NN-scattering phase shifts. The resulting low-energy parameters are shown in table 5, too.

The results for some important phase shifts are shown in figs. 43–49. The solid lines are obtained when V_{eff} (eq. (9.8)) is used in eq. (7.3). The dashed lines result when $M'_{NN}^{\pi\pi}$ is omitted; for the dotted line, $(M'_{NN}^{\pi\pi} + M'_{N\Delta}^{\pi\pi})$ is omitted; the dash-dot curve is based on the use of V_{OBE} only, whereas the dash-double-dot curve is obtained when, in addition, the σ -contribution in V_{OBE} is omitted describing effectively the part of the whole 2π -exchange which is not described explicitly. The error bars are taken from the analysis of ref. [14].

Obviously, a good agreement with empirical phase shifts is obtained. Again, compared to OBE-models, the 3D_2 phase shifts are lowered considerably, i.e. there is a strong improvement, which was already found when only box diagrams were included, see fig. 36. That this effect persists after inclusion of non-iterative diagrams can be mainly traced back to the behaviour of $M'_{NN}^{\pi\pi}$: It is attractive in 3S_1 (because of the sizeable contribution of the stretched-box diagrams just in this partial wave) but

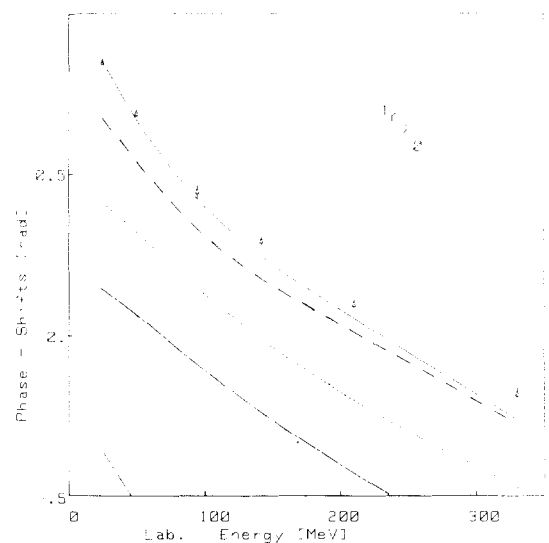


Fig. 43.

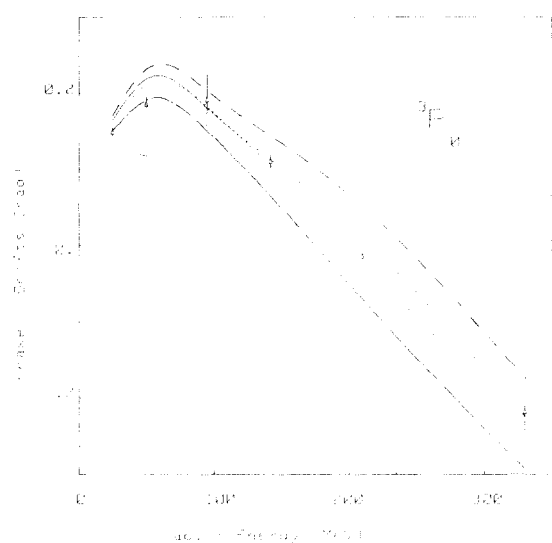


Fig. 44.

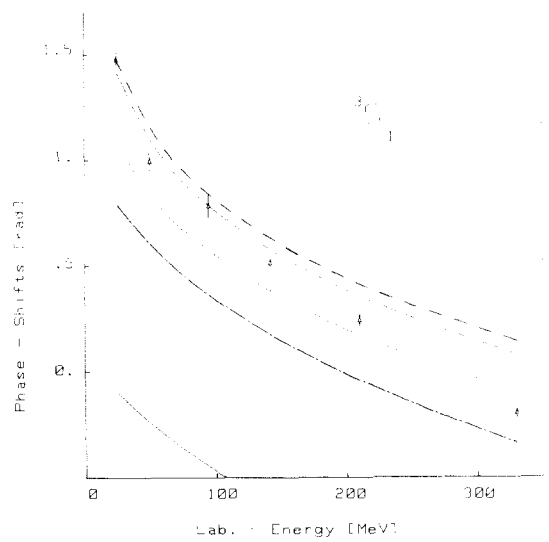


Fig. 45.

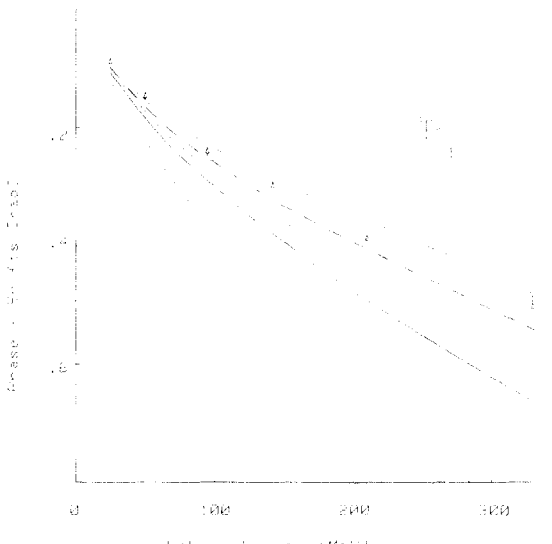


Fig. 46.

negligible in 3D_2 (due to a cancellation between stretched- and crossed-box diagrams in this partial wave). Therefore, a readjustment of 3S_1 will lower 3D_2 .

In general, the stretched-box diagrams of M'_{NN}^π give a small contribution only. The effect is negligible in 1S_0 but sizeable in 3S_1 , which is due to the isospin factor being 1 in 1S_0 but 9 in 3S_1 . Concerning the crossed-box diagrams of M'_{NN}^π , the isospin factor is 5 in 1S_0 , but -3 in 3S_1 , i.e. it even changes sign. Therefore, this contribution is attractive in 1S_0 but repulsive in 3S_1 . There is a strong (repulsive) effect in 3P_0 , even for lower energies. This is in line with what is known already from dispersion-theoretical

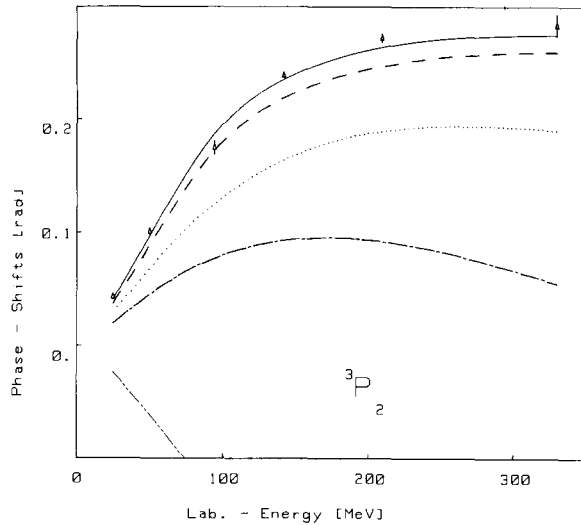


Fig. 47.

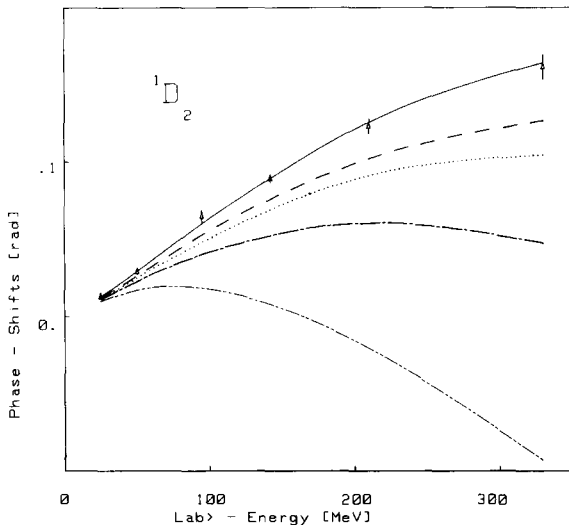


Fig. 48.

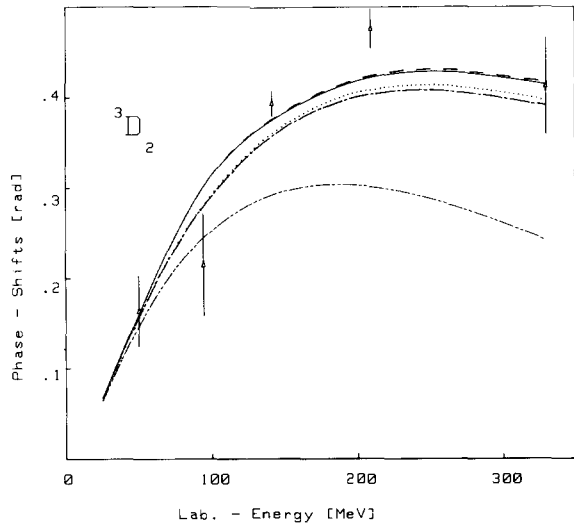


Fig. 49.

Figs. 43–49. Nucleon–nucleon bar phase shifts (in radians) as a function of the nucleon lab energy (in MeV). The error bars are taken from the energy-independent Livermore analysis [14]. Results for the full V_{eff} (eq. (9.8)) are denoted by the solid curves. For the dashed curves, $M'_{\text{NN}}^{\pi\pi}$ has been omitted, while in the dotted curves ($M'_{\text{NN}}^{\pi\pi} + M'_{\Delta\Delta}^{\pi\pi}$) is omitted. The dashed curve contains only the V_{OBE} -part of eq. (9.8), whereas the dash-double-dot curve is obtained when, in addition, the σ -contribution in V_{OBE} is omitted.

calculations. Namely, the crossed-box diagrams build up the long-range (non-resonant) part of the 2π -exchange contribution in the $\rho(1^-)$ -channel.

In order to give a quantitative impression of the size of the effects discussed above in an OBE-language, we note that $M'_{\text{NN}}^{\pi\pi}$ replaces roughly 10% of the σ and 20% of the ρ in the OBEP of ref. [43].

Concerning the non-iterative isobar diagrams ($M'_{\Delta\Delta}^{\pi\pi}$), the figures clearly demonstrate that they are as important as isobar box diagrams ($M_{\Delta\Delta} + M_{\text{NA}}$). (We believe that ρ -exchange will not drastically reduce the importance of $M'_{\Delta\Delta}^{\pi\pi}$.) Especially in isospin-zero states (where M_{NA} does not contribute), the isobar contribution is drastically enlarged, see e.g. ${}^3\text{D}_2$. Consequently, the inclusion of $M'_{\Delta\Delta}^{\pi\pi}$ in the evaluation

of the Δ -probability of the deuteron, which has not been done so far, should lead to a considerable enhancement, too.

9.4. Effects in nuclear matter

According to our general scheme, also the non-iterative diagrams should be suppressed in the medium. The modification of $M'_{NN}^{\pi\pi}$ is studied in detail in the paper of Müther et al. [70]. It turns out that $M'_{NN}^{\pi\pi}$ is suppressed by only 20% (compared to 30% in the case of isobar box diagrams, see section 8) which can be traced back to the relatively short range of non-iterative diagrams involving more high-momentum components. Since, furthermore, $M'_{NN}^{\pi\pi}$ describes roughly 10% of the intermediate-range attraction (yielding about 100 MeV binding at nuclear matter density), the repulsive effect generated by the modification of $M'_{NN}^{\pi\pi}$ is roughly 6 times smaller than for the isobar box diagrams studied before, i.e. only ≈ 2 MeV at empirical nuclear matter density, which is small but not negligible.

Corresponding calculations with $M'_{N\Delta}^{\pi\pi}$ are under way [71]. We expect a repulsive effect of roughly the same size as for $M'_{NN}^{\pi\pi}$: On one hand, $M'_{N\Delta}^{\pi\pi}$ is still shorter-ranged; on the other hand, its contribution is larger.

9.5. Other non-iterative diagrams

For consistency, the non-iterative diagrams involving $\Delta\Delta$ -intermediate states should be included, too. Such calculations are in progress [72]. This will make it possible to test arguments raised in ref. [67] about the combined effect of non-iterative 2π -exchange diagrams involving NN-, $N\Delta$ -, and $\Delta\Delta$ -intermediate states. Furthermore, diagrams with non-iterative (π, α) -exchange ($\alpha = \sigma, \rho, \omega$) are known to contribute sizeably to the medium-range part of the tensor force and are thus of outstanding importance. We have recently finished the evaluation of all these diagrams and are now studying their role in NN-scattering [73]. On the other hand, we believe that such diagrams are already too short-ranged to be noticeably modified at empirical nuclear matter density.

10. Summary and outlook

Recent nuclear matter calculations have shown that

- (a) a precise knowledge of the tensor force in the NN-interaction,
- (b) an explicit description of the intermediate-range attraction, are absolutely essential to obtain saturation at empirical density.

We have seen that strong ρ -exchange (which is favoured from πN -studies) together with some structure at the πNN -vertex points to a rather weak tensor force, characterized by a deuteron D-state probability of 4–5%. Final conclusions can, however, not be made before non-iterative diagrams like those involving (π, α) , $\alpha = \sigma, \rho, \omega$ have been included.

The Δ -isobar plays an outstanding role in an explicit dynamical model for the 2π -exchange contribution. However, not only the iterative isobar box diagrams, but also the non-iterative diagrams (involving NN-, $N\Delta$ -, and $\Delta\Delta$ -intermediate states) have to be considered. According to our calculations, such contributions replace roughly 50% of the σ -exchange in OBE-models providing the intermediate-range attraction. The other part is mainly given by rescattering contributions (involving diagrams in which the two exchanged pions interact). They must be included before a realistic and explicit model for

the total 2π -exchange contribution is obtained, which, in two-body scattering, agrees satisfactorily with the result of dispersion-theoretic models. At present, the rescattering part is still effectively described by σ -exchange in our model. We expect, however, that the main modification of the 2π -exchange contribution occurs in those diagrams already described explicitly.

Up to now, the nuclear matter calculations have been done with our explicit model only in a first-order (two-hole-line) Brueckner calculation. It is essential to study also higher-order contributions (three-hole-line etc.) before one can come to any conclusions regarding the validity of our model.

As a whole, we are deeply convinced that a purely phenomenological treatment of the nuclear force and the nuclear matter problem will not be able to provide a realistic description of the nuclear matter system. A meson theory of the nuclear force is inevitably required. On the other hand, we still believe that a theory of the nuclear force in terms of meson exchange is also the adequate level for this system, i.e. there is good reason to hope that quark degrees of freedom will come into play only at much more extreme physical situations like neutron stars or deep inelastic scattering.

Acknowledgement

It is a deep pleasure for me to thank my teacher, Prof. K. Bleuler, for many stimulating discussions during the course of this work. Special thanks are due to Prof. G.E. Brown for numerous enlightening discussions and critical comments during my stay at NORDITA for the spring semester 1978. Further discussions with Profs. H.A. Bethe, A.M. Green, F. Gross, E. Lomon, J.J. de Swart and R. Vinh Mau are gratefully acknowledged. Finally, I want to take this opportunity to thank Prof. A. Fäßler, Prof. H. Müther, Dr. M. Anastasio and especially Dr. R. Machleidt for the steady and fruitful collaboration in the last years, out of which grew most of the results described in this article.

Appendix

The spin sum of eq. (9.1) can be evaluated with the help of positive-energy nucleon projection operators Λ_+ .

$$\Lambda_+(\mathbf{k}) = \frac{\gamma^0 E_k - \boldsymbol{\gamma} \cdot \mathbf{k} + m}{2m}. \quad (\text{A.1})$$

This gives

$$\begin{aligned} & \sum_{h_1, h_2} \bar{u}_{A_2}(-\mathbf{q}') i\gamma^5 u_{h_2}(-\mathbf{k}) \bar{u}_{h_2}(-\mathbf{k}) i\gamma^5 u_{A_2}(-\mathbf{q}) \bar{u}_{A_1}(\mathbf{q}') i\gamma^5 u_{h_1}(\mathbf{k}) \bar{u}_{h_1}(\mathbf{k}) i\gamma^5 u_{A_1}(\mathbf{q}) \\ &= \frac{m^2}{E_k^2} \bar{u}_{A_2}(-\mathbf{q}') \gamma^5 \Lambda_+(-\mathbf{k}) \gamma^5 u_{A_2}(-\mathbf{q}) \bar{u}_{A_1}(\mathbf{q}') \gamma^5 \Lambda_+(\mathbf{k}) \gamma^5 u_{A_1}(\mathbf{q}) \\ &= \frac{1}{4E_k^2} \bar{u}_{A_2}(-\mathbf{q}') [\gamma^0 E_k + \boldsymbol{\gamma} \cdot \mathbf{k} + m] \gamma^5 u_{A_2}(-\mathbf{q}) \bar{u}_{A_1}(\mathbf{q}') \gamma^5 [\gamma^0 E_k - \boldsymbol{\gamma} \cdot \mathbf{k} + m] \gamma^5 u_{A_1}(\mathbf{q}) \\ &= \frac{1}{4E_k^2} \bar{u}_{A_2}(-\mathbf{q}) [\gamma^0 E_k + \boldsymbol{\gamma} \cdot \mathbf{k} - m] u_{A_2}(-\mathbf{q}) \bar{u}_{A_1}(\mathbf{q}') [\gamma^0 E_k - \boldsymbol{\gamma} \cdot \mathbf{k} - m] u_{A_1}(\mathbf{q}). \end{aligned} \quad (\text{A.2})$$

Since we want to do the integration over \mathbf{k} using polar coordinates, we must get rid of the $\gamma \cdot \mathbf{k}$ -term. Therefore, we expand \mathbf{k} in terms of \mathbf{q} , \mathbf{q}' and $\mathbf{q}' \times \mathbf{q}$

$$\mathbf{k} = a\mathbf{q} + b\mathbf{q}' + c\mathbf{q}' \times \mathbf{q}/|\mathbf{q}' \times \mathbf{q}| \quad (\text{A.3})$$

with

$$a = \frac{\mathbf{q}' \cdot \mathbf{q} \mathbf{q}' \cdot \mathbf{k} - q'^2 \mathbf{q} \cdot \mathbf{k}}{(\mathbf{q}' \cdot \mathbf{q})^2 - q'^2 q'^2}, \quad b = \frac{\mathbf{q}' \cdot \mathbf{q} \mathbf{q} \cdot \mathbf{k} - q^2 \mathbf{q}' \cdot \mathbf{k}}{(\mathbf{q}' \cdot \mathbf{q})^2 - q^2 q'^2}, \quad c = \frac{\mathbf{q}' \times \mathbf{q}}{|\mathbf{q}' \times \mathbf{q}|} \cdot \mathbf{k}. \quad (\text{A.4})$$

Thus, $\gamma \cdot \mathbf{k}$ can be replaced by

$$\gamma \cdot \mathbf{k} = a\gamma \cdot \mathbf{q} + b\gamma \cdot \mathbf{q}' + c\gamma \cdot \frac{\mathbf{q}' \times \mathbf{q}}{|\mathbf{q}' \times \mathbf{q}|}. \quad (\text{A.5})$$

Using the Dirac equation, the expression (A.2) becomes

$$\begin{aligned} & \frac{1}{4E_k^2} \bar{u}_{A_2}(-\mathbf{q}') \left[(aE_q + bE_{q'} - E_k)\gamma^0 + m(1-a-b) - c\gamma \cdot \frac{\mathbf{q}' \times \mathbf{q}}{|\mathbf{q}' \times \mathbf{q}|} \right] u_{A_2}(-\mathbf{q}) \\ & \times \bar{u}_{A_1}(\mathbf{q}') \left[(aE_q + bE_{q'} - E_k)\gamma^0 + m(1-a-b) + c\gamma \cdot \frac{\mathbf{q}' \times \mathbf{q}}{|\mathbf{q}' \times \mathbf{q}|} \right] u_{A_1}(\mathbf{q}). \end{aligned} \quad (\text{A.6})$$

If we choose \mathbf{q} to be in the z -axis and \mathbf{q}' to be in the xz -plane, $\gamma \cdot \mathbf{q}' \times \mathbf{q}/|\mathbf{q}' \times \mathbf{q}| = -\gamma^2$ and terms linear in c disappear after angle integration. Thus (A.2) becomes

$$\begin{aligned} & \frac{1}{4E_k^2} m^2(1-a-b)^2 [\bar{u}_{A_2}(-\mathbf{q}') u_{A_2}(-\mathbf{q}) \bar{u}_{A_1}(\mathbf{q}') u_{A_1}(\mathbf{q})] \\ & + m(1-a-b)(aE_q + bE_{q'} - E_k) [\bar{u}_{A_2}(-\mathbf{q}') \gamma^0 u_{A_2}(-\mathbf{q}) \bar{u}_{A_1}(\mathbf{q}') u_{A_1}(\mathbf{q}) \\ & + \bar{u}_{A_2}(-\mathbf{q}') u_{A_2}(-\mathbf{q}) \bar{u}_{A_1}(\mathbf{q}') \gamma^0 u_{A_1}(\mathbf{q})] \\ & + (aE_q + bE_{q'} - E_k)^2 [\bar{u}_{A_2}(-\mathbf{q}') \gamma^0 u_{A_2}(-\mathbf{q}) \bar{u}_{A_1}(\mathbf{q}') \gamma^0 u_{A_1}(\mathbf{q})] \\ & - c^2 [\bar{u}_{A_2}(-\mathbf{q}') \gamma^2 u_{A_2}(-\mathbf{q}) \bar{u}_{A_1}(\mathbf{q}') \gamma^2 u_{A_1}(\mathbf{q})]. \end{aligned} \quad (\text{A.7})$$

The unpleasant $\gamma^2 \gamma^2$ -term can be replaced by using

$$\gamma^2 \gamma^2 = \gamma \cdot \gamma - (\gamma^1 \gamma^1 + \gamma^3 \gamma^3) = \gamma \cdot \gamma - a' \gamma \cdot \mathbf{q}' \gamma \cdot \mathbf{q}' - b' (\gamma \cdot \mathbf{q}' \gamma \cdot \mathbf{q} + \gamma \cdot \mathbf{q} \gamma \cdot \mathbf{q}') - c' \gamma \cdot \mathbf{q} \gamma \cdot \mathbf{q} \quad (\text{A.8})$$

with

$$a' = \frac{1}{q'^2 \sin^2 \theta}, \quad b' = -\frac{\cos \theta}{q' q \sin^2 \theta}, \quad c' = \frac{1}{q^2 \sin^2 \theta} \quad (\text{A.9})$$

where θ is the angle between \mathbf{q} and \mathbf{q}' . Thus, we obtain using (A.8) and the Dirac equation,

$$\begin{aligned} & \bar{u}_{\Lambda_2}(-\mathbf{q}') \gamma^2 u_{\Lambda_2}(-\mathbf{q}) \bar{u}_{\Lambda_1}(\mathbf{q}') \gamma^2 u_{\Lambda_1}(\mathbf{q}) \\ &= \bar{u}_{\Lambda_2}(-\mathbf{q}') \gamma u_{\Lambda_2}(-\mathbf{q}) \bar{u}_{\Lambda_1}(\mathbf{q}') \gamma u_{\Lambda_1}(\mathbf{q}) + m^2(a' + 2b' + c') \bar{u}_{\Lambda_2}(-\mathbf{q}') u_{\Lambda_2}(-\mathbf{q}) \bar{u}_{\Lambda_1}(\mathbf{q}') u_{\Lambda_1}(\mathbf{q}) \\ &+ (E_{q'}^2 a' + E_q^2 c' + 2E_q E_q b') \bar{u}_{\Lambda_2}(-\mathbf{q}') \gamma^0 u_{\Lambda_2}(-\mathbf{q}) \bar{u}_{\Lambda_1}(\mathbf{q}') \gamma^0 u_{\Lambda_1}(\mathbf{q}) \\ &- m(E_{q'} a' + E_q c' + (E_{q'} + E_q)b') [\bar{u}_{\Lambda_2}(-\mathbf{q}') \gamma^0 u_{\Lambda_2}(-\mathbf{q}) \bar{u}_{\Lambda_1}(\mathbf{q}') u_{\Lambda_1}(\mathbf{q}) \\ &+ \bar{u}_{\Lambda_2}(-\mathbf{q}') u_{\Lambda_2}(-\mathbf{q}) \bar{u}_{\Lambda_1}(\mathbf{q}') \gamma^0 u_{\Lambda_1}(\mathbf{q})]. \end{aligned} \quad (\text{A.10})$$

Eq. (9.1) can finally be written as

$$\begin{aligned} & \langle \mathbf{q}' \Lambda'_1 \Lambda'_2 | M'_{NN,1}^{(1)}(z) | \mathbf{q} \Lambda_1 \Lambda_2 \rangle = \frac{(4\pi)^2}{(2\pi)^6} g_{NN\pi}^4 (3 - 2\tau_1 \cdot \tau_2) \\ & \times \sum_{i=1}^4 A_i(\mathbf{q}' \Lambda'_1 \Lambda'_2; \mathbf{q} \Lambda_1 \Lambda_2) \cdot \int \frac{d^3 k I_i^{(1)}(\mathbf{q}', \mathbf{q}, \mathbf{k}) F_\pi^2[(\mathbf{q}' - \mathbf{k})^2] F_\pi^2[(\mathbf{q} - \mathbf{k})^2]}{16E_k^2 \omega_{q'-k} \omega_{q'-k} D_1^{(1)}(\mathbf{q}', \mathbf{q}, \mathbf{k})} \end{aligned} \quad (\text{A.11})$$

where

$$\begin{aligned} A_1 &= \bar{u}_{\Lambda_2}(-\mathbf{q}') u_{\Lambda_2}(-\mathbf{q}) \bar{u}_{\Lambda_1}(\mathbf{q}') u_{\Lambda_1}(\mathbf{q}) \\ A_2 &= [\bar{u}_{\Lambda_2}(-\mathbf{q}') \gamma^0 u_{\Lambda_2}(-\mathbf{q}) \bar{u}_{\Lambda_1}(\mathbf{q}') u_{\Lambda_1}(\mathbf{q}) + \bar{u}_{\Lambda_2}(-\mathbf{q}') u_{\Lambda_2}(-\mathbf{q}) \bar{u}_{\Lambda_1}(\mathbf{q}') \gamma^0 u_{\Lambda_1}(\mathbf{q})] \cdot \frac{1}{2} \\ A_3 &= \bar{u}_{\Lambda_2}(-\mathbf{q}') \gamma^0 u_{\Lambda_2}(-\mathbf{q}) \bar{u}_{\Lambda_1}(\mathbf{q}') \gamma^0 u_{\Lambda_1}(\mathbf{q}) \\ A_4 &= \bar{u}_{\Lambda_2}(-\mathbf{q}') \gamma u_{\Lambda_2}(-\mathbf{q}) \bar{u}_{\Lambda_1}(\mathbf{q}') \gamma u_{\Lambda_1}(\mathbf{q}) \end{aligned} \quad (\text{A.12})$$

and

$$\begin{aligned} I_1^{(1)} &= m^2[(1 - a - b)^2 - c^2(a' + 2b' + c')] \\ I_2^{(1)} &= 2m[(1 - a - b)(E_q a + E_{q'} b - E_k) + c^2(E_{q'} a' + (E_{q'} + E_q)b' + E_{q'} c')] \\ I_3^{(1)} &= (E_q a + E_{q'} b - E_k)^2 - c^2(E_{q'}^2 a' + 2E_{q'} E_q b' + E_{q'}^2 c') \\ I_4^{(1)} &= -c^2 \\ D_1^{(1)} &= (z - E_{q'} - E_k - \omega_{q'-k})(z - E_{q'} - E_q - \omega_{q'-k} - \omega_{q-k})(z - E_q - E_k - \omega_{q-k}). \end{aligned} \quad (\text{A.13})$$

The contribution of the third diagram in fig. 38 is given by

$$\begin{aligned} & \langle \mathbf{q}' \Lambda'_1 \Lambda'_2 | M'_{NN,1}^{(2)}(z) | \mathbf{q} \Lambda_1 \Lambda_2 \rangle = \frac{(4\pi)^2}{(2\pi)^6} g_{NN\pi}^4 (3 + 2\tau_1 \cdot \tau_2) \\ & \times \sum_{h_1, h_2} \int \frac{d^3 k F_\pi^2[(\mathbf{q}' - \mathbf{k})^2] F_\pi^2[(\mathbf{q} - \mathbf{k})^2]}{4\omega_{q'-k} \omega_{q'-k}} \times \frac{\bar{u}_{\Lambda_2}(-\mathbf{q}') i \gamma^5 u_{h_2}(\mathbf{k} - \mathbf{q} - \mathbf{q}')}{(z - E_{q'} - E_{k-q-q'} - \omega_{q-k})} \end{aligned}$$

$$\times \frac{\bar{u}_{h_2}(\mathbf{k} - \mathbf{q} - \mathbf{q}') i\gamma^5 u_{A_2}(-\mathbf{q}) \bar{u}_{A_1}(\mathbf{q}') i\gamma^5 u_{h_1}(\mathbf{k}) \bar{u}_{h_1}(\mathbf{k}) i\gamma^5 u_{A_1}(\mathbf{q})}{(z - E_k - E_{k-q-q'} - \omega_{q-k} - \omega_{q'-k})(z - E_q - E_{k-q-q'} - \omega_{q'-k})}. \quad (\text{A.14})$$

We obtain for the spin sum

$$\begin{aligned} & \sum_{h_1, h_2} \bar{u}_{A_2}(-\mathbf{q}') i\gamma^5 u_{h_2}(\mathbf{k} - \mathbf{q} - \mathbf{q}') \bar{u}_{h_2}(\mathbf{k} - \mathbf{q} - \mathbf{q}') i\gamma^5 u_{A_2}(-\mathbf{q}) \bar{u}_{A_1}(\mathbf{q}') i\gamma^5 u_{h_1}(\mathbf{k}) \bar{u}_{h_1}(\mathbf{k}) i\gamma^5 u_{A_1}(\mathbf{q}) \\ &= \frac{m^2}{E_k E_{k-q-q'}} \bar{u}_{A_2}(-\mathbf{q}') \gamma^5 \Lambda_+ (\mathbf{k} - \mathbf{q} - \mathbf{q}') \gamma^5 u_{A_2}(-\mathbf{q}) \bar{u}_{A_1}(\mathbf{q}') \gamma^5 \Lambda_+ (\mathbf{k}) \gamma^5 u_{A_1}(\mathbf{q}) \\ &= \frac{1}{4E_k E_{k-q-q'}} \bar{u}_{A_2}(-\mathbf{q}') \gamma^5 [\gamma^0 E_{k-q-q'} - \boldsymbol{\gamma} \cdot (\mathbf{k} - \mathbf{q} - \mathbf{q}') + m] \gamma^5 u_{A_2}(-\mathbf{q}) \\ &\quad \times \bar{u}_{A_1}(\mathbf{q}') \gamma^5 [\gamma^0 E_k - \boldsymbol{\gamma} \cdot \mathbf{k} + m] \gamma^5 u_{A_1}(\mathbf{q}) \\ &= \frac{1}{4E_k E_{k-q-q'}} \bar{u}_{A_2}(-\mathbf{q}') [\gamma^0 E_{k-q-q'} - \boldsymbol{\gamma} \cdot (\mathbf{k} - \mathbf{q} - \mathbf{q}') - m] u_{A_2}(-\mathbf{q}) \bar{u}_{A_1}(\mathbf{q}') [\gamma^0 E_k - \boldsymbol{\gamma} \cdot \mathbf{k} - m] u_{A_1}(\mathbf{q}). \end{aligned} \quad (\text{A.15})$$

Using again the expansion (A.3) for \mathbf{k} and the Dirac equation, (A.15) goes into

$$\begin{aligned} & \frac{1}{4E_k E_{k-q-q'}} \bar{u}_{A_2}(-\mathbf{q}') \left[(E_q(1-a) + E_{q'}(1-b) - E_{k-q-q'}) \gamma^0 - m(1-a-b) + c \boldsymbol{\gamma} \cdot \frac{\mathbf{q}' \times \mathbf{q}}{|\mathbf{q}' \times \mathbf{q}|} \right] u_{A_2}(-\mathbf{q}) \\ & \times \bar{u}_{A_1}(\mathbf{q}') \left[(aE_q + bE_{q'} - E_k) \gamma^0 + m(1-a-b) + c \boldsymbol{\gamma} \cdot \frac{\mathbf{q}' \times \mathbf{q}}{|\mathbf{q}' \times \mathbf{q}|} \right] u_{A_1}(\mathbf{q}). \end{aligned} \quad (\text{A.16})$$

Using the same arguments as before and symmetrizing the result by an appropriate change of integration variables, eq. (A.14) can be written as

$$\begin{aligned} \langle \mathbf{q}' \Lambda'_1 \Lambda'_2 | M'_{NN,1}(z) | \mathbf{q} \Lambda_1 \Lambda_2 \rangle &= \frac{(4\pi)^2}{(2\pi)^6} g_{NN\pi}^4 (3 + 2\boldsymbol{\tau}_1 \cdot \boldsymbol{\tau}_2) \sum_{i=1}^4 A_i(\mathbf{q}' \Lambda'_1 \Lambda'_2; \mathbf{q} \Lambda_1 \Lambda_2) \\ &\times \int \frac{d^3 k I_i^{(2)}(\mathbf{q}', \mathbf{q}, \mathbf{k}) F_\pi^2[(\mathbf{q}' - \mathbf{k})^2] F_\pi^2[(\mathbf{q} - \mathbf{k})^2]}{16E_k E_{k-q-q'} \omega_{q-k} \omega_{q'-k} D_i^{(2)}(\mathbf{q}', \mathbf{q}, \mathbf{k})} \end{aligned} \quad (\text{A.17})$$

with

$$\begin{aligned} I_1^{(2)} &= -m^2[(1-a-b)^2 - c^2(a' + 2b' + c')] \\ I_2^{(2)} &= m(1-a-b)[(E_q(1-a) + E_{q'}(1-b) - E_{k-q-q'}) + (E_k - E_q a - E_{q'} b)] \\ &\quad - 2c^2(E_{q'} a' + (E_{q'} + E_q) b' + E_{q'} c') m \\ I_3^{(2)} &= (E_q(1-a) + E_{q'}(1-b) - E_{k-q-q'})(E_q a + E_{q'} b - E_k) + c^2(E_{q'}^2 a' + 2E_{q'} E_q b' + E_q^2 c') \\ I_4^{(2)} &= c^2 \end{aligned} \quad (\text{A.18})$$

and

$$D_1^{(2)} = (z - E_{q'} - E_{k-q-q'} - \omega_{q-k})(z - E_k - E_{k-q-q'} - \omega_{q-k} - \omega_{q'-k})(z - E_q - E_{k-q-q'} - \omega_{q'-k}). \quad (\text{A.19})$$

The other five crossed-box diagrams of fig. 38 give the same result apart from the energy denominators. In the order of fig. 38, $D_1^{(2)}$ in eq. (A.17) has to be replaced by

$$\begin{aligned} D_2^{(2)} &= (z - E_{q'} - E_k - \omega_{q'-k})(z - E_k - E_{k-q-q'} - \omega_{q'-k} - \omega_{q-k})(z - E_q - E_k - \omega_{q-k}) \\ D_3^{(2)} &= (z - E_{q'} - E_{k-q-q'} - \omega_{q-k})(z - E_k - E_{k-q-q'} - \omega_{q'-k} - \omega_{q-k})(z - E_q - E_k - \omega_{q-k}) \\ D_4^{(2)} &= (z - E_{q'} - E_k - \omega_{q'-k})(z - E_k - E_{k-q-q'} - \omega_{q'-k} - \omega_{q-k})(z - E_q - E_{k-q-q'} - \omega_{q'-k}) \\ D_5^{(2)} &= (z - E_{q'} - E_{k-q-q'} - \omega_{q-k})(z - E_{q'} - E_q - \omega_{q'-k} - \omega_{q-k})(z - E_q - E_k - \omega_{q-k}) \\ D_6^{(2)} &= (z - E_{q'} - E_k - \omega_{q'-k})(z - E_{q'} - E_q - \omega_{q'-k} - \omega_{q-k})(z - E_q - E_{k-q-q'} - \omega_{q'-k}). \end{aligned} \quad (\text{A.20})$$

References

- [1] K. Erkelenz, Phys. Rep. 13C (1974) 191.
- [2] R.V. Reid, Ann. of Phys. 50 (1968) 411.
- [3] K. Holinde and R. Machleidt, Nucl. Phys. A247 (1975) 495.
- [4] K. Holinde and R. Machleidt, Nucl. Phys. A256 (1976) 479.
- [5] M. Lacombe, B. Loiseau, J.M. Richard, R. Vinh Mau, P. Pirès and R. de Tourreil, Phys. Rev. D12 (1975) 1495.
- [6] R.A. Bryan and A. Gersten, Phys. Rev. D6 (1972) 341.
- [7] B.D. Day, Rev. Mod. Phys. 50 (1978) 495.
- [8] H.A. Bethe, Ann. Rev. Nucl. Sci. 21 (1971) 23.
- [9] M.M. Nagels, T.A. Rijken and J.J. de Swart, Phys. Rev. D15 (1977) 2547.
- [10] H. Arenhövel and W. Fabian, Nucl. Phys. A282 (1977) 397.
- [11] C. DeTar, Phys. Rev. D17 (1978) 323.
- [12] G.E. Brown, Chiral Symmetry and the Nucleon–Nucleon Interaction, in: Mesons in Nuclei, eds. M. Rho and D. Wilkinson (North-Holland, 1979).
- [13] D.V. Bugg, A.A. Carter and J.R. Carter, Phys. Lett. 44B (1973) 248.
- [14] M. McGregor, R. Arndt and R. Wright, Phys. Rev. 182 (1969) 1714.
- [15] K. Holinde and H. Mundelius, preprint, to be published.
- [16] R.A. Bjorken and S. Drell, Relativistic Quantum Mechanics (McGraw-Hill, New York, 1964).
- [17] P.A. Verhoeven, thesis, Nijmegen 1976, unpublished.
- [18] G. Höhler and E. Pietarinen, Nucl. Phys. B95 (1975) 210.
- [19] G. Höhler et al., Nucl. Phys. B114 (1976) 505.
- [20] W. Grein, Nucl. Phys. B131 (1977) 255.
- [21] E. Lomon, Proc. Int. Conf. on the Nucleon–Nucleon Interaction, Vancouver (1977) p. 554.
- [22] W. Nutt and B. Loiseau, Nucl. Phys. B104 (1976) 98.
- [23] K. Holinde, K. Erkelenz and R. Alzetta, Nucl. Phys. A194 (1972) 161.
- [24] A.D. Jackson, A. Landé and D.O. Riska, Phys. Lett. 55B (1975) 23.
- [25] A.M. Green, Rep. Progr. Phys. 39 (1976) 1109.
- [26] M. Brack, D.O. Riska and W. Weise, Nucl. Phys. A287 (1977) 425.
- [27] K. Bongardt, H. Pilkuhn and H.G. Schlaile, Phys. Lett. 52B (1973) 271.
- [28] C.A. Dominguez and B.J. Verwest, Phys. Lett. 89B (1980) 333.
- [29] M.M. Nagels et al., Nucl. Phys. B147 (1979) 189.
- [30] M.L. Goldberger and S.B. Treiman, Phys. Rev. 111 (1958) 354.
- [31] J.W. Durso, A.D. Jackson and B.J. Verwest, Nucl. Phys. A282 (1977) 404.
- [32] M. Dillig and M. Brack, J. Phys. G5 (1979) 223.

- [33] R.A. Bryan, C.A. Dominguez and B.J. Verwest, Texas A&M University Report No. ORO-5223-16, unpublished.
- [34] W. Grein and P. Kroll, Nucl. Phys. A338 (1980) 332.
- [35] R. Vinh Mau, Nucl. Phys. A335 (1980) 211.
- [36] K. Holinde, R. Machleidt, A. Faessler and H. Müther, Phys. Rev. C15 (1977) 1932.
- [37] E.E. Salpeter and H.A. Bethe, Phys. Rev. 84 (1951) 1232.
- [38] J. Fleischer and J.A. Tjon, Phys. Rev. D15 (1977) 2537.
- [39] R. Blanckenbecler and R. Sugar, Phys. Rev. 142 (1966) 1051.
- [40] M. Lacombe, B. Loiseau, J.M. Richard, R. Vinh Mau, J. Coté, P. Pirès and R. de Tourreil, Phys. Rev. C21 (1980) 861.
- [41] D. Schütte, Nucl. Phys. A221 (1974) 450.
- [42] e.g. W. Heitler, *The Quantum Theory of Radiation* (Oxford University Press, 1944).
- [43] K. Kotthoff, K. Holinde, R. Machleidt and D. Schütte, Nucl. Phys. A242 (1975) 429.
- [44] K. Kotthoff, R. Machleidt and D. Schütte, Nucl. Phys. A264 (1976) 484.
- [45] G.E. Brown and A.D. Jackson, *The Nucleon-Nucleon Interaction* (North-Holland, Amsterdam, 1976).
- [46] D. Amati, E. Leader and B. Vitale, Phys. Rev. 130 (1963) 750;
W.N. Cottingham and R. Vinh Mau, Phys. Rev. 130 (1963) 735.
- [47] B.D. Day and F. Coester, Phys. Rev. C13 (1976) 1720.
- [48] H. Sugawara and F. Hippel, Phys. Rev. 172 (1968) 1764; 185 (1969) 2046.
- [49] G.E. Brown and W. Weise, Phys. Rep. 22C (1975) 281.
- [50] G. Höhler, H.P. Jacob and R. Strauß, Nucl. Phys. B39 (1972) 237.
- [51] J.W. Durso, M. Saarela, G.E. Brown and A.D. Jackson, Nucl. Phys. A278 (1977) 445.
- [52] H. Nielsen and G. Oades, preprint.
- [53] M. Saarela, thesis, University of Oulu (1977), unpublished.
- [54] P. Haapakoski, Phys. Lett. 48B (1974) 307.
- [55] K. Holinde and R. Machleidt, Nucl. Phys. A280 (1977) 429.
- [56] K. Holinde, R. Machleidt, M.R. Anastasio, A. Faessler and H. Muether, Phys. Rev. C18 (1978) 870.
- [57] H.J. Weber and H. Arenhövel, Phys. Rep. 36C (1978) 279.
- [58] M.R. Anastasio, A. Faessler, H. Muether, K. Holinde and R. Machleidt, Nucl. Phys. A322 (1979) 369.
- [59] K. Holinde and R. Machleidt, Proc. Int. Conf. on the Nucleon-Nucleon Interaction, Vancouver (1977) p. 190.
- [60] M.M. Nagels, T.A. Rijken and J.J. de Swart, Phys. Rev. D17 (1978) 768.
- [61] C. Hajduk and P.U. Sauer, Phys. Rev. C22 (1980) 1304.
- [62] H.A. Bethe, B.H. Brandow and A.G. Petschek, Phys. Rev. 129 (1963) 225.
- [63] J.P. Jeukenne, A. Lejeune and C. Mahaux, Nucl. Phys. A245 (1975) 411.
- [64] M.R. Anastasio, A. Faessler, H. Muether, K. Holinde and R. Machleidt, Phys. Rev. C18 (1978) 2416.
- [65] R. Machleidt and K. Holinde, Nucl. Phys. A, in press.
- [66] W. Manzke and M. Gari, Nucl. Phys. A312 (1978) 457.
- [67] R.A. Smith and V.R. Pandharipande, Nucl. Phys. A256 (1976) 327.
- [68] K. Holinde, R. Machleidt, M.R. Anastasio, A. Faessler and H. Muether, Phys. Rev. C19 (1979) 948.
- [69] K. Holinde, R. Machleidt, A. Faessler, H. Muether and M.R. Anastasio, Non-Iterative Isobar Diagrams and their Effect in NN Scattering, preprint, to be published in Phys. Rev. C.
- [70] H. Muether, A. Faessler, M.R. Anastasio, K. Holinde and R. Machleidt, Phys. Rev. C22 (1980) 1744.
- [71] A. Faessler, H. Muether, K. Holinde and R. Machleidt, in preparation.
- [72] X. Bagnoud, K. Holinde and R. Machleidt, in preparation.
- [73] K. Holinde and R. Machleidt, Proc. Int. Conf. on the Few-Body Problem, Eugene (1980) and to be published.